

THE ROLE OF GLYCEROL IN THE DEGRADATION OF DIBENZOTHIOPHENE

BY *BURKHOLDERIA SP. C3*

A DISSERTATION SUBMITTED TO THE GRADUATE DIVISION OF THE
UNIVERSITY OF HAWAI'I AT MĀNOA IN PARTIAL FULFILLMENT OF THE
REQUIREMENTS FOR THE DEGREE OF

DOCTOR OF PHILOSOPHY

IN

MOLECULAR BIOSCIENCES AND BIOENGINEERING

MAY 2017

BY

CAMILA A. ORTEGA RAMÍREZ

Dissertation Committee:

Qing X. Li, Chairperson
Jon-Paul Bingham
Dulal Borthakur
Sean Callahan
Monika Ward

Keywords: Bioremediation, Polycyclic Aromatic Hydrocarbons, Biodegradation, Glycerol, Biosurfactants, Rhamnolipids

© Camila A. Ortega Ramírez

1. ACKNOWLEDGEMENTS

I would like to express my gratitude to everyone who has assisted me throughout my academic endeavor. First, I want to thank my advisor Dr. Qing X. Li for the opportunity to be a part of his lab, and for his invaluable guidance that has helped me grow professionally and personally. Additionally, I would like to acknowledge the support provided by the grant N00014-12-1-0496 from the Office of Naval Research and a subcontract with the Western Center for Agricultural Health and Safety NIOSH grant 2U54OH007550. I want to thank my committee members Drs. Jon-Paul Bingham, Dulal Borthakur, Sean Callahan and Monika Ward for their suggestions towards the improvement of my dissertation and completion of the Ph.D. degree. I would also like to thank them for their willingness and dedication despite their time constraints. I want to thank Dr. Brandon Yoza for his invaluable help with electron microscopy experiments and for reviewing my thesis and provided me with feedback towards the improvement of my written dissertation. I want to thank Mr. Abraham Kwan for his commitment to the lab and the project. Finally, I want to thank Mr. Travers Ching from Cell Molecular Biology department for helping me with proteomics data normalization and Mr. Jinlong Yang from engineering department who helped me with surface tension experiments. My time in Dr. Li's lab has been memorable and enjoyable, for that I need to thank my advisor and my lab mates. I want to specially mention to Drs. Jing Ge and Margaret Baker, to Mr. Zhibin Liang and Ms. Sofía Doello for their helpful discussions and encouragement. I will always cherish the friendship. Finally, I would like to thank the Microbiology and Biology departments for providing me with TA positions, which has allowed me to complete my graduate education.

2. ABSTRACT

Polycyclic aromatic hydrocarbons (PAHs) are a group of persistent, ubiquitous and carcinogenic chemicals found in the environment. PAHs can be formed anthropogenically and naturally. Dibenzothiophene (DBT) is a sulfur-containing PAH typically used as a model chemical to study biodegradation of PAHs and bioremediation. Biostimulation using more readily metabolized substrates can increase the biodegradation rate of PAHs, but the molecular mechanisms are not well understood. In this thesis, the effects of using glycerol as a co-substrate were investigated during DBT biodegradation by *Burkholderia* sp. C3 with respect to (i) DBT biodegradation kinetics, (ii) bacterial growth, (iii) proteome profiling, (iv) secretion of the biosurfactant rhamnolipid (RL), (v) RL biosynthesis inhibition, (vi) RL characterization and (vii) polyhydroxyalkanoates (PHA) vesicle formation. The results indicated that glycerol enhanced DBT biodegradation and supported bacterial growth, a phenomenon known as cometabolism. Optimized glycerol to DBT molar ratios increased DBT biodegradation rate constants up to 18-fold and enhanced DBT cometabolism by 25-30% at day 1 relative to DBT alone. At day 7 DBT (0.5 mM or 100 ppm) was completely biodegraded at a 100:1 glycerol to DBT molar ratio. Such increases were associated with nearly tripled amounts of RL secreted. RL analysis indicated biosynthesis, secretion and relevance of RLs to the enhanced DBT cometabolism. RLs reduced the surface tension of cultures with a DBT and glycerol mixture from 60-65 to 48-51 mN/m. RL biosynthesis inhibition with 2-bromooctanoic acid at 5 mM decreased DBT biodegradation rate comparable to that with DBT alone. Production of PHA vesicles were induced with glycerol and inhibited with 2 bromoalkanoic acids. RLs and PHA vesicles shared the same lipid precursor. All proteins involved in dTDP-rhamnose sugar precursor and R-3-hydroxydecanoyl-CoA lipid

precursor for RL biosynthesis were accumulated under the conditions tested. RhlABC proteins mediate the final steps in RL formation. The work presented in this dissertation showed that glycerol induces DBT cometabolism at a dose dependent manner over time, which positively associates with bacterial growth, PHA lipid granule formation and RL biosynthesis and secretion. This is the first description of anabolic pathways involved in RL biosynthesis and bromooctanoic acid inhibitory mechanism in a *Burkholderia* species.

3. STUDENT PRODUCTIVITY

3.1. POSTER PRESENTATIONS

- 3.1.1. **Camila A. Ortega Ramírez**, Abraham Kwan and Qing X. Li. Glycerol induced cometabolism of dibenzothiophene by *Burkholderia* sp. C3. CTAHR Symposium, April, 2016, Honolulu, HI. CTAHR Best PhD Student Poster Presentation Award
- 3.1.2. **Camila A. Ortega Ramírez**, Abraham Kwan and Qing X. Li. Glycolipid biosurfactant enhanced degradation of aromatic pollutants. Society for Glycobiology & Japanese Society of Carbohydrate Research Joint Annual Meeting, November, 2014, Honolulu, HI.
- 3.1.3. Qing X. Li and **Camila A. Ortega Ramírez** and Abraham Kwan. Bacterial surfactant enhanced degradation of aromatic compounds: an omics approach of study. 248th Analytical Chemistry Society National Meeting & Exposition, August, 2014, San Francisco, CA.
- 3.1.4. **Camila A. Ortega Ramírez** and Qing X. Li. *In silico* analysis of PAH dioxygenase from *Burkholderia* sp. C3 and its potential use in biodegradation. CTAHR Symposium, April, 2013, Honolulu, HI.

3.2. ORAL PRESENTATIONS

- 3.2.1. **Camila A. Ortega Ramírez**, Abraham Kwan and Qing X. Li. Enhanced cometabolism of dibenzothiophene in *Burkholderia* sp. C3 induced by glycerol. The International Chemical Congress of Pacific Basin Societies, December, 2015, Honolulu, HI.
- 3.2.2. **Camila A. Ortega Ramírez**, Abraham Kwan and Qing X. Li. The biosurfactant rhamnolipids secreted by *Burkholderia* sp. C3 enhance degradation of polycyclic aromatic hydrocarbons. CTAHR Symposium, April, 2014, Honolulu, HI. MBBE Best PhD Student Oral Presentation award.

3.3. MANUSCRIPTS IN PREPARATION

- 3.3.1. **Ortega Ramírez, C. A.**, Kwan, A. and Li, Q. X. 2016. Rhamnolipids induced by glycerol enhance dibenzothiophene cometabolism in *Burkholderia* sp. C3. Submitted to Applied and Environmental Microbiology.
- 3.3.2. **Ortega Ramírez, C. A.** and Li, Q. X. 2016. Glycerol induced mechanisms for degradation of dibenzothiophene in *Burkholderia* sp. C3. In preparation
- 3.3.3. **Ortega Ramírez, C. A.**, Yoza B. and Li, Q. X. 2016. 2-Bromoalkanoic acids inhibit polyhydroxyalkanoate granules formation in *Burkholderia* sp. C3. In preparation

- 3.3.4.** Mouanda N. A., **Ortega Ramírez, C. A.** and Li, Q. X. **2016.** Biodegradation of pyrene by *Bacillus lenichiformis* and *Achromobacter xylooxidans* isolates from the coastal region of Saudi Arabia. In preparation
- 3.3.5.** **Ortega Ramírez, C. A.** and Li, Q. X. 2016. Microbial degradation of heterocyclic aromatic hydrocarbon enhanced by biosurfactant. In preparation

TABLE OF CONTENTS

1.	Acknowledgements.....	i
2.	Abstract.....	ii
3.	Student productivity.....	iv
3.1.	Poster presentations.....	iv
3.2.	Oral presentations.....	iv
3.3.	Manuscripts in preparation.....	iv
4.	Abbreviations.....	xi
5.	Chapter 1: Literature Review.....	1
5.1.1.	Polycyclic Aromatic hydrocarbons (PAHs) and its frequency in the environment.....	1
5.1.2.	Sulfur-containing PAHs: DBT as a model chemical for bioremediation studies.....	3
5.1.3.	Remediation technologies for PAH contaminated soil.....	5
5.1.4.	Bioremediation as an alternative biotechnology.....	10
5.1.5.	Biosurfactants and its potential in bioremediation.....	12
5.1.6.	Bacterial degradation of DBT.....	13
5.1.7.	DBT biodegradation: 4S pathway.....	14
5.1.8.	DBT biodegradation: Kodama or lateral dioxygenation pathway.....	14
5.1.9.	DBT biodegradation: Angular dioxygenation pathway.....	15
5.1.10.	<i>Burkholderia</i> sp. C3, a non-pathogenic environmental isolate.....	17
5.1.11.	Impact of this dissertation.....	17
6.	Chapter 2: Hypotheses, Rationales and Aims.....	19
6.1	Hypothesis 1: Glycerol induces enhanced cometabolism of DBT in <i>Burkholderia</i> sp. C3.....	19
6.1.1.	Rationale: Addition of glycerol as a co-substrate biostimulates DBT biodegradation in C3 via increased biomass.....	19
6.2.	Hypothesis 1: Aims.....	21
6.2.1.	Aim 1:.....	21
6.2.2.	Aim 2:.....	21
6.2.3.	Aim 3:.....	21
6.3	Hypothesis 2: Glycerol stimulates the synthesis of proteins that mediate lipid metabolic pathways and polyhydroxyalkanoates (PHA) lipid granule formation in C322	

6.3.1. Rationale: Glycerol molecule and its assimilation in bacterial cells	22
6.4. Hypothesis 2: Aims	23
6.4.1. Aim 1:	23
6.4.2. Aim 2:	23
6.4.3. Aim 3:	23
6.4.4. Aim 4:	23
6.5. Hypothesis 3: Glycerol induces lipid precursor supply for biosynthesis of RL biosurfactant.....	24
6.5.1. Rationale: Glycerol is readily available in RL anabolic pathways	24
6.6. Hypothesis 3: Aims	26
6.6.1. Aim 1:	26
6.6.2. Aim 2:	26
6.6.3. Aim 3:	26
6.6.4. Aim 4:	26
6.6.5. Aim 5:	26
6.6.6. Aim 6:	26
7. Chapter 3: Methodology	27
7.1. Culturing of <i>Burkholderia</i> sp. C3	27
7.2. Preparation of DBT biodegradation cultures	27
7.3. Extraction and analysis of DBT	28
7.4. Extraction and processing of proteins from C3	30
7.5. Protein Identification	32
7.6. Extraction, restriction digestion and ligation of C3 genomic DNA.....	36
7.7. Identification of <i>rhlABC</i> genes	37
7.8. Extraction and quantification of RL	39
7.9. Characterization of RL congeners via MALDI-TOF-TOF.....	40
7.10. Visualization of polyhydroxyalkanoates lipid vesicles.....	43
7.11. Constrained drop surfactometer analysis	44
7.12. Data calculation.	45
8. Chapter 4: Results	46
8.1 Hypothesis 1: Glycerol induces enhanced cometabolism of DBT in <i>Burkholderia</i> sp. C3	46
8.1.1 Glycerol concentrations correlated with DBT cometabolism and C3 growth..	46

8.1.2. C3 has a third set of proteins involved in DBT degradation	50
8.2 Hypothesis 2: Glycerol stimulates the synthesis of proteins that mediate lipid metabolic pathways.....	55
8.2.1. Inhibition of β -oxidation of fatty acids decreased DBT biodegradation and C3 growth.....	55
8.2.2. Up-regulated proteome: DBT metabolism versus glycerol induced DBT cometabolism.....	58
8.2.3. Proteins involved in lipid metabolic pathways such as β -oxidation and FAS II pathways from C3 are up-regulated in all conditions tested.	62
8.2.4. PHA vesicle formation is induced by glycerol in C3	65
8.3. Hypothesis 3: glycerol induces lipid precursor supply for biosynthesis of RL biosurfactant and polyhydroxyalkanoates lipid vesicles in C3.....	68
8.3.1 RL fortification enhanced DBT biodegradation.....	71
8.3.2 Identification of genes confirmed the potential of RL biosynthesis in C3.....	68
8.3.3. RL biosynthesis induced by glycerol enhances DBT biodegradation in C3 ...	73
8.3.4. Proteins involved in RL synthesis and regulation were accumulated in all conditions tested.....	76
8.3.5. RL congeners were identified and characterized.....	77
9. Chapter 5: Discussion (past tense).....	84
10. Chapter 6: Conclusion and future directions (1 page)	92
11. References.....	95
11.1. Websites cited.....	95
11.2. Papers cited.....	96

LIST OF FIGURES

Figure 1. Clar structure of phenanthrene.	1
Figure 2. DBT metabolic pathways described in microorganisms.	16
Figure 3. Glycerol uptake and early assimilation in <i>Escherichia coli</i> adapted from (70).	20
Figure 4. Biosynthesis of polyhydroxyalkanoates (PHA) and rhamnolipids (RLs) in <i>Pseudomonas</i>	25
Figure 5. HPLC chromatogram of DBT standard.	29
Figure 6. Data normalization.	36
Figure 7. Malto-oligosaccharides spectrum.	42
Figure 8. Chromatograms of extracts of triplicate C3 cell cultures supplemented with 50 mM glycerol and 0.5 mM DBT at day 1.	46
Figure 9. Enhanced DBT biodegradation induced by glycerol vs C3 growth.	47
Figure 10. Putative steps catalyzed by DBT degradative enzymes identified in C3.	54
Figure 11. HEX and OC lipid pathways inhibitors decreased DBT biodegradation and C3 growth.	56
Figure 12. Correlation plot of the relative abundance of proteins extracted from C3 grown under different treatments.	59
Figure 13. Heat map of significant changes in the relative protein abundance in correspondence with treatments.	60
Figure 14. Glycerol induced PHA granules formation in C3. Cells were incubated with 0.5 mM DBT with or without 50 mM glycerol.	66
Figure 15. HEX and OC inhibited the formation of PHA granules in C3 at 2 days of incubation..	67
Figure 16. Cluster of <i>rhlABC</i> genes in C3 involved in RL synthesis.	71
Figure 17. RL fortified enhanced DBT biodegradation.	72
Figure 18. Relationship between DBT biodegradation and RL secretion induced by glycerol in C3 (A) and tensioactive properties of the cultures (B).	74
Figure 19. Relationship between the inhibition of RL biosynthesis by HEX or OC acid (A) and DBT biodegradation (B).	75
Figure 20. Analysis of RL standard via HPLC and MALDI-TOF.	79
Figure 21. Dirhamnolipid Rha-Rha-C ₁₀ -C ₁₀ fragmentation pattern spectrum.	80
Figure 22. RL separation in experimental samples.	82
Figure 23. (A) MALDI-TOF-MS of 4 RL congeners (M1, M2, M3 and M4) identified and (B) LC-Q-ToF-MS2 of Rha-C ₁₀ -C ₁₀ (M1).	83

LIST OF TABLES

Table 1. Elemental atom composition of crude oil from Saudi Arabia from (7).....	2
Table 2. Legal requirements of sulfur in diesel and gasoline (Transport website ⁶). *it became available.....	4
Table 3. Overview of remediation technologies. Adapted from (8, 14).....	6
Table 4. Inverse PCR primer information. T _a : annealing temperature. bp: base pair. Y: cytosine or thymine. K: guanine or thymine. R: adenine or guanosine. B: cytosine, guanine or thymine.	38
Table 5. Enhancement of DBT biodegradation rate constant and DBT half-life is dependent on glycerol concentration.....	49
Table 6. Proteins involved in DBT and degradation of other xenobiotics identified in C3. SC: sequence coverage..	50
Table 7. Influence of bromoalkanoic acid inhibitors in DBT biodegradation rate constant and DBT half-life.....	57
Table 8. Proteins involved in lipid metabolic pathways and PHA formation. NO: Not observed. ACP: acyl carrier protein.	63
Table 9. C3 <i>rhlABC</i> genes homology to other <i>Burkholderia</i> species.....	68
Table 10. Influence of RL fortification and C3 density in DBT biodegradation rate constant and DBT half-life.....	73
Table 11. Proteins mediating RL synthesis in C3.....	76
Table 12. Rha-Rha-C ₁₀ -C ₁₀ dirhamnolipid fragments..	81
Table 13. Full description of significantly abundant proteins (p-value < 0.05)..	114

4. ABBREVIATIONS

PAHs	Polycyclic Aromatic Hydrocarbons
ACN	Acetonitrile
ACP	Acyl Carrier Protein
ANOVA	Analysis of Variance
ATSDR	Agency for Toxic Substances and Disease Registry
AU	Arbitrary Units
CMC	Critical Micelle Concentration
DBT	Dibenzothiophene
DHB	2,5-Dihydroxybenzoic Acid
DP	Degrees of Polymerization
DTT	Dithiothreitol
ESI	Electrospray Ionization
EPA	Environmental Protection Agency
FAS II	De novo Fatty Acid Synthesis
FDP	Fructose-1,6-Diphosphate
FDR	False Discovery Rate
G3P	Glycerol-3-Phosphate
gDNA	Genomic DNA
GO	Gene Ontology
HAA	Hydroxy Alkanoic Acid
HBP	2-hydroxybiphenyl
HEX	2-Bromohexanoic Acid
HPLC	High Performance Liquid Chromatography
IAA	Iodoacetamide

iPCR	Inverse PCR
LB	Luria Bertani
LC-MS	Liquid Chromatograph Mass Spectrometer
<i>m/z</i>	Mass To Charge Ratio
MALDI-TOF	Matrix Assisted Laser Desorption Ionization - Time of Flight
MGF	Mascot Generic Format
MM	Minimal Medium
MS	Mass spectrometry
MS/MS	Tandem Mass Spectrometry
MW	Molecular Weight
NO	Not Observed
NPWSL	National Priority Waste Sites List
OC	2-Bromooctanoic Acid
PHA	Polyhydroxyalkanoic Acid
PL	Priority List
PPM	Parts Per Million
PSM	Peptide-Spectrum-Match
PVDF	Polyvinylidene Fluoride
Rha	Rhamnose sugar
RL	Rhamnolipid
SC	Sequence Coverage
SCE	Supercritical Extraction
SCF	Supercritical Fluid
TEM	Transmission electron microscopy

5. CHAPTER 1: LITERATURE REVIEW

5.1.1. Polycyclic Aromatic hydrocarbons (PAHs) and its frequency in the environment

Polycyclic Aromatic hydrocarbons (PAHs) are environmentally persistent, ubiquitous and carcinogenic chemicals (1–3) containing two or more fused aromatic rings in a linear, angular or clustered arrangement (3). The major sources of PAHs are petrogenic, pyrogenic and biogenic (4). Persistence of PAHs and its high frequency in the environment can be attributed to the aromatic character of the molecule, which confers an unusual low reactivity and high stability (5).

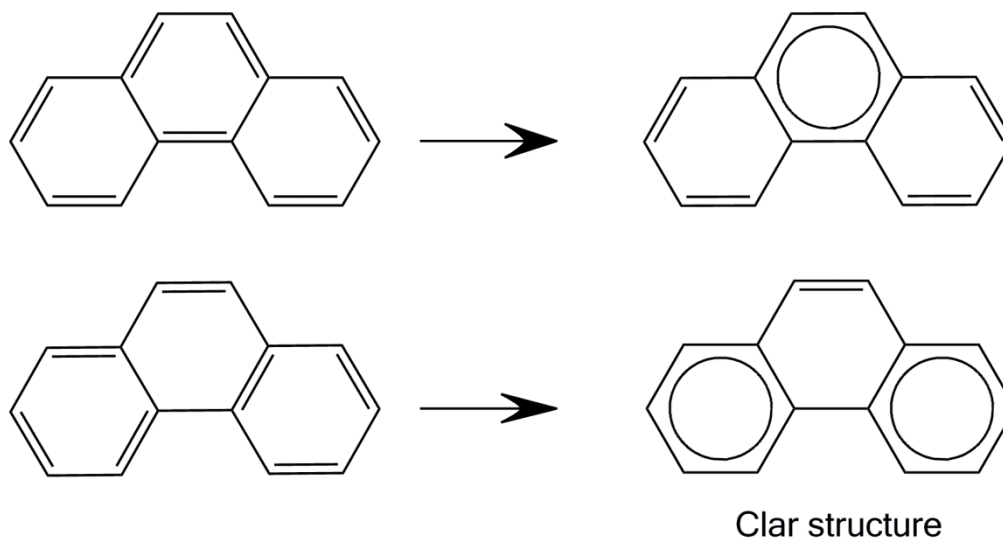


Figure 1. Clar structure of phenanthrene. Only two resonance structures are shown in the figure. Aromatic π -sextets are indicated with a circle. The Clar structure is the resonance structure with the highest number of aromatic π -sextet. Figure adapted from (5).

The aromaticity of a PAH is explained in Clar's postulation which is an extension of $4n+2$ Hückel's rule (3, 6). In Clar's postulation is stated that π -electrons ($2p_z$) are assigned to a PAH in order to obtain the largest number of disjoint aromatic π -sextet. A π -sextet contains six π -electrons in a benzene ring separated by C-C single bond from the adjacent ring (6). The Clar structure of a PAH is the resonance structure that has the highest number of isolated and localized aromatic π -sextet with the least number of localized double bonds (Figure 1). This structure is less active or kinetically more stable than the rest of the resonance structures. Likewise, the π -sextet centers are more aromatic and thus, less reactive than the other rings present in the molecule (5, 6).

Table 1. Elemental atom composition of crude oil from Saudi Arabia from (7).

Component	Fresh Saudi oil (wt%)
Carbon	84.80
Hydrogen	13.00
Sulphur	1.94
Oxygen	<0.50
Nitrogen	0.10
Calorific Value (mJ.K^{-1})	44.64

PAHs are planar molecules composed of carbon and hydrogen atoms; however, as shown in Table 1, sulfur, oxygen and nitrogen atoms may readily substitute in the ring system to produce heterocyclic aromatic compounds (3, 8) such as dibenzothiophene (DBT). Heterocyclics

co-exist with PAHs and other aromatic compounds (methyl PAHs) in the environment (4). Clar's postulate applies to all aromatics compounds with some limitations (5) and for simplicity in this dissertation heterocyclic aromatics will be referred as PAHs. Substitutions can result in molecular distortion of planarity that can potentially lead to more reactive and carcinogenic molecules. Consequently, the carcinogenic and mutagenic potential of PAHs depends on both abiotic and biotic transformations to more reactive metabolites (3), the mixture of PAHs and the organism exposed (9).

The atmosphere, water, soil and biota all act as environmental sinks for PAHs, although soil is the major repository (8). In the United States, PAHs were ranked ninth in the priority list (PL) of hazardous substances by the Environmental Protection Agency (EPA) and the Agency for Toxic Substances and Disease Registry (ATSDR) in 2015. The priority list is a compilation of substances frequently found in the national priority waste sites list (NPWSL) that are determined to have risk to human health, having known toxicity and potential for human exposure (ATSDR website:¹). Currently, there are 1337 sites in the NPWSL (EPA website:²).

5.1.2. Sulfur-containing PAHs: DBT as a model chemical for bioremediation studies

After carbon and hydrogen, sulfur is the most abundant element in PAHs and can exist in organic or inorganic fractions (10). In organic fractions, DBT is a major component, along with benzothiophene, benzonaphthothiophenes and their alkylated homologous (11). Sulfur-containing PAHs in crude oil are of particular concern because of its detrimental effects in

human health, the environment and economy (10, 11). The Clean Air Act in United States established the legal requirements to lower the sulfur content from crude oil (Table 2).

Table 2. Legal requirements of sulfur in diesel and gasoline (Transport website⁵). *it became available.

Sulfur levels in diesel	500 ppm	15 ppm
Highway Diesel Fuel	1993	2006*
No road Diesel Fuel	2007	2010
Locomotive and marine fuels	2007	2012
Marine engine fuels	10,000 ppm (1%)	1000 ppm (0.1%)
IMO* limits	2010	2015
EPA limits		2009
Sulfur levels in gasoline		Year
120 - 300 ppm		2004
30 - 80 ppm		2006

DBT and its analogs are however widely distributed in sediments and urbanized areas (11, 12). Consequently, DBT it is typically used as a model chemical to study spatial distribution and quantification of thermodynamically stable sulfur-containing PAHs (11) and is the chemical of study in this dissertation for its applications in bioremediation.

DBT is a non-alternant PAH with both six- and five-rings fused together in an angular arrangement (Figure 2) (3). It is a hydrophobic compound with a water solubility of 7.9 μM and an octanol-water coefficient (K_{ow}) of 4.44 (12). The lipophilic nature of DBT and other high molecular weight PAHs allows them to concentrate in aquatic animals and bioaccumulate through the food chain possessing an ecotoxicological risk (4). It was shown that dose dependent exposure of DBT to zebrafish embryos disrupted cardiac function. Higher dose was associated with morphological abnormalities at later developmental stages. Mortality was also reported for continuously exposed zebrafish embryos (12). In another study, DBT metabolites were shown to interact with estrogen receptors expressed in T47D human breast adenocarcinoma cell lines. Predicted DBT liver metabolites would also be estrogenic compounds (13). The frequency of DBT and PAHs in urbanized areas, the potential for human exposure and health threat makes them chemicals of concern and thus, need to be environmentally controlled.

5.1.3. Remediation technologies for PAH contaminated soil

In order to effectively remove PAHs, a prior characterization and evaluation of the contaminated site is required (14). Site-specific conditions, which include characteristics of the contaminants (e.g., volatility, concentration, mixture) and soil properties (e.g., permeability, porosity, and pH) are important considerations for effective remediation. There are several technologies for PAH contaminant removal in which the technology of choice will depend on the evaluation of the site, the monetary cost and the technologies available (14). These technologies are summarized in Table 3.

Physicochemical, chemical, thermal and biological are all types of treatments to be applied *in-situ* or *ex-situ* of the remediation site. The main advantage of *in-situ* compared to *ex-situ* technologies is that the polluted soil does not need prior excavation and transportation in order to be treated, making it economically more attractive. However, treatments can require longer times and the uniformity as well as the efficacy is usually unclear. Similarly, the amount of waste to be treated and the moisture content of the soil are key cost drivers to consider *ex-situ* remediation (FRTR website⁴). *In-situ* and *ex-situ* technologies, their advantages and limitations will be discussed briefly in the following paragraphs.

Table 3. Overview of remediation technologies. Adapted from (8, 14).

Classification	Technology
Physicochemical	Solvent (water and organic solvents (15)) or vegetable oils extraction (16) with or without addition of surfactants (17) and/or cyclodextrins. Extraction with supercritical fluid (18, 19) or subcritical fluid. Both extractions complemented with physical agitation or sonication.
Thermal	Incineration, thermal desorption (20), thermally enhanced soil vapor extraction.
Chemical	Chemical oxidation with various oxidants (21) (e.g. hydrogen peroxide, Fenton's reagent, potassium permanganate, activated persulfate), photocatalytic degradation, electroremediation (22)
Biological	Biostimulation (23), bioventilation and bioaugmentation (24) or a mixture of those.

Ex-situ physicochemical treatment utilize physical separation (agitation or ultrasonication) and chemical extraction using a solvent or a supercritical or subcritical fluid (18). Chemical extractions use individual or mixture of chemically compatible solvents, surfactants (e.g. Tween 80) and/or include elevated temperature for PAH desorption from soil particles and extraction into the solvent. The use of non-toxic or biodegradable extraction agents are desirable attributes (8). Silva et al., (15) utilized acetone-ethyl acetate-water (40:50:10 ratio) as an environmental friendly mixture; where ethyl acetate was the main solvent contributing to the removal of xylene, naphthalene and hexadecane. Pollutant recovery efficiency increased with higher liquid to soil ratios, up to 95% (15). Use of sunflower and peanut oil with orbital agitation also showed promising results, however, oil to soil ratio adequate for PAH removal was prohibitively high and may not represent a viable solution (16).

Subcritical fluid extraction utilizes water at high temperature ($100^{\circ}\text{C} < T < 374^{\circ}\text{C}$) and pressure (>221 bars) to retain its liquid state. Under these conditions the, dielectric constant, surface tension and polarity of water are reduced making it an effective alternative solvent (subcritical or superheated water) (14). The same principle is applied in supercritical extraction (SCE), but, a fluid (supercritical fluid: SCF) with a high affinity for PAHs is utilized instead of water. In SCE, excavated soil is placed in a pressure vessel and extracted with a recirculated stream of SCF. Once PAHs are transferred to SCF; the clean soil, the SCF and the solutes are separated by physical methods (18). Librando et al. (19) analyzed the recovery of 6 PAHs from sediment samples with varying pressure from 230–600 bars and at 2 temperatures (50 and 80°C). Different co-solvents with CO_2 as SCF were also tested. The best performance was obtained with 5% methanol as co-solvent, 50°C and 450 bars. These optimized parameters achieved above 90%

recovery of 5 PAHs from spiked soil. They concluded that better recovery was obtained with higher molecular weight PAHs (19), which is an advantage over bioremediation, since there are few microorganism capable of biodegrading high molecular weight PAHs (4). Nonetheless, there are disadvantages of *ex-situ* physicochemical treatments; for instance, PAHs need to be treat it following extraction and solvents used need to be regenerated (8, 16). Extractions need to be scale up to make them more economically feasible (8). Streams by-products can be generated during SCE and must also be treated, which increases the technology cost (18).

Thermal remediation comprises the ex-situ technologies: incineration, thermal desorption and microwave frequency heating. Incineration consist in simply burning the contaminated soil at temperatures up to 1000°C (25). It is one of the most effective and simpler remediation methods for removing oil contamination (14) but it emits toxic gases and uses high amounts of energy (7, 14). Thermal desorption uses heat to physically separate contaminants from soil. For PAH remediation, the temperature required must be higher than a PAHs boiling temperature. During thermal treatments, the number and concentration of PAHs changes due to parasitic reactions. PAHs may be transformed to several isomers, some being more toxic than their parent compound. For example Pope et al., empirically demonstrated that at high temperatures pyrene reacts with acetylene forming cyclopenta[*c,d*]pyrene and phenanthrene forms chrysene, both human cell mutagens (26).

The production of free radicals with high redox potential is the basic principle of chemical oxidation treatments. The free radicals will oxidize through electrophilic addition or via hydrogen subtraction (14). For example, hydrogen peroxide produces hydroxyl radicals ($\cdot\text{OH}$), which are able to react with alkanes and aromatic compounds. Since this reaction is not

considered kinetically fast enough, hydrogen peroxide is co-added with a transition metal (usually iron) as a catalyst to enhance radical formation, a mixture known as Fenton reagent. In a modified Fenton's system in addition to hydroxyl radicals, hydroperoxide radicals ($\text{HO}_2\bullet$), superoxide anions ($\text{O}_2^{\bullet-}$), and hydroperoxide anions (HO_2^-) are also formed. These radicals seem to degrade recalcitrant organic compounds. Efficiency is however impacted by high organic content and PAH adsorption onto soil, relative PAHs concentration and its specific chemical composition and mixture (21).

Electroremediation is an in situ technology where electrodes are inserted directly into the contaminated soil from which a low intensity electrical current is distributed. It has been previously used for the removal of inorganic contaminants; however, recent efforts to expand this technology to remediate PAH contaminated soil are being developed (8). A charged base electromigration of species occurs towards the electrodes. Nonpolar species such as PAHs can migrate with the electro-osmotic flow of an aqueous solution. Addition of solubilizing agents (non-ionic surfactants, cyclodextrins), co-solvents (e.g. ethanol) and/or electrolytes in the aqueous solution are some of the strategies to increase desorption and solubilization of PAHs (22). Application of biosurfactants to this strategy remains to be investigated. After current exposure, soil contaminants are concentrated and recovered from an electrode chamber and subsequently treated (22).

5.1.4. Bioremediation as an alternative biotechnology

Generally, bioremediation is the use of biological metabolisms for the removal of contaminants from the environment. Phytoremediation could also be included in this category; however, it will not be discussed in this dissertation as it is out of the scope of the research presented. Four strategies can be utilized in bioremediation with microorganisms: bioaugmentation, biostimulation, bioventilation or a combination of these. Bioaugmentation refers to the addition or enrichment of specific microorganisms that possess the metabolic capabilities resulting in increased biodegradation rates of pollutants on site (8). This strategy is applicable to sites that have insufficient amount of PAH degrading microbes or when the indigenous microflora does not possess the necessary metabolic capability (27). Typically, consortia of microorganisms are applied to the soil as there is not a single microorganism with the ability to degrade all the contaminants of a particular site (14). Dehydrogenase activity and CO₂ measurements are often two parameters used to determine the potential efficiency of a consortia in situ. Szulc et al., (24) tested ten consortia for hydrocarbon degradation and discovered an association between dehydrogenase activity and CO₂ emitted. The consortium having the highest dehydrogenase activity and CO₂ emission values was selected for bioaugmentation use. They emphasize the need for the selection of an appropriate consortium for improved bioremediation. Their results demonstrated an enhanced removal of diesel oil compared to natural attenuation over a one year period (24).

It is worth noting that the indigenous microflora of a PAH contaminated place can accomplish natural attenuation. In soil column experiments, 88% of PAH loss was attributed to biodegradation by the indigenous soil community (28). However, the rate of biodegradation is

generally lower than in laboratory settings (29). If environmental conditions are limiting factors, biostimulation with nutrients, surfactants and/or additional carbon sources is another strategy to improve biodegradation rates (14). Margesin and Schinner showed that after 447 days biostimulation with N-P-K fertilizer (C/N ratio of 20:1) decreased the hydrocarbon concentration by 66% compared with 41% achieved through natural attenuation (23). In another study, Boonchan et al., (30) tested 5 nonionic surfactants at concentrations below, above and at the critical micelle concentration (CMC). CMC is the minimum concentration required for a surfactant to form micelles. Surfactant micelle formation is one of the mechanisms proposed for PAH solubilization and consequent bioavailability increased (31). Effectively, the solubility of pyrene, fluoranthene and benzo[*a*]pyrene increased 700-, 500- and 10⁴-fold, respectively, with surfactant concentrations above CMC (30). In this experiment the biodegradation rate for 250 ppm pyrene was reduced by 50% using Brij 35, Tergitol NP-10 and Tyloxapol non-ionic surfactants (5-10 g/L). Igepal CA-360 inhibited microbial growth, consequently inhibiting pyrene degradation (30). These results suggest that the efficacy of specific surfactants should be tested under the conditions that it will be utilized. Biostimulation can provide more suitable conditions for both indigenous and exogenous microbial populations (27).

Bioventilation involves the introduction of oxygen to stimulate microbial growth and aerobic reactions. It has been shown to improve degradation efficiency 21% over natural attenuation of biodiesel on a 60 days' time period (14).

In contrast to other remediation technologies, which often result in partial breakdown or by-products, the products of bioremediation are water, gasses and minerals, requiring no further downstream process. Assuming that the necessary metabolic capability is present, biostimulation

through the addition of nutrients or biosurfactants is arguably the most widely used strategy to increase PAH bioavailability (31, 32).

5.1.5. Biosurfactants and its potential in bioremediation

Intentional augmentation of contaminated soil with microorganisms adept at producing biosurfactants is a promising method to improve current bioremediation technologies (24). In addition to catabolic enzymes (4, 33–36), microbial methods to address PAH solubilization and bioavailability may be required as a PAH molecular weight increases, which results in greater resistance to degradation (3, 31, 32). Bioremediation of hydrophobic pollutants is frequently limited by low abundance of microorganisms and poor chemical bioavailability, causing decreased biodegradation kinetics (23, 31).

Biosurfactants interact with PAHs in solution and at water-particle and water-oil interfaces because of the amphipathic nature of their chemical structure. Those interactions make PAHs more soluble and bioavailable (31, 37). The production of both biosurfactants and hydrocarbon degradative enzymes in bacteria from PAH contaminated soil (38–40) and the effects of these biosurfactants on hydrophobic pollutant uptake (41) and biodegradation (37, 42, 43) suggest an evolutionary adaptation by microorganisms to overcome low substrate availability.

5.1.6. Bacterial degradation of DBT

Research on the microbial transformation of PAHs, their catabolic pathways and biodegradation kinetics have been extensively studied (4, 32, 44). Three degradation pathways have been described for DBT (45–49). Catabolism as well as additional metabolic processes for enhanced DBT degradation will depend on the genetic make-up of not only the consortia, but also upon specific species of microorganism. Metabolically removed sulfur from the DBT molecule can be utilized in primary metabolisms for the production of amino acids and enzyme co-factors (10, 47).

The three DBT biodegradation pathways are shown in Figure 2 and discussed in the following subheadings:

5.1.7. DBT biodegradation: 4S pathway

5.1.8. DBT biodegradation: Kodama or lateral dioxygenation pathway

5.1.9. DBT biodegradation: Angular dioxygenation pathway

DBT oxidative enzymes are found in the cytoplasm, requiring transport of the hydrophobic DBT for degradation (50). How can DBT enter the cell membrane? - the mechanism is not clear, however, it was suggested that DBT dispersed by *N,N'*-dimethylformide in water (water/oil phase) may cross the cell membrane through simple diffusion but not in *n*-tetradecane (oil phase), where an ABC-like transport system may have this role (51).

5.1.7. DBT biodegradation: 4S pathway

Initial steps in this pathway are catalyzed by DBT monooxygenase and DBT-sulfone monooxygenase. Both of these flavin-dependent monooxygenases incorporate one oxygen atom into the sulfur atom in two steps process (Figure 2). A flavin reductase is required for full monooxygenases activity (49). A HPBS desulfinate then catalyzes the conversion of hydroxyphenyl benzene sulfonate into 2-hydroxybiphenyl (HBP) and sulfite (49, 52).

The HBP product is highly hydrophobic finding its way back to the oil fraction. No calorific value is lost with this pathway and thus is an ideal desulfurization pathway for fuel processing (47, 53). The *dsz* genes coding for the enzymes involved in the 4S pathway have been described in *Rhodococcus*, *Mycobacterium*, *Corynebacterium*, *Bacillus* and *Stenotrophomonas* species (54–57).

5.1.8. DBT biodegradation: Kodama or lateral dioxygenation pathway

The Kodama pathway is described as a lateral dioxygenation pathway (4, 46). The first and most important step in this pathway is mediated by DBT dioxygenase. Reports indicate that DBT dioxygenase mutants lose their ability to metabolize DBT (58, 59). Ring-hydroxylating dioxygenases incorporate molecular oxygen at 1,2; 3,4 or the 9,10 positions of a PAH (Figure 2). This step is necessary for ortho-, meta- or para-cleavage of the aromatic ring. The position where oxygen will be incorporated would depend on the dioxygenase specificity. The metabolites produced are therefore dependent on DBT initial dioxygenation (4, 34, 48, 60). In 1993, Denome *et al.*, (58) reported a DNA fragment that conferred *Pseudomonas* sp. C18 the capacity to oxidize

DBT. This DNA fragment contains *dox* genes with high sequence similarities to naphthalene, biphenyl, toluene and benzene dioxygenases from *Pseudomonas putida* G7 (*nah* genes) (58, 61). The *nah* genes conferred G7 the ability to degrade naphthalene (62). Several groups of *nah*-like genes and *phn* genes have been described. The *nah*-like and *phn* genes conferred *Pseudomonas* strains the ability to degrade naphthalene and phenanthrene, respectively (61, 62).

5.1.9. DBT biodegradation: Angular dioxygenation pathway

The angular dioxygenation pathway will not be discussed in this dissertation as there are very few reports describing this biodegradation pathway and most of the DBT metabolites have not been identified, as well as microorganisms, with the proper catalytic enzymes (46) (Figure 2).

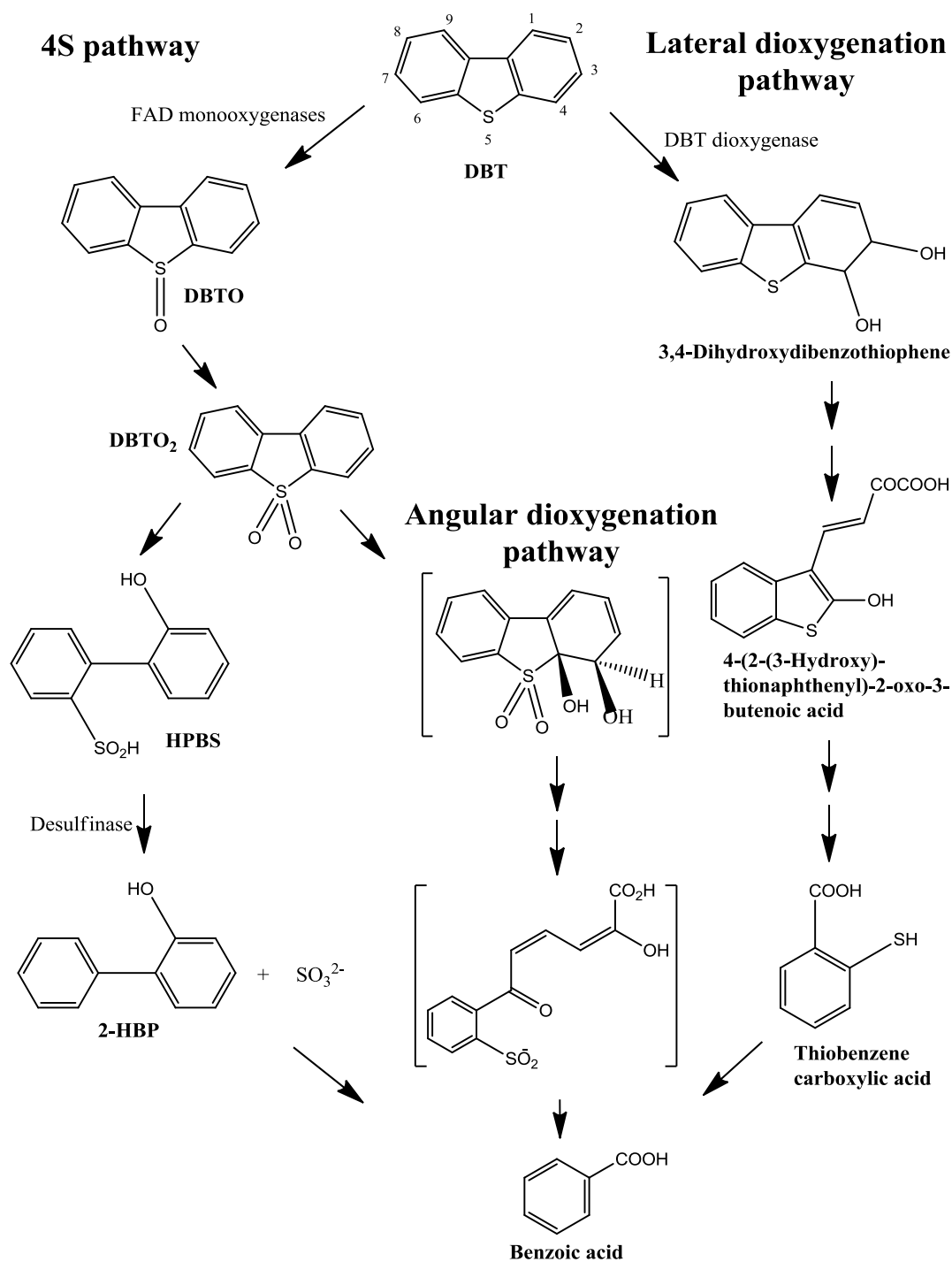


Figure 2. DBT metabolic pathways described in microorganisms. Unstable metabolites in brackets have not been observed directly. Figure was adapted and modified from (45, 46, 49, 59). DBT: dibenzothiophene. DBTO: dibenzothiophene sulfoxide. DBTO₂: dibenzothiophene sulfone. HPBS: hydroxyphenylbenzene sulfonate. 2-HBP: 2-hydroxybiphenyl.

5.1.10. *Burkholderia* sp. C3, a non-pathogenic environmental isolate

Burkholderia sp. C3 is a PAH degrading bacterium isolated from a former oil gasification company site on Hilo, Hawai'i. The waste product generated by the company was a tar rich in PAHs. The tar was buried in a tank after the company was closed in 1965. Later the bottom of the tank was excavated and a portion of the tar with contaminated soil was stored in a plastic sheet in a berm on site. In the year 2000, heavy flooding swept PAH-contaminated silt onto the surface of five Hawai'i County Park soccer fields. In the same year this site was declared an emergency response site by the EPA and samples were taken and analyzed in our laboratory. Thirteen PAHs were identified and 19 bacterial strains were isolated (63). The C3 isolate was able to completely degrade 40 ppm of phenanthrene in 7 days using a 1,2 and 3,4 dioxygenation system (34). Tittabutr et al. (35) then reported the ability of C3 to degrade 7 additional aromatic pollutants. C3 degraded 40 ppm of DBT in 7 days (35). Furthermore, *nag*-like and *phn* cluster of genes were isolated in C3. Both clusters conferred *E. coli* the ability to degrade phenanthrene, naphthalene and DBT to some extent (35).

5.1.11. Impact of this dissertation

This study was designed to investigate glycerol, as a co-substrate, to biostimulate the degradation of DBT by C3. Previously unpublished studies indicated that glycerol enhanced the biodegradation of DBT. Glucose was also investigated as a co-substrate but DBT biodegradation inhibition was detected instead. Early DBT solubilization, foam formation, and DBT degradation were observed in DBT biodegradation cultures induced for 12 hours with glycerol. This was not

observed in cultures with DBT alone, suggesting the secretion of a surfactant agent. In *Pseudomonas* species, glycerol readily enters into glycolysis and β -oxidation and De novo synthesis of fatty acid (FAS II) lipid pathways, affecting the production of rhamnolipids (RLs), a glycolipid biosurfactant and the production of polyhydroxyalkanoic acid (PHA) granules formation (64, 65). There are reports describing the production of RLs in Burkholderia species as well (66, 67). Here, we report up to an 18-fold enhancement in DBT biodegradation induced by glycerol cometabolism in C3. Four mechanisms were induced in C3 by DBT cometabolism with glycerol. (1) Glycerol-induced accumulation of DBT degradative enzymes. All enzymes from DBT, phenanthrene and naphthalene degradation pathways were available for degradation of xenobiotics in C3 treated with 50 mM glycerol. (2) Glycerol supported an increase in C3 biomass. Glycerol assimilated in C3 basal metabolism as phosphorylated glycerol and glycerate. (3) Glycerol-induced accumulation of intracellular PHA granules. Glycerol-induced PHA granule formation at 2 days and this associated with enhanced DBT degradation (4) Glycerol stimulated a dual function in C3 as a RL producer and a DBT degrader. The increase of RL biosynthesis and secretion facilitated biodegradation of DBT in C3. To our knowledge, this is the first study showing a direct association between RL biosynthesis and DBT biodegradation induced by glycerol in Burkholderia species.

6. CHAPTER 2: HYPOTHESES, RATIONALES AND AIMS

6.1 HYPOTHESIS 1: GLYCEROL ENHANCES COMETABOLISM OF DBT IN *BURKHOLDERIA SP. C3*

6.1.1. Rationale: Glycerol as a co-substrate biostimulates DBT biodegradation in C3 via increased biomass

There are many parameters affecting bioremediation of PAHs-contaminated sites. Besides an appropriate microbial consortium, type and concentration of nutrients and the actual site conditions (e.g. soil moisture, pH, temperature) are stressor factors that have an effect on biodegradation efficiencies (27). This study was designed to follow a biostimulation strategy to investigate the influence of glycerol in the DBT biodegradation ability of C3. Glycerol is the main by-product in the production of biodiesel. It is obtained during transesterification of vegetable oils and animal fats, accounting for about 10% (w/w) of biodiesel. Biodiesel is one of the most promising alternative fuels, although its current production cost is relatively high. New applications of glycerol would make biodiesel production more cost-effective (68, 69).

Glycerol is a small uncharged molecule that can cross the cell membrane through passive diffusion. However, under low extracellular glycerol concentrations, bacterial cells limited to passive uptake have a growth disadvantage (69). The gene products of the *glp* regulon participate in facilitated diffusion and metabolism of glycerol and its derivatives in *Escherichia coli*. *GlpF* is a highly selective channel for non-ionic compounds (69). Not to be confused with glycerol-3-

phosphate (G3P) transporter (GlpT), which uptakes G3P (70). Interaction of GlpF with glycerol kinase (GlpK) stimulates glycerol phosphorylation by the same enzyme. It was shown that the K_m of GlpK decreased upon interaction with GlpF (71). Intracellular G3P can be further metabolized aerobically via G3P dehydrogenase (GlpD) or anaerobically via G3P dehydrogenase (GlpA) as shown in Figure 3.

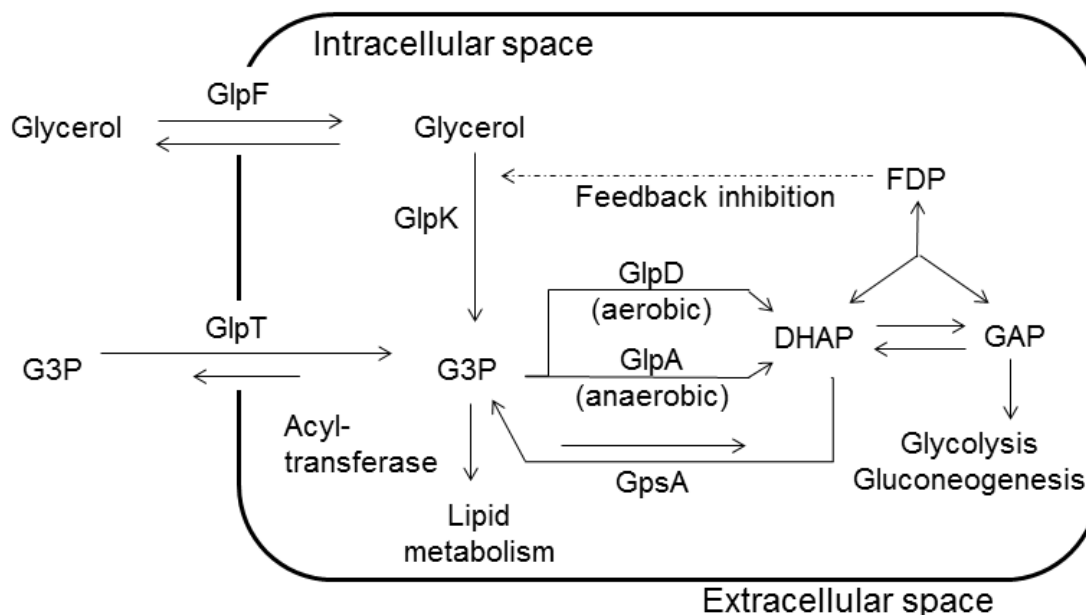


Figure 3. Glycerol uptake and early assimilation in *Escherichia coli* adapted from (70). Substrates: G3P, glycerol-3-phosphate; DHAP, dihydroxyacetone phosphate; GAP, glyceraldehyde-3-phosphate, FDP, fructose-1,6-diphosphate. Proteins: GlpF, glycerol facilitator; GlpT, glycerol-3-phosphate transporter; GlpK, glycerol kinase; GlpD, glycerol-3-phosphate dehydrogenase; GlpA, glycerol-3-phosphate dehydrogenase and GpsA, glycerol-3-phosphate synthase.

If supplied into basal metabolism, glycerol can support bacterial growth and possibly enhanced the biodegradation rate of DBT, simply by increasing the biomass of C3. For aerobic metabolism, GlpK phosphorylates glycerol into G3P which is then converted to

dihydroxyacetone phosphate by G3P dehydrogenase (70). Glycerol can also enter to glycolysis via glycerate-3-phosphate. GlpK has four binding sites for glycerol and for fructose-1,6-diphosphate (FDP). Feedback inhibition by FDP is the dominant repressing mechanism for glycerol utilization in the presence of glucose (70). In order to determine the glycerol effects on DBT co-utilization and C3 growth the aims below were proposed:

6.2. HYPOTHESIS 1: AIMS

6.2.1. Aim 1: Determine the optimum concentration of glycerol to induce DBT cometabolism in C3

6.2.2. Aim 2: Measure C3 growth with different concentrations of glycerol in the presence and absence of 0.5 mM DBT

6.2.3. Aim 3: Analyze proteins involved in DBT and glycerol degradation from C3 cultured with treatments: A, 0.5 mM DBT; B, 50 mM glycerol; C, 0.5 mM DBT with 50 mM glycerol; and D, 0.5 mM DBT with 50 mM glycerol and 2 mM 2-bromooctanoic acid (OC).

6.3 HYPOTHESIS 2: GLYCEROL STIMULATES THE SYNTHESIS OF PROTEINS THAT MEDIATE LIPID METABOLIC PATHWAYS AND POLYHYDROXYALKANOIC (PHA) LIPID GRANULE FORMATION IN C3

6.3.1. Rationale: Glycerol molecule and its assimilation in bacterial cells

Glycerol is used for carbohydrate and lipid synthesis in bacteria (Figure 3). G3P can be directly used by G3P acyltransferase for biosynthesis of L-1-phosphatidyl-glycerol. The end products and intermediaries of this biosynthetic pathway served then as substrates for the synthesis of phospholipids such as phosphatidylcholines, phosphatidylethanolamine and cardiolipins (BioCyc website⁶). In 1964, Tepper et al., (72) demonstrated that glycerol-grown *Mycobacterium phlei* cells had higher non-essential lipid content than glucose-grown cells (72). Glycerol readily enters into β -oxidation and *De Novo* synthesis of fatty acid (FAS II) pathways. These pathways produce the lipid precursor for the biosynthesis of PHAs lipid storage granules (73, 74).

Pseudomonas species have two PHA synthase genes (*phaC1* and *phaC2*) found in the mclPHA gene cluster. Additionally in this cluster, PHA depolymerase (*phaZ*), a transcriptional activator (*phaD*) (75) and two phasin proteins (*phaF1*) are also coded. It is proposed that phasins have a structural role in granule formation and stabilization (76). PHA utilization and storage increased the production of molecules with tension-lowering properties (77) such as RL (78). Similarly, PHA accumulation affected cell-surface hydrophobicity (77) and increased heat-stress tolerance (78). All features relevant for fitness in a hydrocarbon-contaminated environment.

Inhibition of β -oxidation and FAS II by 2-bromoalkanoic acids suppresses the biosynthesis of PHAs in *Pseudomonas* species (64, 65). It was proposed that 2-bromoalkanoic acid may target PhaG involved in producing the acyl carrier protein (ACP)-lipid precursor for PHA synthesis (65, 79). Does C3 forms PHA granules and do these enhanced DBT degradation? If PHA granule accumulation has an effect on DBT biodegradation in C3 induced by glycerol, the use of 2-bromoalkanoic acid should not only inhibit degradation of DBT, but also the production of PHA granules.

6.4. HYPOTHESIS 2: AIMS

6.4.1. Aim 1: Determine the effect of 2-bromohexanoic (HEX) and OC acid, inhibitors of β -oxidation and FAS II lipid pathways at 2 and 5 mM concentrations on DBT biodegradation induced by 50 mM glycerol and measure C3 growth

6.4.2. Aim 2: Profile proteins from C3 cultured with treatments: A 0.5 mM DBT; B, 50 mM glycerol; C, 0.5 mM DBT with 50 mM glycerol; and D, 0.5 mM DBT with 50 mM glycerol and 2 mM OC.

6.4.3. Aim 3: Analyze proteins involved in PHA synthesis from C3 cultured with treatments: A 0.5 mM DBT; B, 50 mM glycerol; C, 0.5 mM DBT with 50 mM glycerol; and D, 0.5 mM DBT with 50 mM glycerol and 2 mM OC.

6.4.4. Aim 4: Visualize PHA lipid granules in C3 grown with 0.5 mM DBT with or without 50 mM glycerol and with 2 mM of OC or HEX inhibitor

6.5. HYPOTHESIS 3: GLYCEROL INDUCES LIPID PRECURSOR SUPPLY FOR BIOSYNTHESIS OF RL BIOSURFACTANT

6.5.1. Rationale: Glycerol is readily available in RL anabolic pathways

PHA and RL synthesis have a close metabolic relationship. PhaG utilizes R-3-hydroxydecanoyl-CoA to produce PHA or R-3-hydroxyoctanoyl-CoA can be further converted to hydroxylalkanoic acid (HAA), lipid precursor for RL synthesis (Figure 4) (74). RL is a glycolipid biosurfactant extensively studied in *Pseudomonas* species and its potential in the bioremediation field (37, 38, 80, 81). Biosynthesis of RL involves the anabolic pathways shown in Figure 4. Biosynthesis of dTDP-L-rhamnose is accomplished in several steps by RmlABCD from the substrate, D-glucose-1-phosphate (82). The lipid precursors of HAA by HAA synthase (RhIA) are supplied from both β -oxidation and FAS II pathways. β -Oxidation pathway produces R-3-hydroxydecanoyl-CoA via an enoyl-CoA hydratase/isomerase (RhIYZ), which is subsequently utilized by RhIA to produce HAA (64). FAS II pathway produces R-3-hydroxyacyl-ACP that is directly used by RhIA to synthesize HAA (83). Additional steps catalyzed by RhIG and PhaG to produce HAA have also been described in literature (65, 73, 84). HAA and dTDP-L-rhamnose are reacted via the catalysis of rhamnosyltransferase 1 (RhIB) to produce monorhamnolipids (85, 86). Monorhamnolipids can then react with another dTDP-L-rhamnose under the catalysis of rhamnosyltransferase 2 (RhIC) to produce dirhamnolipids (87).

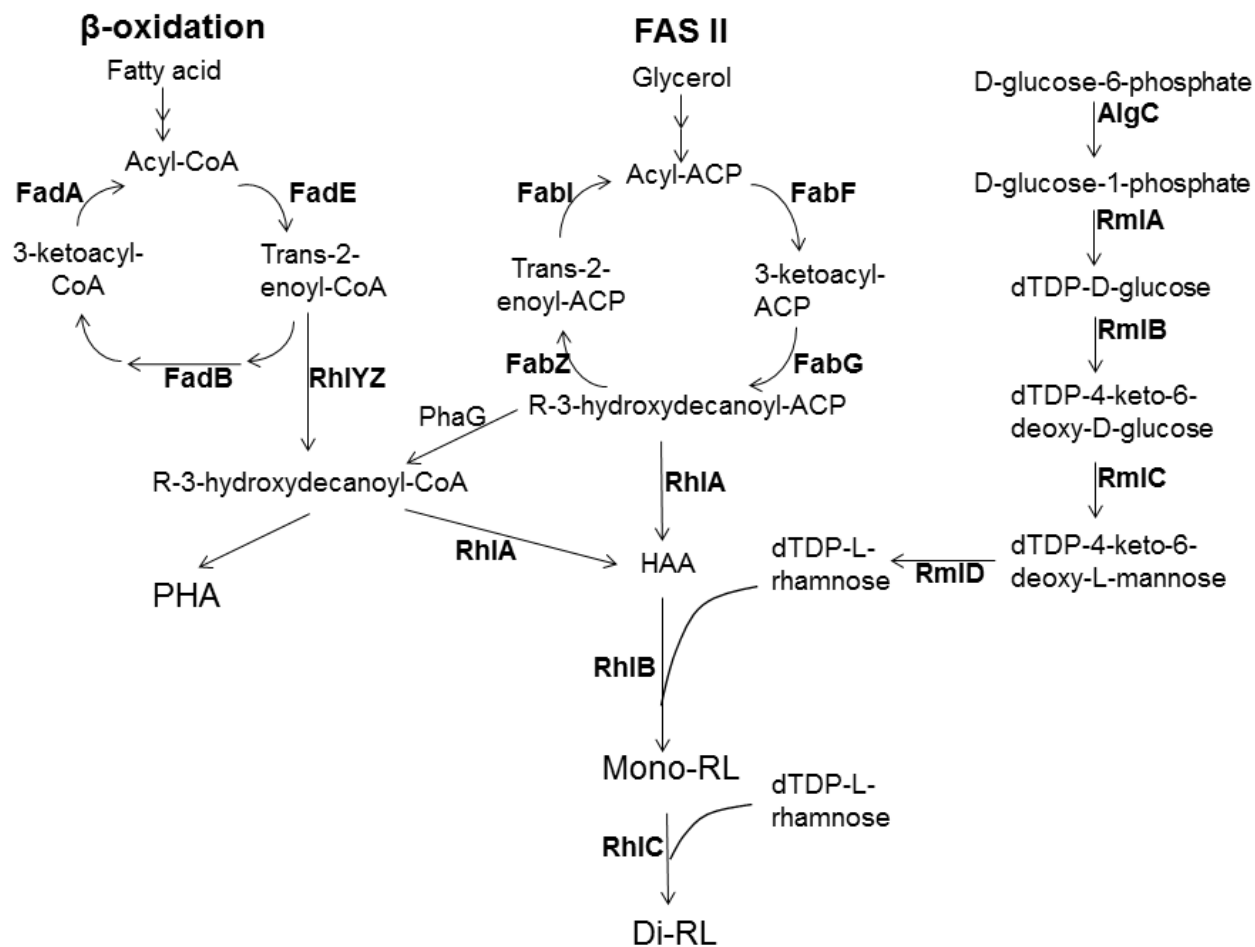


Figure 4. Biosynthesis of polyhydroxyalkanoates (PHA) and rhamnolipids (RLs) in *Pseudomonas*. Figure was adapted and modified from (64, 73, 88) Glycerol directly supplies into *De novo* synthesis of fatty acid pathway (FAS II). Mono-RL: Monorhamnolipid. Di-RL: Dirhamnolipid. ACP: acyl carrier protein.

Is C3 producing RLs and do these enhance DBT degradation? If RL have an effect on DBT biodegradation, the use of 2-bromoalkanoic acid should inhibit degradation of DBT and RLs. The aims below were designed to answer these two interrogations.

6.6. HYPOTHESIS 3: AIMS

6.6.1. Aim 1: Identify *rhlABC* genes in which their genetic products catalyze the main steps on RL biosynthesis

6.6.2. Aim 2: Quantify the effects of RL standard on DBT degradation and C3 growth

6.6.3. Aim 3: Determine the tensioactive properties of the DBT biodegradation cultures

6.6.4. Aim 4: Determine the effects of HEX and OC, β -oxidation and FAS II pathways inhibitors on DBT biodegradation induced by different glycerol concentration and RL synthesis

6.6.5. Aim 5: Analyze proteins involved in RL synthesis from C3 cultured with treatments: A 0.5 mM DBT; B, 50 mM glycerol; C, 0.5 mM DBT with 50 mM glycerol; and D, 0.5 mM DBT with 50 mM glycerol and 2 mM OC.

6.6.6. Aim 6: Characterize RL congeners via HPLC separation and MALDI-TOF/TOF identification

7. CHAPTER 3: METHODOLOGY

7.1. CULTURING OF *BURKHOLDERIA* SP. C3

C3 growth from glycerol stock at -80°C. C3 was plated from a 20% (v/v) glycerol stock at -80°C and incubated at 30°C for two days in LB agar. No more than 3 consecutive plate transfers were done as less consistent results might be obtained which would be attributed to C3 cell mutations. After a third transfer, C3 cells were newly plated from a 20% (v/v) glycerol stock stored at -80°C.

C3 preparation for DBT biodegradation cultures. C3 cells from LB plates were grown overnight in LB rich medium at 30°C and washed three times with minimal medium (MM) (89) by centrifugation at 5850 g for 7 min. C3 cells were then adjusted to an OD₆₀₀ of 0.5 in MM, of which 0.5 mL were inoculated to each of the tubes at a concentration of approximately 0.05 OD₆₀₀. The cultures inoculated at 0.20 OD₆₀₀ were prepared in the same manner. In C3 growth curves, cultures with glycerol, but without DBT were also prepared.

7.2. PREPARATION OF DBT BIODEGRADATION CULTURES

DBT biodegradation cultures preparation. Test tubes were baked at 450°C for a minimum of 3 h. A stock solution of 5 mg/mL (5000 parts per million; ppm) of DBT dissolved in acetone was prepared. In each test tube, 100 µL of DBT stock solution was added, followed by complete evaporation of acetone under N₂ gas. Five mL of MM and an appropriate volume of 50% (v/v) aqueous glycerol solution were then added. The final concentration of DBT was 0.5

mM (100 ppm), while the final concentration of glycerol was as follows: 0, 0.05, 0.5, 5, 50, 200 or 500 mM. In the RL biosynthesis inhibition experiments, the final concentration of HEX and OC was 2 or 5 mM. The appropriate volume to add was calculated using density of HEX and OC. In the RL fortification experiments, the final RL concentration was 20 µg/mL resuspended in water. Cultures were incubated in a rotary shaker at 30°C at 200 rpm. Autoclaved C3 cells were used as controls. All experiments were done in at least three biological replicates.

7.3. EXTRACTION AND ANALYSIS OF DBT

DBT extraction. DBT was extracted from biodegradation cultures incubated for 0, 1, 4, 7 and 10 days and analyzed according to Akhtar et al., (90). After the culture was acidified to pH 2-3 with HCl, DBT was extracted with ethyl acetate by vortex 3 times for 2 min. Between vortex intervals, tubes were open for at least 1 min to prevent bubble formation. Long glass blue capped tubes were used to ensure an increased mixing area. The upper layer (organic phase) was collected and filtered with a 0.2 µm (pore size) polyvinylidene fluoride (PVDF) membrane. PVDF membranes were used to filter organic solvents.

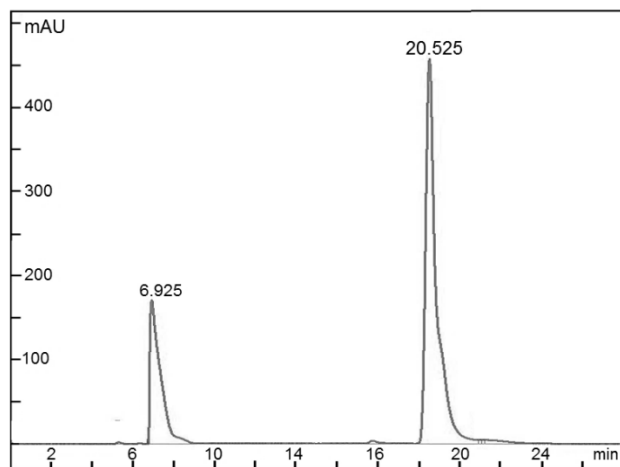


Figure 5. HPLC chromatogram of DBT standard. Standard concentration used was 100 ppm. Ethyl acetate (solvent peak) and DBT retention times were 6.925 and 20.525 minutes, respectively. AU: arbitrary units. All experiments were done at least in triplicates.

DBT analysis with HPLC. DBT was analyzed on an Agilent 1100 series high performance liquid chromatograph (HPLC) equipped with an Aqua C18 column (150 x 4.60 mm, 5 μ m) (Phenomenex, Inc.) and detected at 245 nm. Mobile phase was 60% aqueous ACN and the flow rate was 1 mL/min. An injection volume of 10 μ L was used for standards and experimental samples. The total chromatographic run was 25 min. Experimental samples were quantified with a DBT standard curve ranging from 5-100 ppm. Standard was resuspended in ethyl acetate. Retention time (RT) of ethyl acetate was 6.9 min, whereas, RT of DBT was 20.5 min as shown in Figure 5.

7.4. PROTEIN EXTRACTION AND PREPARATION

Protein extraction. C3 cells were collected from biodegradation cultures at day 2, washed 3 times with mQ water and the proteome was extracted according to a previously reported method (91) with few modifications. A lysis buffer was prepared by mixing 9 mL of a 9 M urea solution with 1 mL of 10x protease inhibitor solution. Protease inhibitor solution was prepared from Sigmafast™ protease inhibitor tablet (Sigma-Aldrich, Milwaukee, WI). After complete removal of medium by centrifugation at 5850 g, cell pellets were resuspended in 700 µL of lysis buffer followed by immediate vortex to ensure a complete and uniform sample. Otherwise, cells would clump together making a less effective cell membrane disruption. This cell suspension was added to a 300 µL of lysis buffer solution in a screw cap vial that was 2/3 prefilled with 0.5 mm (diameter) glass beads (BioSpec Products, Bartlesville, OK). Cell membranes were disrupted by 6 cycles of bead-beating at a maximum speed for 60 s on a mini-beadbeater (BioSpec Products) and on ice for 60 s. Cell debris was removed by centrifugation at 20,817 g for 15 min.

Protein quantification and visualization. A supernatant was collected and protein concentration was measured with Bradford protein assay (Bio-Rad, Hercules, CA). If protein concentration was below 1.2 mg/mL, protein extracts were run through an Amicon Ultra-0.5 mL centrifugal filter (3K cut-off; Millipore, Bay city, MI) to concentrate proteins on the filter. The filter was then washed with 500 µL of mQ water. An amount of 36 µg of protein was loaded on a

12% SDS-PAGE run at 100 V constant for 1 hour and 30 min. Protein bands were visualized with Coomassie blue.

Protein sample preparation for LC-MS. From each gel lane, 12 to 14 gel fractions (1 mm³) were obtained and washed with 25 mM ammonium bicarbonate (NH₄HCO₃)/50% ACN until gel pieces became clear. The protein disulfide bonds were reduced with dithiothreitol (DTT) incubated at 56°C for 30 min. The exposed cysteine residues were alkylated with iodoacetamide (IAA) at room temperature for 20 min. Gel pieces were dehydrated with 100% ACN prior to the DTT reduction and IAA alkylation steps to ensure a full absorption of the solutions. Washing with 100 mM NH₄HCO₃ and dehydration with 100% ACN was followed prior in-gel protein digestion with Trypsin/Lys-C Mix, Mass Spec Grade (Promega, Fitchburg, WI) at 37°C for 16-18 hrs. Protein digests were desalted and concentrated with Pierce[®] C18 tips (Thermo Scientific, Rockford, IL) and then analyzed on a Bruker nanoLC-amaZon speed ion trap mass spectrometer system (Bruker Daltonics, Billerica, MA). The peptides were separated on a C18 analytical column (0.1×150 mm, 3 μ, 200 Å, Bruker) with gradient elution from 5%-65% ACN in 0.1% formic acid for 80 min after 2-min running delay. After 90 min elution, the mobile phase was changed to 95% ACN in 0.1% formic acid and remained for 10 min, followed by column equilibration with 5% ACN in 0.1% formic acid for 20 min for the next run. The flow rate was 800 nL/min. The peptides were detected using a capillary voltage of 1600 and the temperature of the heated capillary was 149.5°C. A survey scan from *m/z* 400-3000 was followed by data-dependent MS/MS of the 10 most abundant ions and 0.5 Da instrument error. Dynamic

exclusion was set to repeat the same precursor ion twice and followed by excluding it for 0.8 min.

7.5. PROTEIN IDENTIFICATION AND ANALYSIS

Raw file conversion software. Raw files (file type = BAF) were converted to mascot generic format (.mgf) and .xml with DataAnalysis software (Bruker Daltonics). Other software such as ProteoWizard (92, 93), software package available for download at <http://proteowizard.sourceforge.net/> can be used for free access. If so, 32-bit version must be used because the 64-bit version is not currently compatible with the 64-bit Bruker peak picker. A filter for peak picking of all MS levels using the vendor peak picker option should be applied.

Raw file conversion with DataAnalysis software. Mass spectrometry (MS) and tandem MS (MS/MS) compounds are found on the basis that the MS/MS spectra of a specific compound contains an identical parent ion within a narrow mass to charge ratio (m/z) and time range. When compounds contained more than one MS/MS spectrum, DataAnalysis software selects the best MS spectrum (higher intensity and best resolution) as precursor MS spectrum. Apex was used as the peak picking algorithm and absolute intensity threshold was set to 100. Parameters for MS and MS/MS compound find were selected based on the capabilities of the instrument utilized. These parameters were: Intensity threshold = 100,000, RT window = 0 and option = fragments qualified by amino acids was checked. Even though a peptide molecular mass ($M+H^+$) is automatically generated in DataAnalysis, MS and MS/MS spectra were deconvoluted via

resolved-isotope deconvolution method prior to compound identification. For this, the minimum percentage abundance of a signal relative to the largest one in the spectrum was set to 5 for MS and MS/MS and the maximum charge was set to auto. Finally, the compounds were exported to .xml and .mgf file formats checking the global charge limitation option and setting the intensity threshold for non-deconvoluted ions to 50 and export N most abundant non-deconvoluted ions to 500. The same parameters were used for each .raw file generated.

Protein database and database search. Database containing canonical and isoform 2,628,482 protein sequences from *Burkholderiales* (Uniprot taxonomy: 80840) was downloaded in FASTA format from the UniProt Knowledgebase on April 4, 2016. Additional databases were constructed based on metabolic pathway and/or organism of interest. For xenobiotic degradation: canonical and isoform 35 protein sequences from “*Burkholderia* sp C3” and “*Burkholderia* sp DBT1” (searched terms) was downloaded in FASTA format from the UniProt Knowledgebase on October 26, 2016. For lipid metabolism and RL synthesis: canonical and isoform 492 protein sequences from “*Burkholderia*” (Uniprot taxonomy: 32008, fixed searched term) and the different protein names (variable term) was downloaded in FASTA format from the UniProt Knowledgebase on April 4, 2016. For PHA synthase: canonical and isoform 23 protein sequences from PHA synthase and *Burkholderiales* (fixed searched terms) was downloaded in FASTA format from the UniProt Knowledgebase on October 25, 2016.

The database search was conducted with Myrimatch search engine (94) and the configuration used was as follows: Instrument type = Ion Trap, Precursor Mass = auto, Enzyme

= Trypsin/P, Average precursor tolerance 1.5 m/z , Fragment tolerance = 0.5 m/z and Mono precursor tolerance = 10 ppm. Modifications = carbamidomethyl (fixed) and Methionine oxidation (variable).

Data normalization. Spectral counts of proteins identified in each treatment were obtained with IdPicker software. Treatments were: A, 0.5 mM DBT; B, 50 mM glycerol; C, 50 mM glycerol and 0.5 mM DBT; D, 50 mM glycerol, 0.5 mM DBT and 2 mM OC. Filters to match peptide to MS/MS spectra were: Maximum false discovery rate (FDR) of 1% and 1 minimum spectrum per peptide (PSM) and per match. In order to match peptides to proteins, a minimum of 2 distinct peptides and spectra and 2 minimum additional peptide were allowed (95, 96). Data were normalized according to (97) assumption that MS/MS intensities are equal to 1 and without considering the peptide length. A $\text{Log}_{10}(\text{normalized count} + 1)$ was applied and the normalized data was compared to the raw data (Figure 6). An analysis of variance (ANOVA, p-value <0.05) was done to search for statistically significant protein abundance changes with DEseq (98). In order to create a matrix for the statistical design, a principal component analysis was done. This analysis showed that glycerol and the interaction of glycerol*DBT are the principal factors having an effect on the data clustering, thus DBT was excluded as a factor in the design. To define the value of the glycerol*DBT interaction term, the DBT degradation rate values were used. The rate to which the inhibitor decreased DBT biodegradation (treatment D) relative to treatment C was calculated and inputted in the matrix. The Matrix design was as follows:

Treatment	Glycerol term	Glycerol*DBT interaction term
A	0	0
B	1	0
C	1	0.7
D	0	0.7

The logFC term was calculated and is shown in Table 6, Table 8, Table 11 and Table 13. This value represents the effect size of the glycerol*DBT interaction term. When the LogFC is upregulated, indicates that the glycerol*DBT interaction had a positive effect on the protein abundance of treatments that contained this interaction (Treatments C and D). It has the opposite effect if the LogFC is downregulated. A p-value was also shown for each protein of these tables. Graphs were done with InfernoRDN (Previously DANTE) -omics software (98). Proteins that were detected in the 3 biological replicates were considered for the analysis.

Pathway and GO search. Excel files were re-formatted (e.g. column 1 = gene name), converted to a tab delimited file and uploaded to MetaCyc database (Private account) to search for biological relevance of the significant proteins detected (Table 13). A smart table was created (November 17, 2016) and the molecular function, biological process (Gene Ontology terms, GO) and pathway involved of each protein was searched.

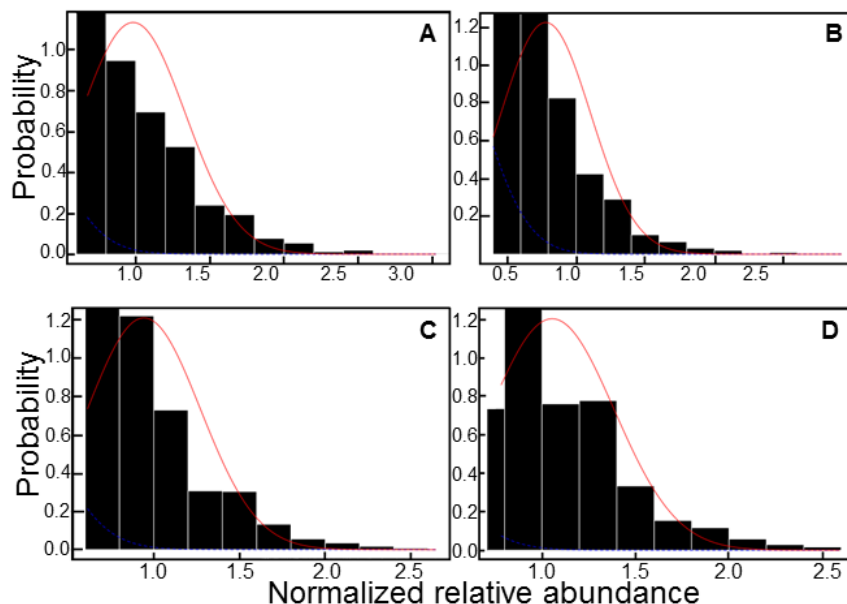


Figure 6. Data normalization. Treatments were: A, 0.5 mM DBT; B, 50 mM glycerol; C, 50 mM glycerol and 0.5 mM DBT; D, 50 mM glycerol, 0.5 mM DBT and 2 mM OC. Biological replicates were 1, 2 and 3. Data followed a more normal trend after normalization.

7.6. EXTRACTION, RESTRICTION DIGESTION AND LIGATION OF C3 GENOMIC DNA

Genomic DNA (gDNA) of C3 was extracted with an ultraclean microbial DNA isolation kit from MO BIO laboratories according to the manufacturer's instruction. Two micrograms of gDNA were digested using 20 units of HindIII and 20 units of NdeI. Digestions were incubated at 37°C for 3 h. Restriction enzyme was heat inactivated at 65°C for 20 min. Proper digestion for inverse PCR (iPCR) with fragments above 1 Kb was checked on a 1% agarose gel. One microgram of digested DNA was self-ligated with 9 units of ligase. Ligations were incubated at 15°C overnight in a thermocycler. Self-ligated gDNA was precipitated and washed with ethanol and resuspended in DNase free water.

7.7. IDENTIFICATION OF *RHLABC* GENES

Primer design. Degenerative primers were designed based on conserved regions of 13 *rhlB* and 55 *rhlC* gene sequences from *Burkholderia* species collected from the NCBI database and using Geneious Pro 5.6.7 (Biomatters limited, Auckland, New Zealand) multiple sequence alignment default options. Inverse PCR was done using a high fidelity polymerase (Finnzymes, Thermo Scientific), degenerate primers for *rhlB* and self-ligated genomic DNA as template. PCR products were sequenced in duplicate and primers were designed based on the newly sequenced PCR product until a complete self-ligated plasmid was assembled.

Table 4. Inverse PCR primer information. T_a: annealing temperature. bp: base pair. Y: cytosine or thymine. K: guanine or thymine. R: adenine or guanosine. B: cytosine, guanine or thymine.

Primer name	Primer sequence (5' → 3' direction)	T _a (°C)
rhlB_F	F GCTACGTGTCGGTGCAGGTGTC	40
rhlB_R	R CGTCGTTGAACAGCGCAAACCC	
rhlseq_F1	F TGCTGTGTCTGTTTCCGGACTG	60
rhlseq_R1	R GCCACGCGGAATCGTCAGACGC	
rhlseq_F2	F TTCGATAACGCACAGCGCGTCG	60
rhlseq_R2	R CCATTGCGCGCCGATCAGCACG	
rhlseq_F3	F ATCAGTTCGATAACGCACAGCG	60
rhlseq_R3	R GCGATACTGTGAATACGCACGG	
rhlseq_F4	F GAGAGTGTCATTCTGATCAACG	60
rhlseq_R4	R CGAAGTAATCGAAAATCGCTGT	
Plasmid check F1	F GAAGCAGGCTTTGCCGAATTAC	60
Plasmid check R1	R GCGTGGAAAGATAGCGGTAGTT	
Plasmid check F2	F AGTCGGGCTATCGCTGATTTTC	60
Plasmid check R2	R AACATCTGCCTCAATAGCAGCC	
Plasmid check F3	F CTACCGCTATCTTTCCACGCTC	60
Plasmid check R3	R GGCGATGTTTGTGATGTTTGCA	
rhlC_F	F GCGCTGTTCGAYCAGGAYTCG	62
rhlC_R	R GCCGATCCGRTGCKBCAGCA	

DNA sequence assembly and identification. Sequences were assembled using Geneious Pro 5.6.7. Open reading frames (ORFs) were identified using the fgenesB bacterial operon and gene prediction program on March 11, 2016 (<http://www.softberry.com/>). Sequence homology was determined using UniProt Knowledgebase (<http://www.uniprot.org/>) and gene cluster homology was determined using *Burkholderia* Genome database (<http://burkholderia.com/>) and BLASTX algorithm accessed on May 4, 2016. The complete set of primer pairs utilized for identification of *rhlABC* genes is specified in Table 4.

7.8. EXTRACTION AND QUANTIFICATION OF RL

RL extraction. RLs were extracted according to Abdel-Mawgoud et al. (99). Briefly, cells were removed at day 2 by centrifugation at 5850 g for 10 min and filtration with a 0.2 μm pore size. The medium was extracted with ethyl acetate 3 times. The extracts were combined and dried under a gentle stream of N_2 gas, followed by resuspending the residues in 0.5 mL of methanol. The same procedure was applied to a RL standard (50 $\mu\text{g/mL}$) dissolved with 5 or 50 mM glycerol in MM.

RL quantification. RLs were quantified using an orcinol assay (100) [0.19% orcinol (w/v) in 53% sulfuric acid (v/v)]. An aliquot of 250 μL of sample was collected, dried and resuspended in 250 μL of water. To 100 μL of RL extract, or varying concentrations of a RL standard, 900 μL of the orcinol solution was added. Mixtures were incubated for 30 min at 80°C. Absorbance was read at 421 nm. A RL standard curve was prepared in a range of 0 and 500

µg/mL. The remaining 250 µL resuspended in methanol was used for HPLC fractionation and RL identification via matrix assisted laser desorption ionization (MALDI)–time of flight (TOF).

7.9. CHARACTERIZATION OF RL CONGENERS VIA MATRIX ASSISTED LASER DESORPTION IONIZATION-TIME OF FLIGHT/TIME OF FLIGHT (MALDI-TOF/TOF)

RL fractionation. RLs extracted were fractionated according to (99) on an Agilent 1100 series HPLC equipped with an Aqua C18 column (150 x 4.60 mm, 5 µm particle size; Phenomenex, Inc.) and detected at 241 nm. RLs were eluted within a 10 min 70 to 90% ACN/water gradient. Both solvents (ACN/water) also contained 2 mM ammonium acetate, pH 8.0-8.5. Three RL fractions were collected at 4-5 (F1), 5-6 (F2) and 7-8 (F3) min as shown in Figure 20. These fractions were dried to completion in a speed vacuum at 45°C and resuspended in 10 µL of 10% ACN/water. Samples were desalted with Pierce® C18 tips (Thermo Scientific) with the following modifications: Trifluoroacetic acid was not used as is recommended for peptide desalting. F1 and F2 samples were bound to the C18 tip 10 times, washed 5 times with 5% ACN and eluted with 10 µL of 70% ACN. The same tip can be used for multiple times of the sample cleanup and concentration. Samples were dried to completion at 45°C and resuspended in 2 µL of 50% ACN containing 40 mg/mL of 2,5-dihydroxybenzoic acid (DHB). One µL of matrix was spotted on the target plate, air-dried and then 1 µL of sample/matrix mixture was spotted.

RL identification. RL congeners were identified on a MALDI-TOF/TOF ultraflex III mass spectrometer (Bruker Daltonics) operated in positive, reflectron mode following the procedures from (101) with modifications. Matrix was 40 mg/mL of DHB dissolved in 50% ACN/water. The instrument was calibrated with degree of polymerization (DP) series: maltotriose hydrate (DP3, MW: 504.44 g/mol), maltotetraose (DP4, MW: 666.57 g/mol), maltopentaose (DP5, MW: 828.71 g/mol) and maltohexose (DP6, MW: 990.85 g/mol) (102). Each DP series formed M-Na⁺ and M-K⁺ adduct ions as can be observed in Figure 7. A 500 μM aliquot of each DP series was dissolved in mQ water. Five μL of each DP series was mixed with 20 μL of DHB matrix to a final concentration of 62.5 μM. Two μL of this mixture was spotted on a MALDI target plate and air-dried for 5 min. Spots consisted of DHB matrix crystals at the surroundings and a uniform mixture in the middle. The instrument m/z range used was 300 to 1200 with 50 pulsations per laser shot and 38-50% laser intensity. Ions were suppressed below 300 Da. Malto-oligosaccharides were found beside DHB matrix crystals.

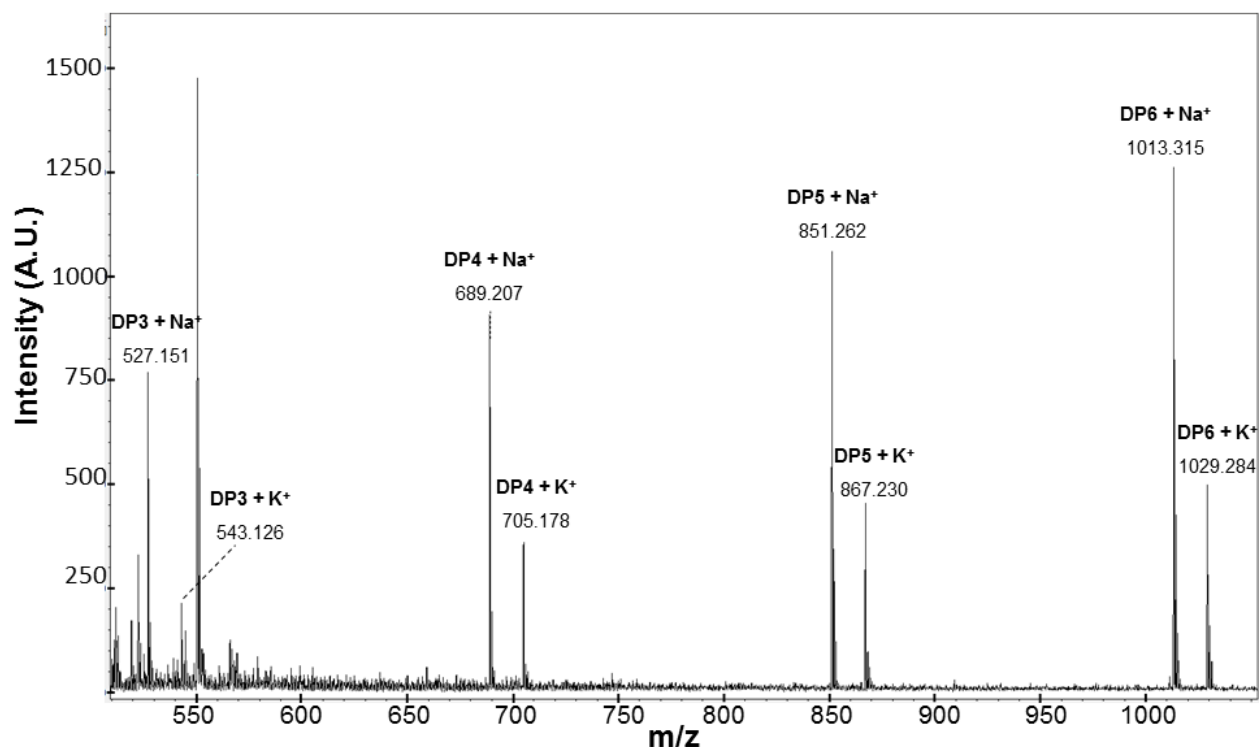


Figure 7. Malto-oligosaccharides spectrum. DP3: Maltotriose hydrate (MW: 504.44 g/mol), DP4: maltotetraose (MW: 666.57 g/mol), maltopentaose (DP5, MW: 828.71 g/mol), maltohexose (DP6, MW: 990.85 g/mol). DP series formed Na⁺, K⁺ and rarely [M-H+ Na₂]⁺ adduct ions. AU: arbitrary units.

A RL standard, containing a mixture of Rha-Rha-C₁₀-C₁₀ and Rha-C₁₀-C₁₀ congeners, was used as control and for training purposes. For MS/MS on RL congeners, MALDI-TOF/TOF ultraflex^{III} mass spectrometer (Bruker Daltonics) operated in lift mode for low molecular mass. Flexi Analysis and Compass Isotope Pattern software (Bruker Daltonics) were used for mass spectral analysis. RL peaks were assigned using an in silico database created according to the RL congeners reported in (37) with an 0.5 Da error mass. Molecular weight and expected adduct ions were calculated with Compass IsotopePattern. Lipids and di-lipids ranging from C₈ to C₁₆ and one and two rhamnose sugars were also included in the database as K⁺ or Na⁺ adduct ions, respectively. RL congeners formed M-Na⁺ and M-K⁺ and rarely [M-H+ Na₂]⁺ adduct ions.

For tandem mass spectrometry of experimental samples an Agilent 1200 LC system coupled to an Agilent 6520A liquid chromatograph-quadrupole time-of-flight mass spectrometer (LC-Q-TOF-MS) system (Agilent Technologies, Mississauga, ON, Canada) was used. A volume of 20 μ L of sample was injected into the LC system. LC separation was carried out on a Luna C18 column (100 mm \times 2.0 mm, 3 μ m particle size) (Phenomenex Com., Torrance, CA, USA). LC mobile phases were (A) 5mM aqueous ammonium formate buffer at pH 3.3; (B) acetonitrile. The mobile phase flow rate was 0.3 mL/min. The gradient for LC system started at 5% B, increasing to 95% B in 15 min, and was held for 15 min. Afterwards, the mobile phase composition was returned to initial conditions and the column was allowed to equilibrate for 10min between runs. The electrospray ionization (ESI) interface was operated in negative mode and the capillary voltage was 4000 V. The fragmentor and skimmer voltages were 180 V and 80 V, respectively. Nitrogen was used as drying and nebulizing gas, and helium was used as the collision gas when the system was operated in MS/MS mode. The gas temperature was 350 $^{\circ}$ C, dry gas flow rate was 10 L/min and nebulizer pressure was 25 psi. Full-scan data acquisition was performed by scanning from m/z 50 to 1700. When operated in the MS/MS mode, the collision energy was 20 eV.

7.10. VISUALIZATION OF POLYHYDROXYALKANOATES LIPID GRANULES

Transmission electron microscopy (TEM). Specimens were fixed with 2.5% glutaraldehyde and 0.1M calcium chloride in 0.1M sodium cacodylate buffer, pH 7.2 for a week, washed in 0.1M cacodylate buffer for 2 x 30 min, followed by postfixation with 1% (v/v) OsO₄

in 0.1M cacodylate buffer for 1 hour. Cells were dehydrated in a graded ethanol series (30%, 50%, 70%, 85%, 95%, 100%), substituted with propylene oxide, and embedded in LX112 epoxy resin. Ultrathin (60-80 nm) sections were obtained on an RMC Powertome ultramicrotome, double stained with uranyl acetate and lead citrate, viewed on a Hitachi HT7700 TEM at 100 kV and photographed with an AMT XR-41B 2k x 2k CCD camera. TEM images were taken at the microscopy facility in the Microbiology department, University of Hawai'i at Mānoa.

7.11. CONSTRAINED DROP SURFACTOMETER ANALYSIS

C3 cells in the culture were removed by centrifugation. The supernatant was dried at 60°C and the residues were resuspended in 0.1 mL of water. RL standard solutions were prepared by dissolving RL in MM. Both RL standard solutions and samples were sonicated for 3 min. An aliquot of 15 μL was placed onto a hydrophilic knife-sharp circular edge pedestal to form a droplet. After 30 s, the volume of the droplet was reduced to approximately 8.00 μL . The surface tension, surface area and droplet volume were calculated according to an axisymmetric drop shape analysis algorithm (103). At the beginning of the experiment, the pedestal was submerged in ethanol and sonicated for 10 min. The pedestal was cleaned with chloroform between measurements, and the instrument was calibrated with pure water to 72.8 mN/m. Experiments were done at Dr. Zuo's laboratory in Engineering department, University of Hawai'i at Mānoa.

7.12. DATA CALCULATION.

DBT degradation curves fitting. Time course points were drawn with standard errors of the mean (SEM) bars representing variation of 3 or 6 biological replicates. Degradation curves were fitted with a first-order kinetic equation, $C = C_0 \times e^{-kt}$, where k is the DBT biodegradation rate constant and C is the concentration measured at time t. DBT half-life ($t_{1/2}$) was calculated with $t_{1/2} = \frac{\ln 2}{k}$. Software OriginPro version 8.5 was used for graphing, fitting data points and calculating the degradation rate constant.

Statistical analysis. Multifactorial ANOVA with unequal sample sizes (n, 15 or 30) was used to calculate statistical significance (p, 0.001) using IBM SPSS Statistics 19 software. P-value was set at 0.001 when the null hypothesis of homogeneity of variances was rejected. Least significant difference (LSD) and Tukey *post-hoc* tests were used for further exploration of the results. DBT degradation was used as the dependent factor. Incubation time, glycerol concentrations, type of inhibitor and concentrations used, RL fortification and initial inoculum were all set as fixed effects. Separate test were run depending upon fixed effects used.

8. CHAPTER 4: RESULTS

8.1 HYPOTHESIS 1: GLYCEROL INDUCES ENHANCED COMETABOLISM OF DBT IN *BURKHOLDERIA* SP. C3

8.1.1 Glycerol concentrations correlated with DBT cometabolism and C3 growth

The effects of glycerol in DBT degradation by C3 were studied with HPLC. Figure 8 shows chromatograms of 50 mM glycerol and 0.5 mM DBT biological triplicates extracted at day 1. The DBT concentration of triplicates was 0.335, 0.358 and 0.349 mM corresponding to retention times 20.492, 20.442 and 20.467, respectively. The retention times of ethyl acetate and DBT matched DBT standard shown in Figure 5.

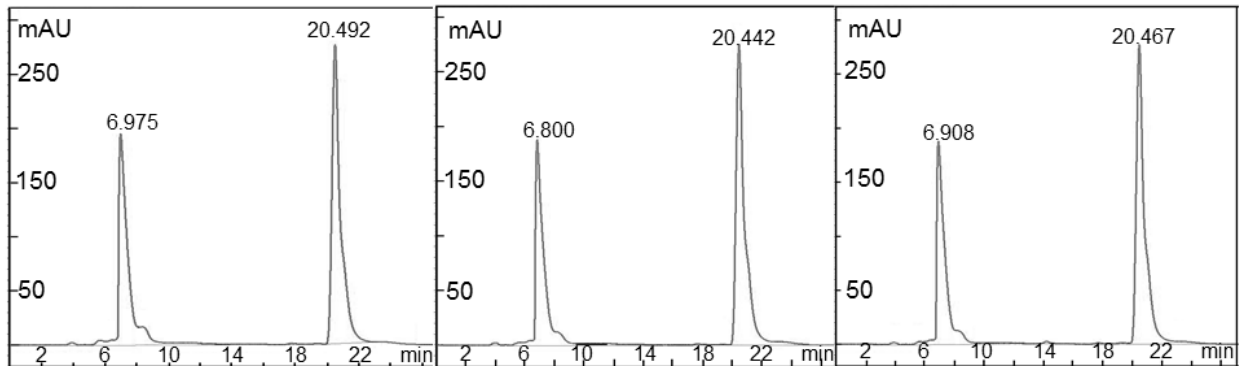


Figure 8. Chromatograms of extracts of triplicate C3 cell cultures supplemented with 50 mM glycerol and 0.5 mM DBT at day 1. First and second peaks correspond to ethyl acetate and DBT, respectively.

DBT degradation rates were quantified using different glycerol concentrations and in the presence of HEX or OC inhibitors. Generally, there was a small variation between biological

replicates as was observed in figures with small SEM values. The SEM using inhibitors was higher than without inhibitors.

Glycerol enhanced DBT biodegradation while supporting bacterial growth, a phenomenon known as cometabolism (Figure 9). DBT as a sole carbon source did not support C3 growth. A 0.05 OD₆₀₀ was observed after a 10-day incubation which was equal to that of the initial inoculum. DBT has no apparent benefit to the metabolizing bacteria.

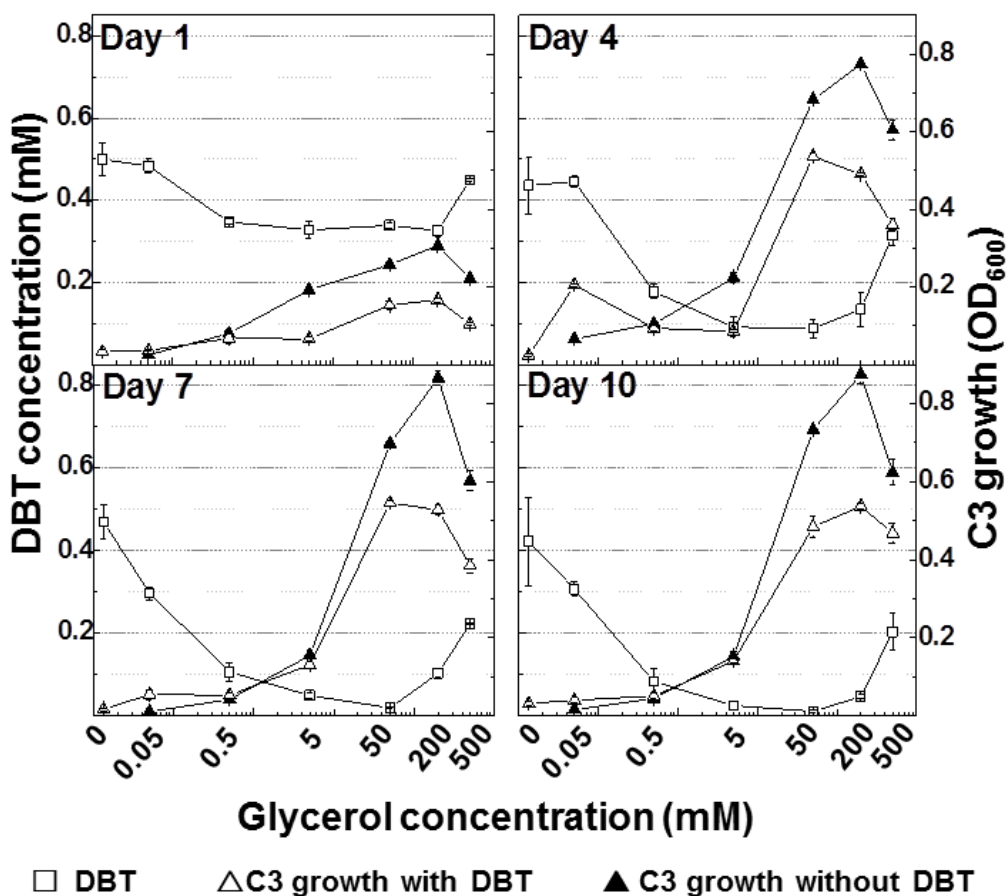


Figure 9. Enhanced DBT biodegradation induced by glycerol vs C3 growth. Concentrations of glycerol at 0.05, 0.5, 5, 50, 200 and 500 mM were used to give a DBT to glycerol molar ratio of 1:0.1, 1:1, 1:10, 1:100, 1:400 and 1:1000. Negligible degradation of DBT was observed in controls with autoclaved C3, but was not shown.

Glycerol-induced DBT cometabolism correlated with C3 growth. Interestingly, C3 growth in DBT-glycerol mixtures was inhibited when compared to glycerol alone. Growth rates varied with the glycerol concentration used and incubation time. For example, mixtures of 0.5 mM DBT with glycerol ranging from 50 to 500 mM exhibited reduced growth as much as 0.3 OD₆₀₀ relative to glycerol alone. DBT did not inhibit growth at lower concentrations of glycerol (0.05-5 mM). An increase in C3 growth using high concentrations of glycerol relative to DBT was observed starting at day 4. It is possible that more DBT may be co-absorbed with glycerol. Therefore, such growth inhibition with 50 to 500 mM glycerol concentrations may be associated to either DBT and DBT metabolites toxicity or both.

Enhanced DBT biodegradation was dependent upon glycerol to DBT ratio and incubation time. Glycerol to DBT molar ratios at 1:1, 10:1, 100:1 and 400:1 (0.5, 5, 50 and 200 mM of glycerol, respectively) enhanced DBT cometabolism by 25-30% after 1 day of incubation. C3 degraded 92% of 0.5 mM DBT at day 10 in cultures containing 0.5 mM glycerol. However, at this glycerol concentration C3 growth remained at 0.05 OD₆₀₀. Evidencing that increased biomass was not the only cause for the enhanced DBT cometabolism. Glycerol (0.05 mM) at a molar ratio of 0.1:1 to DBT did not show enhancement of DBT degradation in C3 at day 1 and 4 of incubation; whereas at day 7 and 10, it enhanced DBT biodegradation by 25-30% relative to no addition of glycerol (Figure 9). In cultures at 100:1 glycerol (50 mM) to DBT molar ratio, C3 degraded 100% of 0.5 mM (100 ppm) DBT after 7 days of incubation. This optimal glycerol concentration was utilized during the remainder of experiments. Dose dependent effects of glycerol on the degradation rate constant and DBT half-life are shown in Table 5. DBT half-life decreased from 27.5 to 1.5 days in cultures containing glycerol. Similarly, up to 18-fold increase

in the DBT degradation rate constant was observed at glycerol to DBT molar ratios of 0.1:1, 1:1, 10: 1, 100:1, 400:1 and 1000:1. Negligible DBT degradation was observed using cultures with autoclaved bacteria as controls.

Table 5. Enhancement of DBT biodegradation rate constant and DBT half-life is dependent on glycerol concentration. Exponential decay equation, $C = C_0 \times e^{-kt}$ was used for fitting “N” data points where k is rate constant and t is time in day. *Relative to rate constant of 0.5 mM DBT.

Substrate	Rate constant (Days ⁻¹)	R ²	Half-life (Days)	N	Fold change*
0.5 mM DBT	0.025±0.01	0.63	27.5	30	0.0
0.05 mM glycerol & 0.5 mM DBT	0.064±0.01	0.84	10.8	15	1.6
0.5 mM glycerol & 0.5 mM DBT	0.359±0.09	0.90	1.9	15	13.2
5 mM glycerol & 0.5 mM DBT	0.390±0.05	0.99	1.8	15	14.5
50 mM glycerol & 0.5 mM DBT	0.479±0.02	0.99	1.5	30	18.0
200 mM glycerol & 0.5 mM DBT	0.229±0.02	0.99	3.0	15	8.1
500 mM glycerol & 0.5 mM DBT	0.113±0.00	1.00	6.1	15	3.5
0.5 mM DBT (autoclaved C3)	0.002±0.01	0.31	287.6	27	-0.9
50 mM glycerol & 0.5 mM DBT (autoclaved C3)	0.009±0.00	0.99	70.44	15	-0.6

8.1.2. Proteins involved in DBT degradation in C3

The proteins involved in DBT degradation identified through LC-MS in C3 are shown in Table 6. Interestingly, the majority of these proteins were also found in C3 containing only 50 mM glycerol. The results indicated that glycerol alone can induce the expression of proteins involved with degradation of DBT and other PAHs.

Table 6. Proteins involved in of degradation of xenobiotics identified in C3. NO: Not observed. Treatments were: A, 0.5 mM DBT; B, 50 mM glycerol; C, 50 mM glycerol and 0.5 mM DBT; D, 50 mM glycerol, 0.5 mM DBT and 2 mM OC. Proteins were extracted at day 2. Three biological replicates were analyzed in each treatment. Mean normalized value is shown in each treatment. The LogFC represents the glycerol*DBT interaction term. *The relative abundance among treatment showed significant differences (p-value<0.05).

UniProt ID	Description	Relative abundance by Treatment				LogFC	P-value
		A	B	C	D		
G5L3J5	Hydratase aldolase (DbtE)*	1.98	1.27	2.33	2.40	1.97	0.000
Q93CN9	Extradiol dioxygenase (DbtC)	1.82	0.96	1.43	1.91	0.32	0.576
Q93CN7	Putative monooxygenase α -subunit	2.02	1.62	2.02	1.87	0.41	0.421
Q93NA7	Dioxygenase β - subunit (DbtAd)*	1.83	NO	1.83	2.30	2.01	0.001
Q93NA6	Dihydrodiol dehydrogenase (DbtB)	1.63	0.88	1.28	1.35	-0.11	0.857
Q93CN6	Putative hydrolase	0.97	1.09	0.93	1.30	-0.02	0.973
Q93NA8	Dioxygenase α - subunit (DbtAc)	1.59	1.00	1.44	1.60	0.12	0.837
C7DQZ5	Dehydrogenase (PhnF)	1.03	1.08	1.23	0.74	-0.47	0.400

Table 6 (continued). Proteins involved in degradation of xenobiotics identified in C3.

NO: Not observed. Treatments were: A, 0.5 mM DBT; B, 50 mM glycerol; C, 50 mM glycerol and 0.5 mM DBT; D, 50 mM glycerol, 0.5 mM DBT and 2 mM OC. Proteins were extracted at day 2. Three biological replicates were analyzed in each treatment. Mean normalized value is shown in each treatment. The LogFC represents the glycerol*DBT interaction term. *The relative abundance among treatment showed significant differences (p-value<0.05).

UniProt ID	Description	Relative abundance by treatment				LogFC	P-value
		A	B	C	D		
C7DQY7	Cis-naphthalene dihydrodiol dehydrogenase (NahB)	1.49	1.64	1.46	1.13	-0.98	0.095
C7DQY6*	PAH dioxygenase small subunit	1.45	1.40	1.12	0.92	-1.28	0.036
C7DQY8	Salicylaldehyde dehydrogenase (NagF)	1.38	1.24	1.82	1.96	-2.41	0.066
C7DQY1	Ferredoxin reductase (NagAa)	1.32	1.36	1.36	1.34	-0.17	0.762
C7DQZ1	Gentisate-1,2-dioxygenase (NagI)	1.40	1.09	1.12	1.20	-0.08	0.903
C7DR01	Dihydrodiol dehydrogenase (PhnB)	1.17	1.06	1.13	0.82	-0.50	0.448
C7DQZ7	Extradiol dioxygenase (PhnC)	1.34	0.95	1.38	1.20	0.34	0.577
C7DQY5	PAH dioxygenase large subunit	1.31	0.76	1.30	1.10	0.41	0.503
C7DQZ3	Salicylate-5-hydroxylase large oxygenase component (NagG)	NO	1.01	1.29	0.69	0.53	0.431
C7DQZ6	Hydratase/aldolase (PhnE)	NO	0.75	1.19	1.30	0.88	0.205
C7DQY9	1,2-Dihydroxynaphthalene dioxygenase (NahC)	1.23	NO	NO	1.24	-0.72	0.328
C7DQZ2	Fumarylacetoacetate hydrolase	0.72	0.79	0.70	0.53	-0.27	0.729
C7DQZ0	Reductase component of salicylate-5-hydroxylase (NdsA)	1.02	0.75	1.05	0.41	-0.09	0.899
C7DQZ7	Extradiol dioxygenase (PhnC)	1.34	0.95	1.38	1.20	0.34	0.577

Table 6 (continued). Proteins involved in degradation of xenobiotics identified in C3.

NO: Not observed. Treatments were: A, 0.5 mM DBT; B, 50 mM glycerol; C, 50 mM glycerol and 0.5 mM DBT; D, 50 mM glycerol, 0.5 mM DBT and 2 mM OC. Proteins were extracted at day 2. Three biological replicates were analyzed in each treatment. Mean normalized value is shown in each treatment. The LogFC represents the glycerol*DBT interaction term. *The relative abundance among treatment showed significant differences (p-value<0.05).

UniProt ID	Description	Relative abundance by treatment				LogFC	P-value
		A	B	C	D		
C7DQY5	PAH dioxygenase large subunit	1.31	0.76	1.30	1.10	0.41	0.503
C7DQZ3	Salicylate-5-hydroxylase large oxygenase component (NagG)	NO	1.01	1.29	0.69	0.53	0.431
C7DQZ6	Hydratase/aldolase (PhnE)	NO	0.75	1.19	1.30	0.88	0.205
C7DQY9	1,2-Dihydroxynaphthalene dioxygenase (NahC)	1.23	NO	NO	1.24	-0.72	0.328
C7DQZ2	Fumarylacetoacetate hydrolase	0.72	0.79	0.70	0.53	-0.27	0.729
C7DQZ0	Reductase component of salicylate-5-hydroxylase (NdsA)	1.02	0.75	1.05	0.41	-0.09	0.899
C7DR00	Dioxygenase β -subunit (PhnAd)	NO	0.60	NO	NO	-1.01	0.289
C7DQZ8	Isomerase (PhnD)	0.23	NO	0.44	0.53	1.04	0.415
R9W162	Aromatic-ring-hydroxylating dioxygenase*	1.73	0.42	1.58	2.17	1.39	0.033
A0A0M4NP56	Naphthalene-1,2-dioxygenase*	1.68	NO	1.66	1.76	1.26	0.044
A0A0D5V FY1	Glycerol-3-phosphate dehydrogenase (GlpD)*	NO	1.07	1.94	NO	1.76	0.003
A0A0D5V9F3	sn-glycerol-3-phosphate import ATP-binding (UgpC)	NO	0.51	0.82	NO	0.32	0.729
A0A0D5V FT7	Glycerol Kinase (GlpK)	NO	1.54	1.46	NO	-0.24	0.648
A0A0D5V C54	Glycerate kinase	NO	0.86	0.46	NO	-1.22	0.201

Proteins expressed by C3 during phenanthrene and naphthalene degradation (35) were also observed when exposed to DBT. The presence of proteins involved in naphthalene degradation suggested that after the first aromatic ring is removed from DBT, degradation subsequently follows naphthalene metabolic pathway. Similarly, identification of phenanthrene (C7DR00) and naphthalene (A0A0M4NP56) dioxygenase subunits suggested broad enzyme specificity towards DBT degradation and this was independent of glycerol supplementation..

Interestingly, a set of proteins specifically involved in DBT degradation was identified for first time in C3 and the putative catalytic steps are shown in Figure 10. These proteins were initially reported on *Burkholderia fungorum* sp. DBT1. In the study, DbtAc and DbtC insertional DBT1 mutants lost their capacity to metabolize DBT (59). The identified enzymes suggest that C3 degrades DBT through lateral dioxygenation pathway.

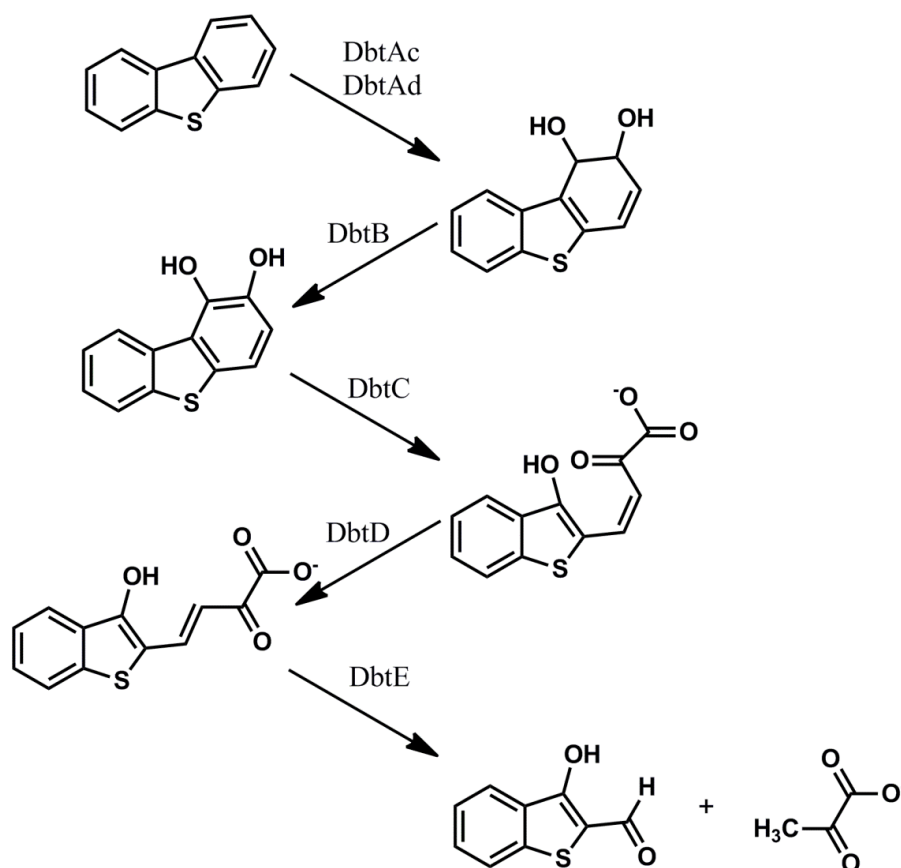


Figure 10. Putative steps catalyzed by DBT degradative enzymes identified in C3. Enzymes: DbtAc, DBT dioxygenase α subunit; DbtAd, DBT dioxygenase β subunit; DbtB, Dihydrodiol dehydrogenase; DbtC, Extradiol dioxygenase; DbtD, isomerase; DbtE: hydratase-aldolase.

Regarding glycerol utilization, at day 2 GlpD (A0A0D5VFY1) is significantly up-regulated (p -value <0.005) in comparison to GlpK (A0A0D5VFT7), which suggests that most of the glycerol has been assimilated as glycerol-3-phosphate. The presence of G3P transporters supports this indication. C3 can also assimilate glycerol as glycerate-3-phosphate by glycerate kinase (A0A0D5VC54). The absence or low abundance of these proteins in treatment D indicated that OC inhibited initial glycerol assimilation in C3.

8.2 HYPOTHESIS 2: GLYCEROL STIMULATES THE SYNTHESIS OF PROTEINS THAT MEDIATE LIPID METABOLIC PATHWAYS

8.2.1. Inhibition of β -oxidation of fatty acids decreased DBT biodegradation and C3 growth

HEX and OC strongly inhibited C3 growth and DBT degradation. At 2 mM, inhibition of DBT degradation was greater with HEX than with OC before 4 days of incubation. Interestingly, unlike C3 growth, the DBT biodegradation ability of C3 was restored at 7-10 days of incubation (Figure 11). At this inhibitor concentration, the rate constant decreased from 0.479 to 0.324 day⁻¹ with HEX and to 0.375 day⁻¹ with OC (Table 7).

At 5 mM, OC had greatly inhibited DBT degradation in comparison to HEX. In terms of cell growth, C3 reached 0.2 OD₆₀₀ at both 2 mM and 5 mM OC concentrations, but 5 mM had a greater negative effect on DBT degradation. In cultures with HEX, C3 reached 0.5 OD₆₀₀ at 5 mM, whereas at 2 mM, C3 only reached 0.2 OD₆₀₀. Opposite results were obtained on DBT degradation; a 5 mM HEX concentration had a greater inhibitory effect than a 2 mM. The observations suggested that glycerol enhanced cometabolism is the results of several metabolic mechanisms and not only those involved with enhanced growth. At 5 mM, rate constants decreased from 0.479 to 0.162 day⁻¹ with HEX and to 0.033 day⁻¹ with OC (Table 7).

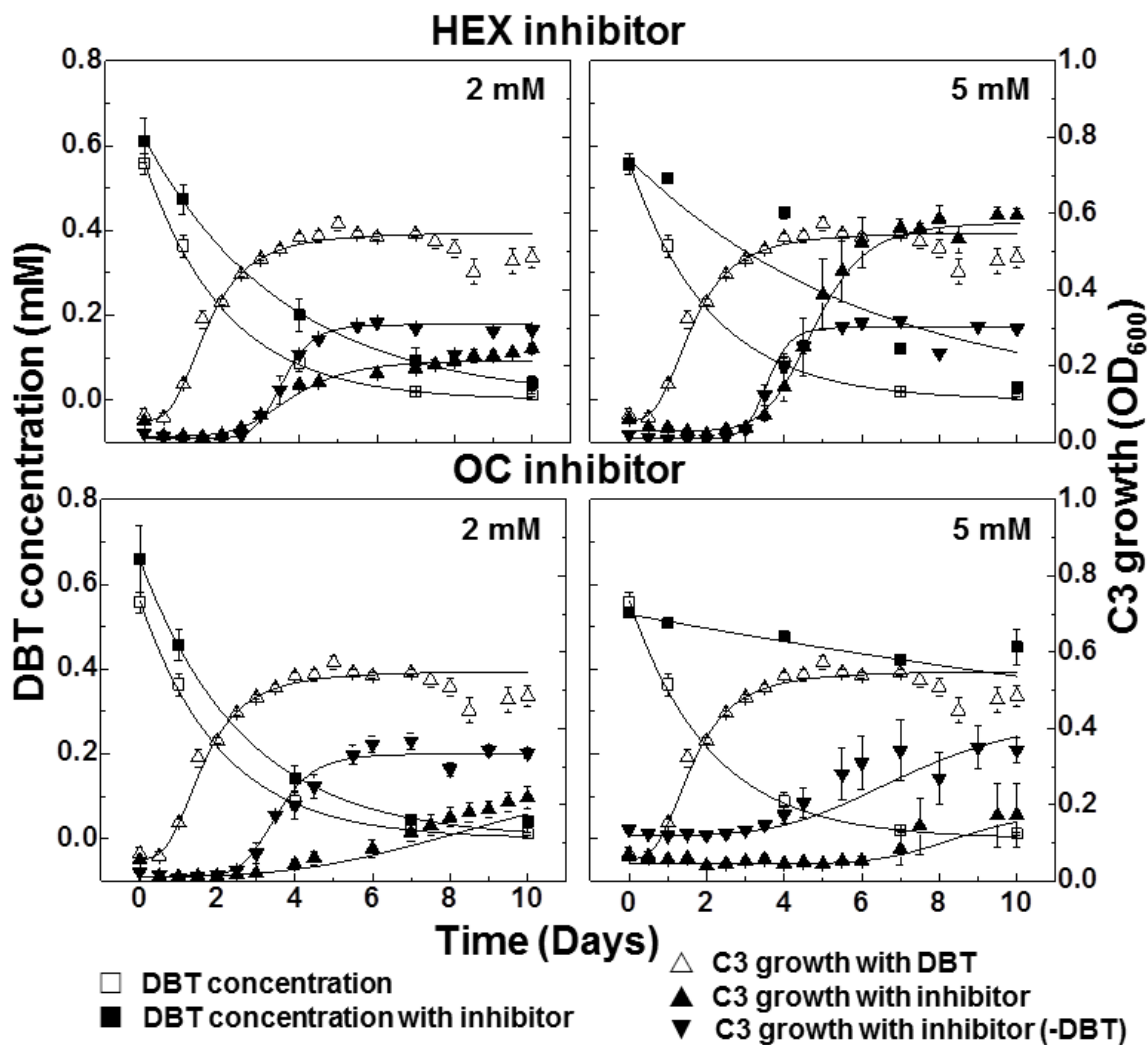


Figure 11. HEX and OC lipid pathways inhibitors decreased DBT biodegradation and C3 growth. All curves were tested with a 50 mM glycerol concentration. The final concentration of 2-bromohexanoic acid (HEX) and 2-bromooctanoic acid (OC) were at 2 mM or 5 mM. An exponential decay equation, $C = C_0 \times e^{-kt}$, was used for fitting data points of degradation curves. Error bars represent variation among 3 or 6 samples. Inhibitors concentration significantly affected DBT degradation (p-value<0.001).

HEX and OC inhibited bacterial growth in cultures supplemented with glycerol alone. C3 reached 0.3 OD₆₀₀ when cultured with 50 mM glycerol and 2 mM or 5 mM HEX. In cultures with 50 mM glycerol and 2 mM or 5 mM OC, C3 reached 0.35 OD₆₀₀ at 4 days. HEX had

slightly greater effects on bacterial growth than OC. Thus, OC was used for proteome profiling experiments. Additionally at 2 mM, HEX and OC had similar effects on bacterial growth in cultures containing DBT in addition to glycerol. For both inhibitors, C3 reached 0.2 OD₆₀₀ at the end of the incubation period. Thus, this concentration was used during the remainder of the experiments.

Table 7. Influence of bromoalkanoic acid inhibitors in DBT biodegradation rate constant and DBT half-life. Exponential decay equation, $C = C_0 \times e^{-kt}$ was used for fitting “N” data points where k is rate constant and t is time in day. *Relative to rate constant of 0.5 mM DBT.

Treatment	Rate constant (Day ⁻¹)	R ²	Half-life (Day)	N	Fold change*
0.5 mM DBT	0.025±0.01	0.63	27.5	30	0.0
50 mM glycerol & 0.5 mM DBT	0.479±0.02	0.99	1.6	30	18.0
2 mM HEX & 50 mM glycerol & 0.5 mM DBT	0.324±0.00	1.00	2.14	15	11.8
2 mM OC & 50 mM glycerol & 0.5 mM DBT	0.374±0.03	0.97	1.9	30	13.8
5 mM HEX & 50 mM glycerol & 0.5 mM DBT	0.162±0.05	0.88	4.28	15	5.4
5 mM OC & 50 mM glycerol & 0.5 mM DBT	0.032±0.00	0.98	21.45	15	0.3

DBT biodegradation kinetics experiments showed that the inhibitory effects were dependent upon the concentration used and the inhibitor (Figure 11). This was investigated with a multifactorial ANOVA followed by post-hoc tests. Type of inhibitor (OC, HEX or without; 3 levels), concentration (0, 2 or 5 mM; 3 levels) and incubation time (5 levels) were used as fixed

factors. Inhibitor suppressed DBT biodegradation by 15%. Chain-length specificity of inhibitor was not a significant factor. The concentration used (either 2 or 5 mM) had a 42% significant effect on DBT degradation (multifactorial ANOVA p-value <0.001). Regarding incubation time, pairwise comparison showed that incubating for 7 days or 10 days did not make a significant difference (p-value =0.831). All other pairwise comparisons were significant (p-value <0.001).

8.2.2. Up-regulated proteome: DBT metabolism versus glycerol induced DBT cometabolism

In order to determine additional mechanisms induced by glycerol, the C3 proteome was profiled under 4 different treatments. The treatments were: A, 0.5 mM DBT; B, 50 mM glycerol; C, 50 mM glycerol and 0.5 mM DBT; D, 50 mM glycerol, 0.5 mM DBT and 2 mM OC.

Proteomes correlation plot (

Figure 12) showed that the relative abundance of proteins detected in C3 grown using DBT (treatment A) were more correlated with proteins detected in C3 grown with glycerol/DBT treated with OC (treatment D). Similarly, the relative abundance of proteins identified in C3 grown using glycerol (treatment B) correlated better with proteins from glycerol with DBT (treatment C) than any other treatment. There was also correlation between treatments C and D. Small variation between biological replicates was also observed.

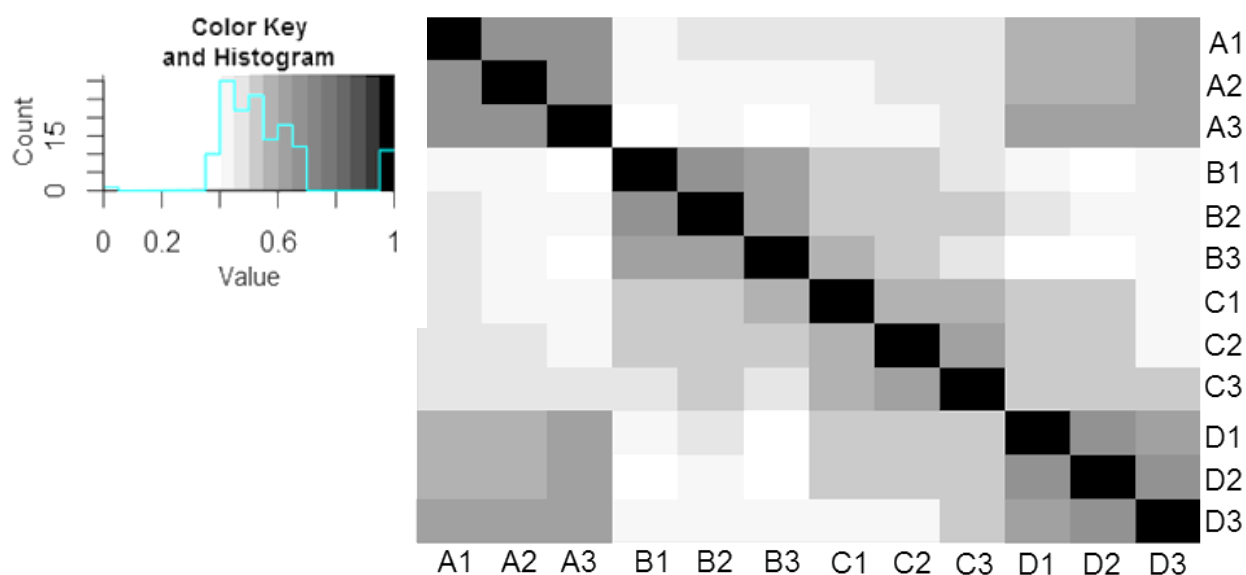


Figure 12. Correlation plot of the relative abundance of proteins extracted from C3 grown under different treatments. A total of 1935 proteins were used for plotting. Proteins were extracted at day 2. Treatments were: A, 0.5 mM DBT; B, 50 mM glycerol; C, 50 mM glycerol and 0.5 mM DBT; D, 50 mM glycerol, 0.5 mM DBT and 2 mM OC. Biological replicates are 1, 2 and 3.

The same correlation between treatments was observed in proteins with significant changes in relative abundance (P -value <0.05 , Figure 13). The changes in relative abundance of proteins extracted from cells treated with OC inhibitor (treatment D) had higher similarity to proteins extracted from cells grown with DBT (treatment A). The analysis shown in Table 6 supported these findings. OC inhibitor is suppressing glycerol assimilation at the proteomic level, and thus this correlation.

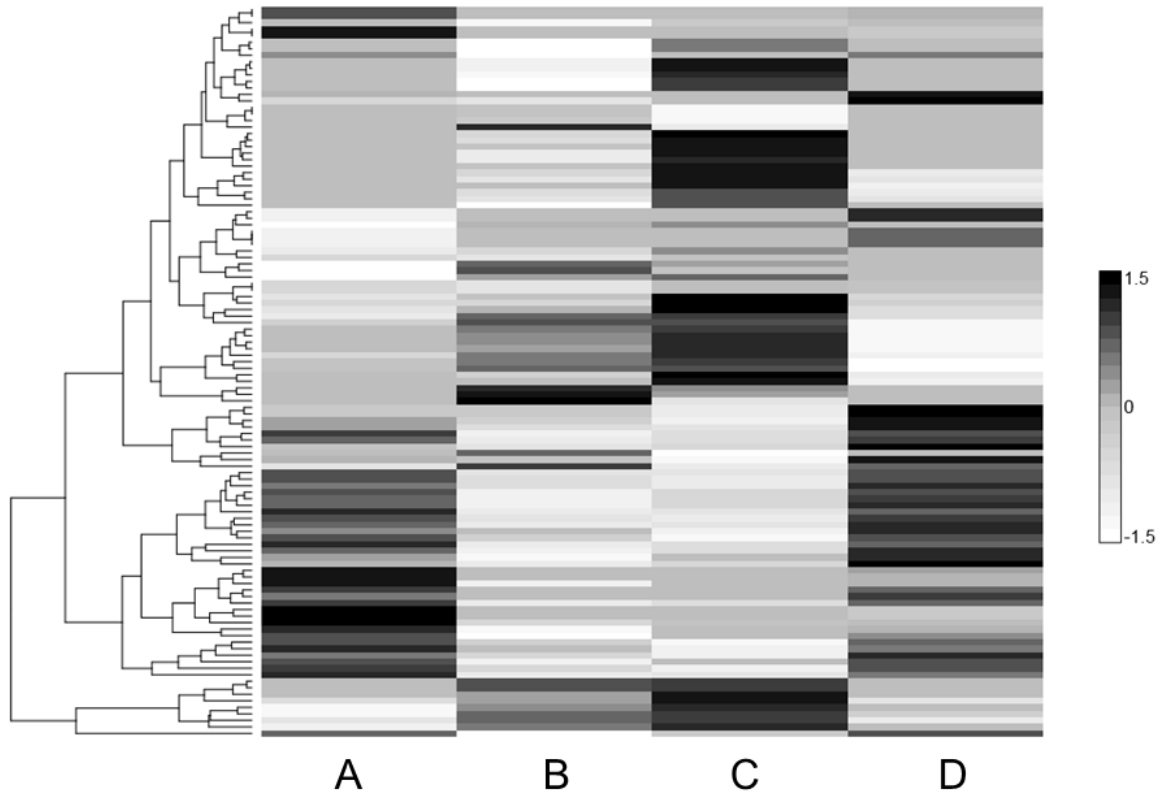


Figure 13. Heat map of significant changes in the relative protein abundance in correspondence with treatments. Plot shows the relative abundance of 122 proteins (p -value < 0.05). Proteins were extracted at day 2. Treatments were: A, 0.5 mM DBT; B, 50 mM glycerol; C, 50 mM glycerol and 0.5 mM DBT; D, 50 mM glycerol, 0.5 mM DBT and 2 mM OC. Mean values of normalized values were used.

Many of the proteins depicted in Figure 13 were related to protein translation and proper folding cell processes. For example, 3 50S (B1JU41, B5WTF5 and A0A0D5V6G6) ribosomal subunits, RNA polymerase sigma factor RpoD (A0A0D5VLP3) and RNA polymerase-binding transcription factor DksA (A0A0D5VEZ5) were detected and showed significant upregulated LogFC. Protein synthesis and correct folding are cellular mechanisms in response to a chemical stress (104).

Similarly, chaperones DnaK (A0A0D5VFX6) and HtpG (A0A0D5V7V8) and elongation factor G (A0A0D5VCE6) were detected and the LogFC was down-regulated, denoting these proteins were not important for cellular processes when the cells were exposed to DBT and Glycerol. However, down-regulation of the LogFC value does imply the presence of these proteins in cells exposed to DBT alone or glycerol alone and hence the importance of comparing the different treatments. Arginine-tRNA ligase (A0A0D5VB61), Aspartate-tRNA ligase (A0A0D5VFE6), Glycine-tRNA ligase beta subunit (A0A0D5VAC2), Isoleucine-tRNA ligase (A0A0D5VEQ0) and Threonine-tRNA ligase (A0A0D5V9J4), also were significantly down regulated. These proteins involved in protein biosynthesis were abundant in cells exposed to glycerol. Figure 9 evidenced that C3 is more metabolically active and reached a higher OD₆₀₀ with glycerol alone, which would explained the higher abundance of these proteins in treatment B.

Tautomerase (A0A0M3TVK8) a protein involved in cellular metabolism of aromatic compounds (GO:0006725) was significantly up-regulated. In *Pseudomonas stutzeri*, this protein is part of the salicylate metabolic pathway. Additionally, FMN-dependent NADH-azoreductase (A0A0D5V7V5) involved in reductive cleavage of aromatic azo compounds was also significantly up-regulated. Along with a putative monooxygenase alpha subunit (Q93CN7), naphthalene 1,2-dioxygenase (A0A0M4NP56) and 2,3-dihydroxy-2,3-dihydrophenylpropionate dehydrogenase (Q93NA6). These results agreed with the ones from Table 6, both suggest that glycerol induces the expression of proteins involved in xenobiotic degradation.

The LogFC of enzymes poly(R)-hydroxyalkanoic acid synthase (A0A0Q5H1G7) and poly(R)-hydroxyalkanoic acid synthase, class I (A9BZX2 and W6X074) were significantly up-

regulated. These enzymes are involved in the production of PHA for granule formation (105). The regulation of these enzymes suggested that lipid metabolism is stimulated by glycerol. Hence, lipid metabolic pathways were investigated more in depth in the next sub-chapter.

Additional proteins with general (e.g. aldolase) and uncharacterized functions (9 proteins) were also significant. The full list of proteins that showed significant changes in relative abundance among treatments is found in the Annexed (Table 13).

8.2.3. Proteins involved in β -oxidation and FAS II pathways from C3 were up-regulated in the presence of glycerol

Glycerol assimilation can affect lipid metabolic pathways. The proteins found in C3 related to lipid metabolism are shown in **Table 8**. Proteins involved in FAS II and β -oxidation pathways were identified in all treatments (A, B, C and D). FabG is a key enzyme in R-3-hydroxydecanoyl-ACP synthesis via FAS II pathway (73). The relative abundance of FabG was >1 in all treatments. The preceding step catalyzed by FabF was up-regulated with glycerol, however, these up-regulation was not statistically significant. FadE from β -oxidation was up-regulated and the p-value was 0.089. The evidence suggests that both FAS II and β -oxidation pathways were active in C3.

Table 8. Proteins involved in lipid metabolic pathways and PHA formation. ACP: acyl carrier protein. NO: Not observed. Treatments were: A, 0.5 mM DBT; B, 50 mM glycerol; C, 50 mM glycerol and 0.5 mM DBT; D, 50 mM glycerol, 0.5 mM DBT and 2 mM OC. Proteins were extracted at day 2. Three biological replicates were analyzed in each treatment. Mean normalized value is shown in each treatment. The LogFC represents the glycerol*DBT interaction term. *The relative abundance among treatment showed significant differences (p-value<0.05).

UniProt ID	Protein description	Relative abundance by treatment				LogFC	P-value
		A	B	C	D		
Q63S87	β -oxoacyl-ACP synthesis (FabF)	NO	0.62	1.38	NO	0.78	0.235
A0A0D5VAR9	3-oxoacyl-ACP-reductase (FabG)	1.32	1.06	1.36	1.45	-0.58	0.328
A0A0D5VAC6	3-hydroxy -ACP-dehydratase (FabZ)	0.98	NO	NO	1.10	1.39	0.140
K8R0G3	Acyl-CoA dehydrogenase (FadE)	NO	NO	0.69	NO	1.99	0.089
Q3JVY2	Enoyl-CoA hydratase/3-hydroxyacyl-CoA dehydrogenase (FadB)	NO	1.15	1.14	NO	-0.20	0.768
A0A0Q5H1G7	Poly(R)-hydroxyalkanoic acid synthase*	0.23	0.00	0.83	0.80	2.77	0.011
W6X074	Poly(R)-hydroxyalkanoic acid synthase, class I*	0.41	0.00	0.54	0.95	2.09	0.043
A9BZX2	Poly(R)-hydroxyalkanoic acid synthase, class I*	0.00	0.13	0.83	0.80	2.51	0.017
D8P4I5	Poly-beta-hydroxybutyrate polymerase	0.23	0.37	0.49	1.05	1.62	0.077
A0A0D5VF95	Cyclopropane-fatty-acyl-phospholipid synthase	NO	0.95	1.52	0.26	0.58	0.338
A0A0N1KL01	Phasin family protein*	2.03	2.13	2.26	1.96	-1.34	0.005

Table 8 (continued). Proteins involved in lipid metabolic pathways and PHA formation. ACP: acyl carrier protein. NO: Not observed. Treatments were: A, 0.5 mM DBT; B, 50 mM glycerol; C, 50 mM glycerol and 0.5 mM DBT; D, 50 mM glycerol, 0.5 mM DBT and 2 mM OC. Proteins were extracted at day 2. Three biological replicates were analyzed in each treatment. Mean normalized value is shown in each treatment. The LogFC represents the glycerol*DBT interaction term. *The relative abundance among treatment showed significant differences (p-value<0.05).

UniProt ID	Description	Relative abundance by treatment				LogFC	P-value
		A	B	C	D		
A0A0D5VHK5	Phasin family domain protein	NO	1.57	1.78	0.80	0.46	0.443
I7A5Y0	PHA synthesis regulatory protein (PhaR)	0.94	0.42	0.46	0.26	-1.01	0.281
A0A0D5VCV0	Phosphatidylethanolamine-binding family protein*	0.23	0.66	0.96	1.24	2.01	0.030

The relative abundance of phasin and Poly(R)-hydroxyalkanoic acid synthase proteins (**Table 8**) suggested that C3 may be forming PHA granules in cultures with glycerol. PHA granule formation is widely suggested for lipid storage when a high concentration of carbon source is provided (73). Interestingly, phasin A0A0N1KL01 was also found in cells grown with DBT alone, which suggested that PHA lipid synthesis and possible granule formation may be an additional mechanism in enhanced DBT degradation.

Cyclopropane-fatty-acyl-phospholipid synthase (A0A0D5VF95) is involved in formation of cyclopropane membrane fatty from S-adenosyl-L-methionine and phospholipid olefinic fatty acid. S-adenosyl-L-methionine-dependent methyltransferase (A0A0D5VPL5) was also up-

regulated (LogFC = 0.82). This enzyme utilizes S-adenosyl-L-methionine to methylate proteins, small molecules, nucleic acids and lipids (108, 109).

8.2.4. PHA granule formation is induced by glycerol in C3

PHA synthases were identified in the 4 treatments (**Table 11**). These proteins bound to the surface of PHA granules, catalyzing its formation and aggregation. Similarly, phasin proteins were up-regulated in cultures supplemented with 50 mM glycerol. Phasins attach to PHA granules (105) and a role in determination of PHA volume-to-surface ratio (105) and granule stabilization (76) was proposed. Proteome profiling suggested that glycerol induced C3 to synthesize PHA granules. TEM images of C3 taken at 2 or 7 days of incubation with 0.5 mM DBT with or without 50 mM glycerol were acquired for PHA granule visualization (Figure 14). Glycerol induced PHA lipid granule formation inside C3 cell at 2 days of incubation. PHA granules were not seen in cells cultured with DBT alone at day 2. After 7 days of incubation PHA granule formation induced by glycerol was more prominent. Interestingly, there were C3 cells cultured with DBT alone that after 7 days of incubation showed PHA granules, but this was not the overall culture. Proteomics data also supported this evidence (Table 8). A clear separation between DBT and C3 cell membrane was observed, evidencing either exopolysaccharide secretion or chemical interactions between DBT and C3.

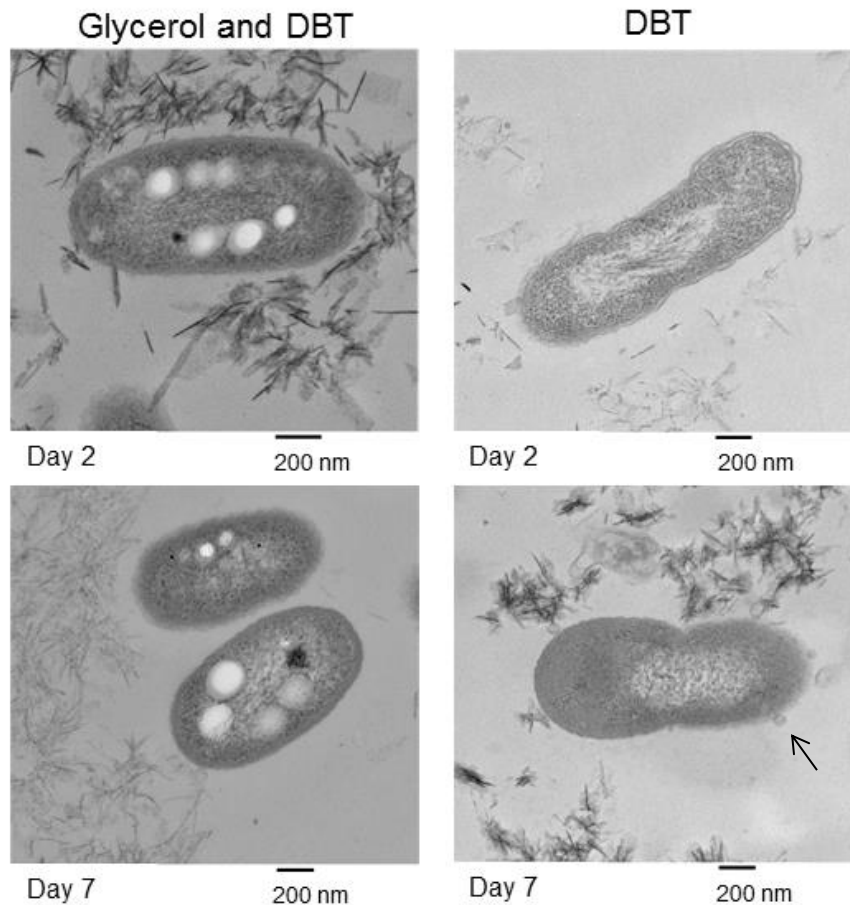


Figure 14. Glycerol induced PHA granules formation in C3. Cells were incubated with 0.5 mM DBT with or without 50 mM glycerol. Cell membrane vesicle detachment is shown by arrow. DBT crystals can be observed surrounding C3 cells. Images were taken at day 2 or 7 of incubation. PHA vesicles were between 100-200 nm in diameter.

Cell membrane detachment of vesicles was also observed and was more noticeable in C3 cells cultured with DBT as the only carbon source. (Figure 14, indicated by arrow). PHA granules are showed as white rounded structures of 100–200 nm in diameter. TEM sample preparation involves the fixing of cells into a solid support from which cross sections are cut, limiting the amount of information that can be obtained, including the PHA granules size range.

However, the trend was that smaller granules were observed at the earlier stage of incubation (Day 2), whereas, bigger ones were observed at the later stage of incubation (Day 7).

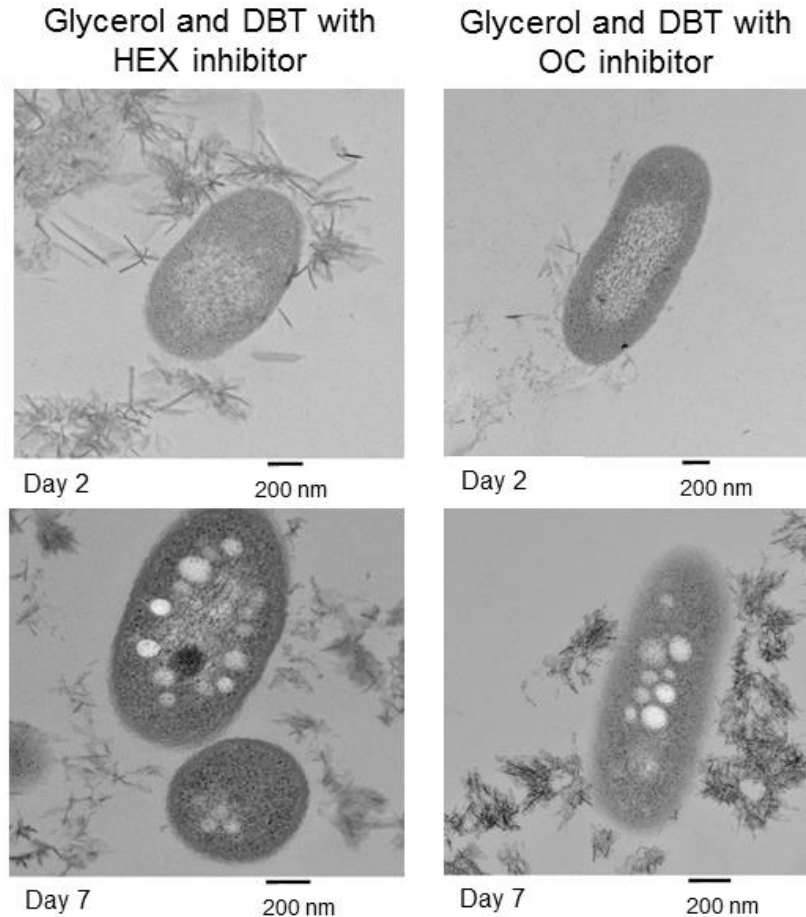


Figure 15. HEX and OC inhibited the formation of PHA granules in C3 at 2 days of incubation. Cells were incubated with 0.5 mM DBT and 50 mM glycerol. HEX or OC inhibitors were added at 2 mM final concentration. DBT crystals can be observed surrounding C3 cells. Images were taken at day 2 or 7 of incubation. PHA vesicles were between 100-200 nm in diameter.

It was shown that HEX and OC negatively affected DBT degradation. Phasin protein profiling suggested that OC inhibited PHA lipid granule formation. The use of HEX and OC was investigated for PHA granule formation inhibition. It was expected that at early stages (Day 2),

HEX and OC will inhibit granule formation and that at day 7 the ability in C3 would be restored. The results shown in Figure 15 agreed with the expectations. PHA lipid formation was inhibited at day 2 and restored at day 7 with both HEX and OC inhibitors. According to the kinetics analysis shown in Figure 11, there is a strong association between DBT degradation and PHA granule accumulation in C3.

8.3. HYPOTHESIS 3: GLYCEROL INDUCES LIPID PRECURSOR SUPPLY FOR BIOSYNTHESIS OF RL BIOSURFACTANT

8.3.1 Identification of genes confirmed the potential of RL biosynthesis in C3

We observed that DBT-glycerol cultures exhibited foam formation (data not shown), suggesting the possible secretion of a biosurfactant. Glycerol can readily enter into FAS II and β -oxidation pathways and these pathways were active in C3 under all the conditions tested (**Table 8**; Treatments A, B, C and D).

Our protein profiling and TEM results showed that PHA vesicle formation was induced in cultures with glycerol and DBT. PHA and RL molecules share the lipid precursor obtained from either or both FAS II or β -oxidation for their biosynthesis (Figure 4). Accordingly, the genes involved in RL biosynthesis in C3 were investigated to confirm the potential ability of C3 for RL secretion.

Table 9. C3 *rhlABC* genes homology to other *Burkholderia* species. bp: basepair. BLASTP algorithm and UniProt database were used to find sequence homology.

UniProt ID	Protein name	Organism	Identity (%)	Query length (bp)
H8WGC8	Rhamnosyltransferase 1, subunit A	<i>B. glumae</i>	78.4	1009
A0A0D5VKY2	Isoprenylcysteine carboxyl methyltransferase	<i>B. fungorum</i>	99.3	450
C4I4U9	Rhamnosyltransferase I, subunit B	<i>B. pseudomallei</i> MSHR3446	99.8	1131
A0A135HB09	MFS transporter	<i>B. thailandensis</i>	64.5	107
Q3JLM3	Rhamnosyltransferase I subunit C	<i>B. pseudomallei</i>	72.3	298

Primers were designed to target conserved regions of 13 *rhlB* sequences from *Burkholderia* species. A DNA sequence (280 bp) matching Rhamnosyltransferase I subunit B from *Burkholderia pseudomallei* (99.8% identity) was obtained. This sequence was used to design inverse PCR primers. The full self-ligated plasmid was 3284 bp. A search for bacterial operons identified 3 ORFs located on the positive plasmid strand. These ORFs were determined to be the *rhlA*, *rhlB* and isoprenylcysteine carboxyl methyltransferase genes (

Table 9). Further analysis showed a 4th gene to be the *MFS transporter*, which was partially sequenced.

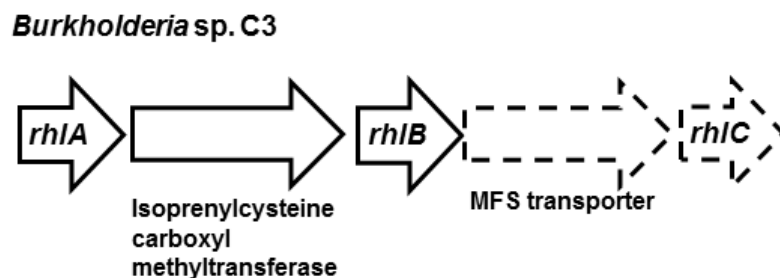


Figure 16. Cluster of *rhlABC* genes in C3 involved in RL synthesis. Solid line arrows represent genes fully sequenced. Dashed line arrows represent genes partially sequenced. *Burkholderia* database was used to find gene cluster homology to other *Burkholderia* species.

The gene *rhlC* (298 bp) was not found in the self-ligated plasmid and was obtained using degenerate primers instead. Comparisons of the gene cluster to those of *Burkholderia* species suggested the *rhlABC* gene cluster proposed in Figure 16.

8.3.2 RL fortification and enhanced DBT biodegradation

In addition to *rhlABC* genes to further test the effects of RLs on DBT degradation, 20 µg/mL of a mixture of two RL congeners (Rha-Rha-C₁₀-C₁₀ and Rha-C₁₀-C₁₀) was added to cultures at 0.05 and 0.2 inocula (OD₆₀₀) containing 0.5 mM DBT (100 ppm). RL congeners did not support bacterial growth. Furthermore, addition of RL congeners dispersed DBT aggregates normally found at the surface of liquid cultures generating many small precipitates. It is possible that the increased biodegradation rates shown in **Table 10** are the result of pseudomicelle formation, increasing the DBT contact surface area and thus DBT toxicity to the bacterial cells. This may explain the decreased on OD₆₀₀ at day 1 (Figure 17).

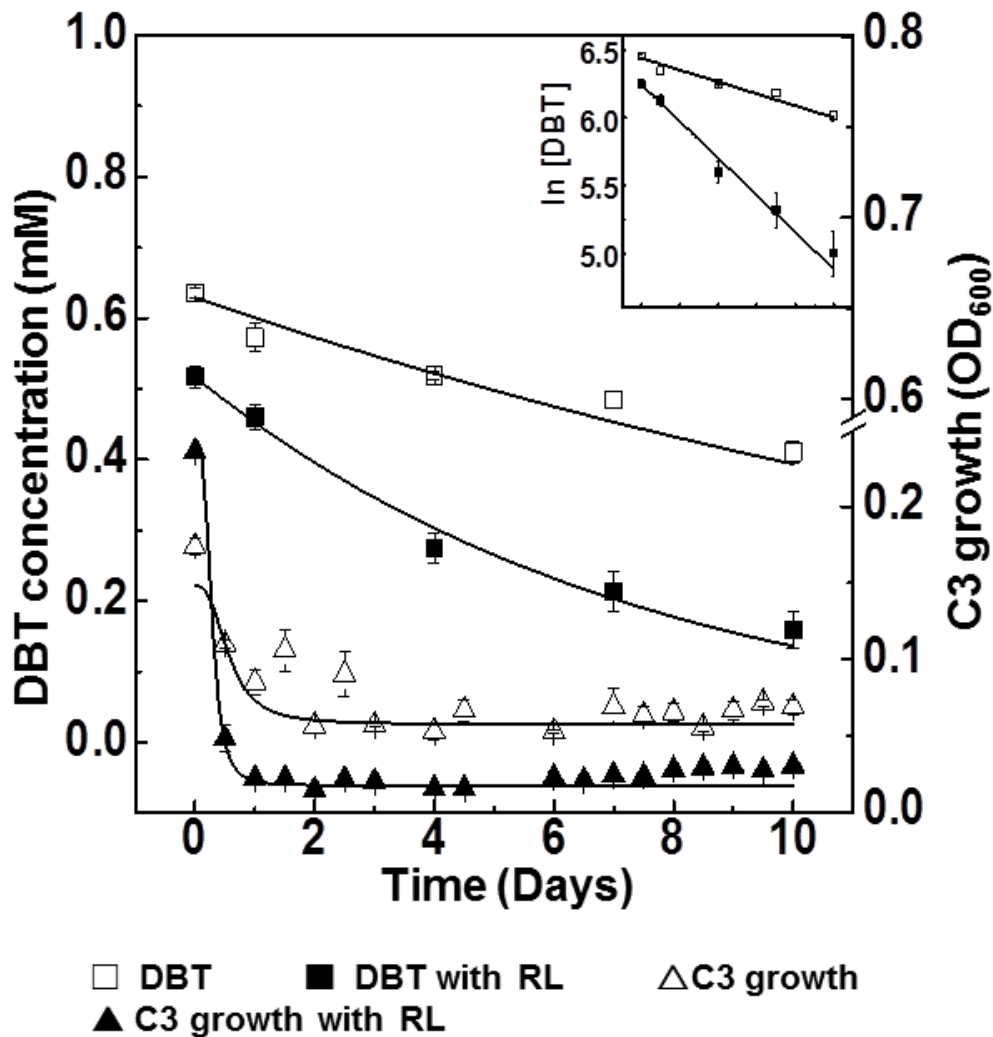


Figure 17. RL fortified enhanced DBT biodegradation. Twenty $\mu\text{g}/\text{mL}$ of RL (solid symbols) was added into C3 inocula at 0.2 OD_{600} . An exponential decay equation, $C = C_0 \times e^{-kt}$, was used for fitting data points of degradation curves. Inset: semi ln fitting.

A multifactorial analysis with incubation time, RLs fortification and inoculum as fixed factors showed that incubation time and RLs were significant factors ($p\text{-value} < 0.001$) accounting for 49% and 37%, respectively (Figure 17).

Table 10. Influence of RL fortification and C3 density in DBT biodegradation rate constant and DBT half-life. The final RL concentration was 20 µg/mL. Exponential decay equation, $C = C_0 \times e^{-kt}$, was used for fitting “N” data points where k is rate constant and t is time in day. Relative to rate constant of 0.5 mM DBT with * 0.05 OD₆₀₀ C3 inoculum and ** 0.2 OD₆₀₀ C3 inoculum.

Treatment	Rate constant (Day ⁻¹)	R ²	Half-life (Day)	N	Fold change
0.5 mM DBT (0.05 OD ₆₀₀ C3 inoculum)	0.025±0.01	0.63	27.5	30	0.0
0.5 mM DBT with RL (0.05 OD ₆₀₀ C3 inoculum)	0.053±0.01	0.91	14.0	30	1.1*
0.5 mM DBT (0.2 OD ₆₀₀ C3 inoculum)	0.047±0.00	0.98	15.8	15	0.7*
0.5 mM DBT with RL (0.2 OD ₆₀₀ C3 inoculum)	0.133±0.01	0.95	5.2	30	1.8**

The RL mixture fortified at 20 µg/mL increased the DBT biodegradation rate constant at both OD₆₀₀ 0.05 and 0.2 cultures (from 0.025 to 0.053 day⁻¹ and from 0.047 to 0.133 day⁻¹, respectively) as shown in **Table 10**.

8.3.3. RL biosynthesis induced by glycerol enhances DBT biodegradation in C3

RLs are amphipathic molecules with surface tension reduction properties. They are glycolipids with 1 or 2 rhamnose sugars attached (37). An orcinol assay is commonly used to measure the levels of RLs (via rhamnose sugar) (110). RL biosynthesis and secretion, induced by varying concentrations of glycerol, associated well with the amount of DBT degraded (Figure 18A). Surface tension measurements further confirmed the biosurfactant production (Figure 18B). The DBT-glycerol cultures achieved 48-51 mN/m surface tension in comparison with 60-65 mN/m of the DBT cultures and with 55-62 mN/m of the glycerol cultures over the time

course. A greater reduction in surface tension relates to a higher biosurfactant concentration until the critical micelle concentration (CMC) is reached (31).

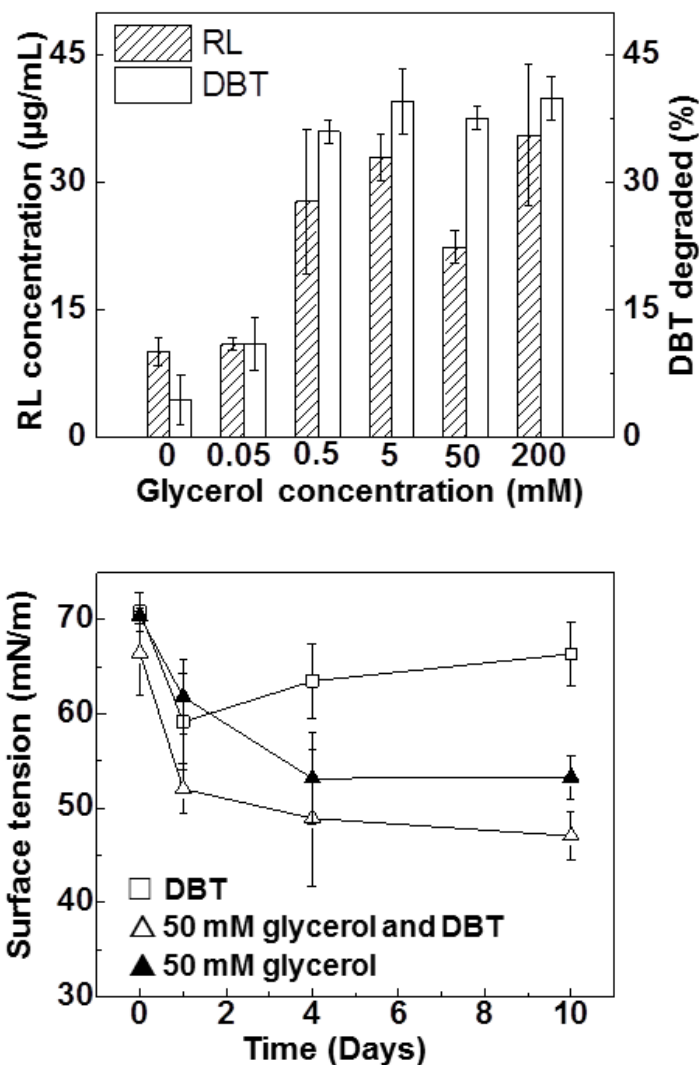


Figure 18. Relationship between DBT biodegradation and RL secretion induced by glycerol in C3 (A) and tensioactive properties of the cultures (B). Concentrations of DBT in the culture media were measured after 24 hours. RLs were extracted from a cell free 5 mL culture after 2 days of incubation. Reference surface tension of water: 72.8 mN/m.

It has been reported that 2-bromoalkanoic acids (HEX and OC) inhibit RL biosynthesis (64, 65). If RLs secreted by C3 play a role in DBT biodegradation, HEX and OC should decrease DBT biodegradation via RL biosynthesis inhibition.

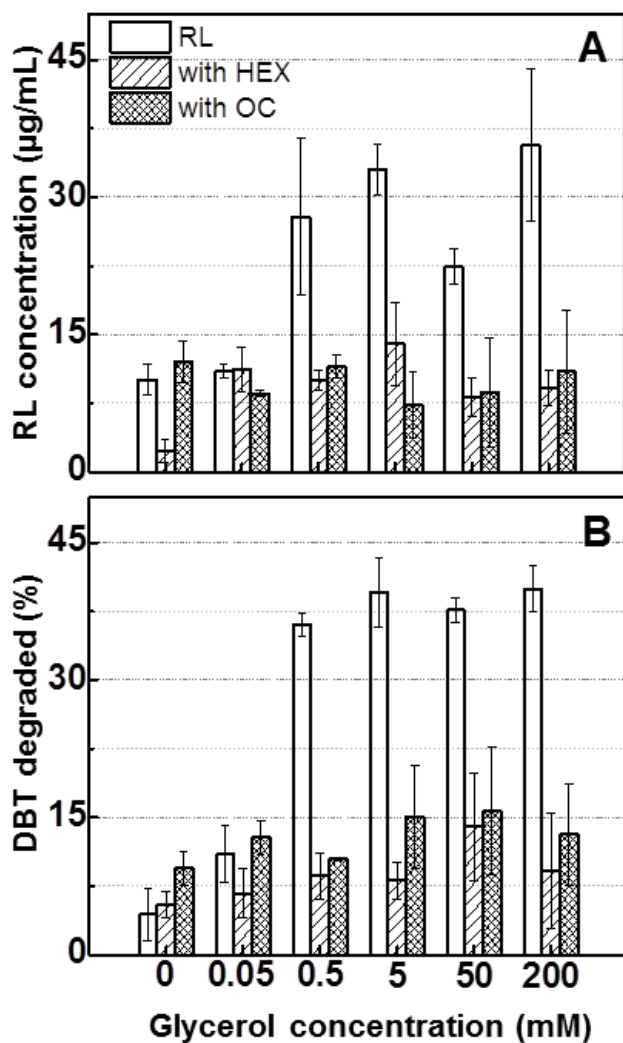


Figure 19. Relationship between the inhibition of RL biosynthesis by HEX or OC acid (A) and DBT biodegradation (B). 2-Bromohexanoic acid (HEX) and 2-bromooctanoic acid (OC) were at 2 mM final concentration. (A) DBT biodegradation cultures were treated with either HEX or OC inhibitors for 24 hours. (B) RLs were extracted from a cell free 5 mL culture after 2 days of incubation.

The results shown in Figure 19 evidenced that the decrease in RL biosynthesis by HEX and OC inhibition was strongly associated with decreased DBT degradation ability in C3.

8.3.4. The proteins involved in RL synthesis were identified

Table 11. Proteins mediating RL synthesis in C3. NO: Not observed. Treatments were: A, 0.5 mM DBT; B, 50 mM glycerol; C, 50 mM glycerol and 0.5 mM DBT; D, 50 mM glycerol, 0.5 mM DBT and 2 mM OC. Proteins were extracted at day 2. Three biological replicates were analyzed in each treatment. Mean normalized value is shown in each treatment. The LogFC represents the glycerol*DBT interaction term. *The relative abundance among treatment showed significant differences (p-value<0.05).

UniProt ID	Protein description	Relative abundance by treatment				LogFC	P-value
		A	B	C	D		
U1XYV8	HAA synthase (RhIA)	0.85	NO	0.86	1.09	1.52	0.090
A0A0B6RU44	Rhamnosyltransferase 1 (RhIB)	1.46	1.02	NO	1.28	-0.57	0.407
C4I4U9	Rhamnosyltransferase 1 (RhIB)	0.85	0.81	NO	1.34	-1.20	0.274
Q3JLM3*	Rhamnosyltransferase 2 (RhIC)*	1.00	0.43	NO	NO	-4.34	0.001
A2RWE5	Rhamnosyltransferase 2 (RhIC)*	0.94	0.43	NO	NO	-4.34	0.001
E1TAD4	Phosphoglucomutase/ phosphomannomutase (AlgC)	0.45	0.62	0.97	0.54	0.68	0.360
B4ECS6	dTDP-glucose 4,6-dehydratase (RmlB)	NO	0.13	0.24	0.27	0.84	0.503
H6TI92	dTDP-4-dehydrorhamnose-3,5-epimerase (RmlC)	1.13	NO	0.58	1.24	0.91	0.233
Q2SYI1	dTDP-4-dehydrorhamnose reductase (RmlD)*	1.22	0.60	1.10	1.52	2.73	0.030

Biosynthesis of RLs requires R-3-hydroxydecanoyl-ACP or -CoA lipid precursor produced from FAS II and/or β -oxidation pathways, respectively (64, 73, 74) and biosynthesis of dTDP-L-rhamnose sugar precursor. Once lipid and sugar precursor are produced, RhlABC mediates the formation of mono- or dirhamnolipids. **Table 8****Table 11** lists the relative abundance of the enzymes detected in the 4 treatments (A, B, C and D), the LogFC and P-value. These enzymes are responsible for RL biosynthesis. For example, the anabolic enzymes AlgC and RmlBCD involved in dTDP-L-rhamnose biosynthesis were detected in all treatments (**Table 11**). RmlD catalyzes the final step from dTDP-4-keto-6-deoxy-L-mannose to dTDP-rhamnose and the LogFC was significantly up-regulated (p-value<0.05). RmlC was also up-regulated. Both RmlD and RmlC relative abundance suggests that synthesis of RL sugar precursors is not inhibited by OC. Additionally, the relative abundance of RmlC in treatment A and D suggest that the synthesis of dTDP rhamnose is delayed with DBT alone or in the treatment containing OC.

Enzymes from FAS II and/or β -oxidation pathways were detected in the 4 treatments (A, B, C and D), indicating these pathways are active in C3. FabG is a key enzyme in R-3-hydroxydecanoyl-ACP synthesis via FAS II pathway (73). The relative abundance of FabG was >1 in all treatments, but treatment B was slightly lower than treatments A, C and D. However, the LogFC was down-regulation. The preceding step catalyzed by FabF was up-regulated in treatment C. β -oxidation enzymes FadB and FadE were abundant in treatment C (**Table 11**). We are unsure which is the main pathway providing the lipid precursor for RL synthesis. The data suggest that both FAS II and β -oxidation pathways are involved in the synthesis of RL lipid precursor. However, it is uncertain which pathway dominates in providing the lipid precursor for RL synthesis.

RhlA produces HAA which is then utilized by RhlB for monorhamnolipid biosynthesis (88). RhlA (U1XYV8) was identified and the LogFC showed up-regulation. Agreeing with Hypothesis 3 glycerol induces lipid precursor supply for biosynthesis of RL biosurfactant. Regarding rhamnosyltransferases, two RhlB and RhlC were identified and contrary to the expectations their LogFC were down-regulated (**Table 11**). These proteins are involved in the direct formation of mono-(85, 86) and di-rhamnolipids (87), respectively.

8.3.5. Identification of RL congeners secreted by C3

A RL standard containing a mixture of Rha-Rha-C₁₀-C₁₀ and Rha-C₁₀-C₁₀ congeners was used for HPLC and MALDI-TOF/TOF method development and to identify RLs in experimental samples. The RL standard that was resuspended in methanol was purified through HPLC and analyzed via MALDI-TOF. Fractions F1, F2, and F3 were collected the results are shown in Figure 20.

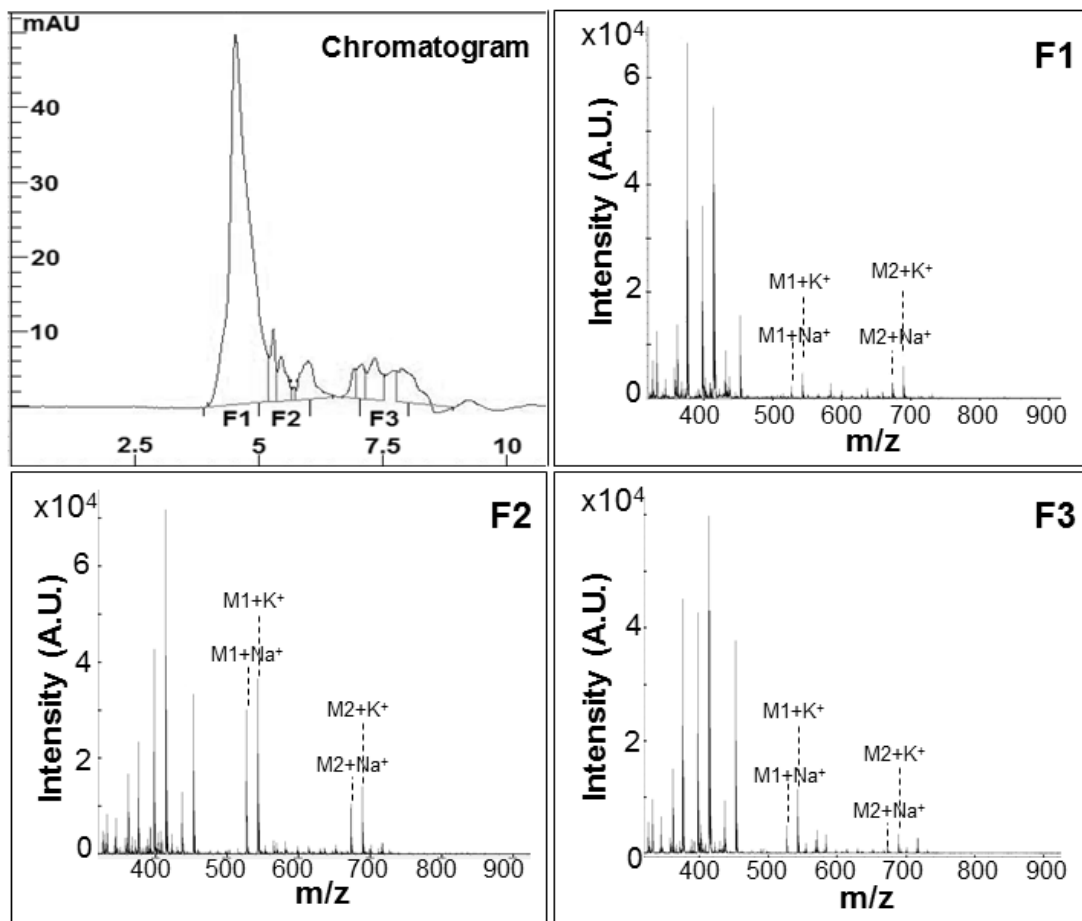


Figure 20. Analysis of RL standard via HPLC and MALDI-TOF. Chromatograms of RL standard were shown. Fractions were collected at 4-5 (F1), 5-6 (F2) and 7-8 (F3) minutes. Standard with two RL congeners (M1 and M2) were found as Na^+ and K^+ adducts in F1, F2 and F3 fractions. RL congener M1: Rha- C_{10} - C_{10} and RL congener M2: Rha-Rha- C_{10} - C_{10} .

Rha- C_{10} - C_{10} (M1) and Rha-Rha- C_{10} - C_{10} (M2) congeners were found in all chromatographic fractions analyzed, but F2 fraction contained higher amounts of as shown by the intensity axis in Figure 20. RL congeners formed Na^+ , K^+ and rarely $[\text{M}-\text{H} + \text{Na}_2]^+$ ions adducts. Congeners forming $[\text{M}-\text{H} + \text{Na}_2]^+$ ions are not shown.

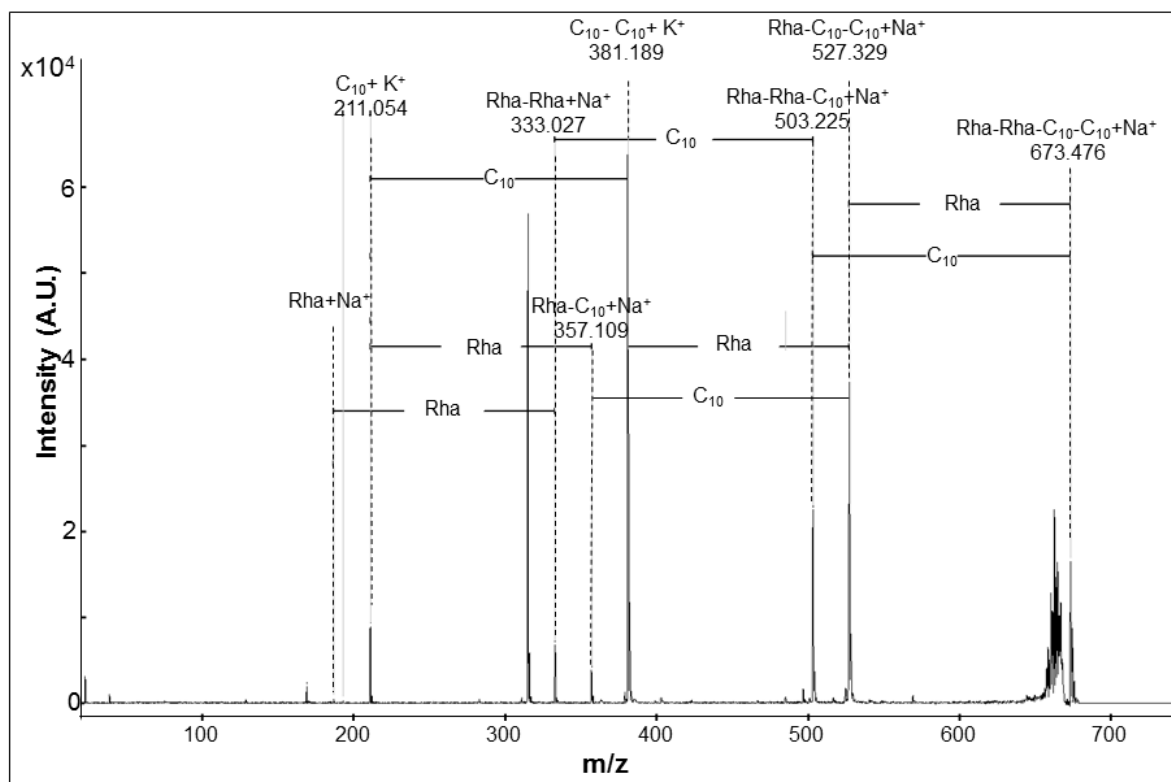


Figure 21. Dirhamnolipid Rha-Rha-C₁₀-C₁₀ fragmentation pattern spectrum. Spectrum was obtained with MALDI-TOF/TOF. Rha: rhamnose sugar. RL congeners formed Na⁺, K⁺ and rarely [M-H+ Na₂]⁺ ions adducts. Lipid fragments (C₁₀-C₁₀ or C₁₀) formed K⁺ adducts. Rhamnose fragments (Rha-Rha or Rha) formed Na⁺ adducts.

After RL peaks were assigned, full fragmentation of Rha-Rha-C₁₀-C₁₀, m/z 673.476 corresponding to [M+Na]⁺ adduct ion was achieved via MALDI-TOF/TOF (Figure 21). In addition to RL congeners, lipid fragments (C₁₀-C₁₀ or C₁₀) consistently formed K⁺ adduct ions and rhamnose sugar fragments (Rha-Rha or Rha) formed Na⁺ adduct ions. Glycolipid peaks formed mainly Na⁺ adduct ions, which were seen in tandem mass spectrometry (e.g. Rha-C₁₀ + Na⁺).

A RL molecule consist in either 1 or 2 rhamnose sugars attached through an O-glycosidic bond to 1 or 2 β -hydroxy fatty acids, with the lipid portion linked by an ester bond (37). RLs are easily fragmented molecules. All potential fragments were observed in tandem MS. The expected and observed ions are described in Table 12. A lipid fragment minus two hydrogens was consistent in lipid fragment loss. For example, if a C₁₀ (C₁₀H₂₀O₂) fragment was lost, the mass loss was 170.1463, instead of 172.1463.

Table 12. Rha-Rha-C₁₀-C₁₀ dirhamnolipid fragments. Molecular weight and expected adduct ions mass was calculated with Compass IsotopePattern.

Fragment	Molecular Formula	Expected M+Na ⁺	Observed M+Na ⁺	Expected M+K ⁺	Observed M+K ⁺
Rha-Rha-C ₁₀ -C ₁₀	C ₃₂ H ₅₈ O ₁₃	673.3769	673.336	689.3509	680.308
Rha-Rha-C ₁₀	C ₃₂ H ₄₀ O ₁₁	503.2285	503.225		
Rha-C ₁₀ -C ₁₀	C ₂₆ H ₄₈ O ₉	527.3190	527.291	543.2929	543.262
C ₁₀ -C ₁₀	C ₂₀ H ₄₀ O ₄			381.2703	381.189
Rha-C ₁₀	C ₁₅ H ₂₈ O ₇	357.178	357.109		
Rha-Rha	C ₁₂ H ₂₂ O ₉		333.027		
Rha	C ₆ H ₁₂ O ₅	187.0576	187.0110		
C ₁₀	C ₁₀ H ₂₀ O ₂			211.1094	211.054

RL congeners were eluted between 4 and 6 minutes (Figure 20). The sample chromatograms (Figure 22) aligned well with RL standard chromatograms (Figure 20). Two fractions named, F1 and F2 were collected from experimental samples with 0.5 mM DBT and

either 50 mM glycerol or not. Fractions from cultures treated with 2 mM of HEX or OC inhibitors were also collected and chromatograms are shown in Figure 22.

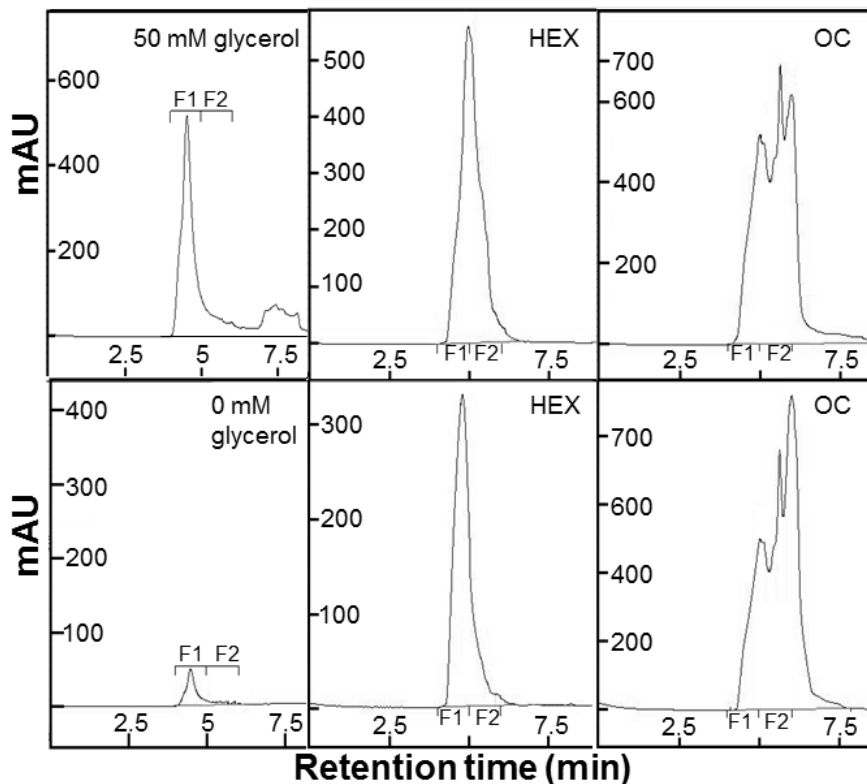


Figure 22. RL separation in experimental samples. RLs were extracted at day 2 from cell free supernatant cultures. C3 was cultivated with **top row:** 50 mM glycerol/0.5 mM DBT and 50 mM glycerol/0.5 mM DBT with HEX or OC inhibitor (2mM). **Bottom row:** 0.5 mM DBT and 0.5 mM DBT with HEX or OC inhibitor (2 mM). F1: fraction 1 collected at 4-5 min. F2: fraction 2 collected at 5-6 min. AU: arbitrary units.

The peak intensity on the 50 mM glycerol chromatogram was approximately 10-fold higher than the peak on the 0 mM glycerol chromatogram, supporting the results showed in Figure 18. Glycerol induced an increase in RL production. It is noteworthy that multiple peaks occurred at the OC chromatograms.

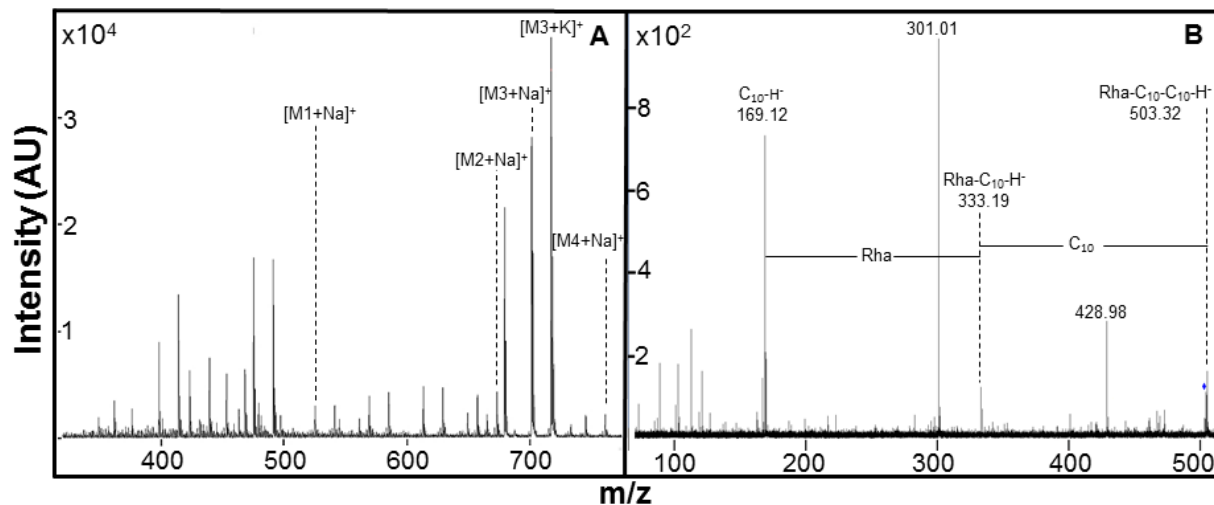


Figure 23. (A) MALDI-TOF-MS of 4 RL congeners (M1, M2, M3 and M4) identified and (B) LC-Q-ToF-MS2 of Rha-C10-C10 (M1). MS1 spectrum of HPLC fraction 2 (F2) is shown in (A). RL congeners were identified with MALDI TOF. Rha: rhamnose sugar. RL congeners identified: Rha-C₁₀-C₁₀ (M1+Na⁺), Rha-Rha-C₁₀-C₁₀ (M2+Na⁺), Rha-Rha-C₁₀-C₁₂ (M3+Na⁺), Rha-Rha-C₁₀-C₁₂ (M3+K⁺) and Rha-Rha-C₁₂-C₁₂ (M4+K⁺). Peaks from (A) were assigned with a 0.5 Da error mass.

We assigned the most intense peaks to RL congeners. In 50 mM glycerol, C3 secreted the congeners Rha-C₁₀-C₁₀ (M1+Na⁺), Rha-Rha-C₁₀-C₁₀ (M2+Na⁺), Rha-Rha-C₁₀-C₁₂, which was identified in the sodium (M3+Na⁺) or potassium (M3+K⁺) adduct ion form and Rha-Rha-C₁₂-C₁₂ (M4+Na⁺). Monorhamnolipid congener Rha-C₁₂-C₁₂ was identified in 0 mM glycerol and with HEX or OC inhibitors (either in 50 or 0 mM glycerol) but the data is not shown. Peaks M1 and M2 were confirmed with tandem mass spectrometry. The mass spectrum of Rha-C₁₀-C₁₀ is shown in Figure 23B. Loss of C₁₀ acyl chain and rhamnose sugar fragments (Rha) were observed.

9. CHAPTER 5: DISCUSSION

Polycyclic aromatic hydrocarbon (PAH) biodegradation on liquid cultures with single carbon source depends on bacterial strain, type of PAH and PAH concentration. Seo et al. showed that *Arthrobacter sp.* P1-1 and *Sinorhizobium sp.* C4 degrade less than 10% of 40 ppm phenanthrene at day 1, whereas *Mycobacterium sp.* JS19b1^T and *Burkholderia sp.* C3 degrade 20-25% and 60-65%, respectively (63). Another study shows that *Mycobacterium sp.* strains czh-101 and czh-3 degrade less than 20% and 100% of 100 ppm phenanthrene at day 7, respectively (111). C3 degrades 100% of 40 ppm naphthalene and phenanthrene at day 3 and 94% of 40 ppm DBT at day 7 (35). Our results indicate that C3 degrades 11-12% of 100 ppm at day 7. A decrease in DBT biodegradation efficiency in C3 at a higher DBT concentration might be related to its toxicity. PAHs hydrophobicity (lipophilic nature) and carcinogenicity influences their toxicity (1, 3, 31, 32).

Co-substrate experiments with DBT and glycerol neither exhibit a carbon catabolite repression phenomenon nor an antagonistic effect, which has been reported for other co-substrate mixtures (32, 111, 112). Instead, a cometabolism effect was observed. It is noteworthy that the term cometabolism is used to describe either of the following molecular processes: (1) broad substrate specificity of catabolic enzymes; (2) imperfect coupling between enzyme specificity and gene regulation; (3) xenobiotic compounds metabolism of a consortium with mutual metabolic reliance and (4) co-substrate effects on the metabolism of a xenobiotic compound (113). The results indicated that biostimulation with glycerol supports C3 growth and induced molecular processes 2 and 4. Phn enzymes involved in phenanthrene degradation in C3 (35)

were detected in the 4 treatments analyzed. Phenanthrene is a 3-ring PAH highly similar to DBT. Dioxygenases broad specificity has been reported in the literature for degradation of biphenyl, 2,4-dinitrotoluene and DBT (114–116). Phenanthrene and DBT crossed-over metabolic points in were proposed in *Mycobacterium aromativorans* JS199B1 (116). The protein profiling results (Table 6) indicated that DBT, phenanthrene and naphthalene crossed-over pathways in C3 and this was independent of glycerol supplementation. For phenanthrene and naphthalene degradation two sets of genes were reported (35). The results showed a third set of enzymes for DBT degradation (Table 6). This enzyme set is involved in DBT degradation through lateral dioxygenation pathway (Figure 10), previously showed in *Burkholderia sp.* DBT1 (59), currently known as *Burkholderia fungorum* DBT 1 (117).

Glycerol supplementation induced the expression of proteins involved in PAHs degradation (Table 6) and changes in lower aromatic pathways, which was evidenced by up-regulation of tautomerase (A0A0M3TVK8) a protein involved in cellular metabolism of aromatic compounds (GO:0006725), FMN-dependent NADH-azoreductase (A0A0D5V7V5), 2,3-dihydroxy-2,3-dihydrophenylpropionate dehydrogenase (Q93NA6) and catechol-2,3-dioxygenase (Q9RB89). Cometabolites can supply energy to support bacterial growth and may also function to induce several catabolic enzymes for degradation of the non-growth substrate (32).

Upon absorption, glycerol underwent immediate phosphorylation followed by conversion into dihydroxyacetone-3-phosphate by GlpD (A0A0D5V7V5) and thus entered glycolysis as D-glyceraldehyde-3-phosphate (Figure 3). This supported cell growth and consequently enhanced DBT biodegradation. There is an association between chemical biodegradation enhancement and

increase in bacterial growth (40, 81). The experiments showed that cometabolism enhancement and C3 growth are dependent upon the glycerol to DBT molar ratio used and the incubation time. For example, at 0.1:1 and 100:1 glycerol to DBT molar ratio, the DBT biodegradation rate constant was enhanced by 1.6-fold and 18-fold, respectively. Meanwhile, a 7 day incubation time is necessary for C3 to biodegrade 100% of DBT at a 100:1 glycerol to DBT molar ratio and 10 days to degrade 90-95% at a 10:1 molar ratio (Fig. 1, Table 1). Interestingly, at 1:1 glycerol to DBT molar ratio C3 degraded 92% of 0.5 mM DBT at day 10 but, at this glycerol concentration C3 growth remained at 0.05 OD₆₀₀.

Glycerol supplies into several metabolic pathways (Figure 3). In addition to glycolysis and gluconeogenesis, glycerol supply into lipid metabolic pathways in C3. The use of HEX and OC, inhibitors of β -oxidation and FAS II pathways (64, 65), was investigated at 2 and 5 mM concentrations. In cultures supplemented with glycerol alone, exponential growth phase was delayed in approximately 2 days. C3 reached 0.3 and 0.35 OD₆₀₀ with HEX and OC, respectively. Generally, the C3 growth curve phases were similar with either 2 mM or 5 mM. However, when a DBT-glycerol mixture was supplemented, the C3 growth and DBT degradation were highly compromised. At the protein level, the relative abundance of GlpD (A0A0D5VFX1) in treatment D (with OC inhibitor) was lower than in treatments B and C, which could partially explain the suppressed C3 growth (Figure 11).

Protein profiling revealed additional mechanisms that were affecting DBT degradation. Detection of cyclopropane-fatty-acyl-phospholipid synthase (A0A0M3TVX7) indicated cell membrane changes. Cyclopropane-fatty-acyl-phospholipid synthase mutants of *Pseudomonas putida* DOT-T1E were less resistant to toluene. The mutants contained decreased levels of 9,10-

methyl hexadecanoic and 11,12-methyl octadecanoic acids in their membrane when compared to wild-type. These changes did not affect membrane fluidity. Organic solvents m-xylene, ethylbenzene and propylbenzene also decreased survival rate of DOT-T1E mutant strain (118). Cyclopropane-fatty-acyl-phospholipid are non-essential components of cell membranes that provided organic solvent tolerance (118). Toluene tolerance protein A0A0D5VI71 has a LogFC value of 1.40 (p-value = 0.062) and its relative abundance in treatment C was 1.38. DBT degradation may produce toluene metabolites toxic for C3. Significantly up-regulated proteins suggested that C3 secreted several metabolites that warrant further metabolomics studies. Proteomics and metabolomics studies were reported in C3 in response to carbaryl. They reported that the most prominent metabolic changes were associated with biosynthesis and metabolisms of amino acid, sugars, PHA, lipids and cofactors (104).

Phasin proteins were abundant in all treatments. Phasins are analogs to oleosins and they associate to PHA granules. They determine the surface-to-volume ratio and prevent coalescence with other cell components (105). PHA granules are mainly described for carbon and energy storage when carbon supplied is not a limiting factor (105). York et al., reported that phasin accumulation was dependent on expression of PHA synthase in *Ralstonia eutropha* (119). Additionally, PHA synthase proteins involved in PHA biosynthesis were significantly upregulated (**Table 8**). Phasins were previously proposed as reporters of PHA production (119). C3 grown with glycerol accumulated intracellular PHA granules and this were produced by day 2 and remained at day 7 (Figure 14). When C3 was grown in DBT alone granules were not observed at day 2, contrary to the regulation of phasin (A0A0N1KL01). Intracellular PHA granules were observed in a small number of cells at day 7. It is interesting that on a limited

carbon supply C3 favored PHA granule formation. HEX and OC at 2 mM inhibited granule formation only at day 2. In addition to carbon and energy storage, PHA granules may have other roles involved in DBT and xenobiotics degradation. It was proposed that *Bacillus sp.* CYR1 produced high levels of PHA from phenol, naphthalene and 4-chlorophenol (120). Production of PHA was reported in C3 in response to carbaryl, NB and glucose, where, the lowest levels were measured with carbaryl, followed by NB and glucose (104). Di Martino *et al.*, (77) indicated that PHA accumulation influences biosurfactant production. PHA mutant *Pseudomonas sp.* KA-08 showed less surface tension reduction than wild type when cultured in PHA accumulating conditions. PHA production also affected outer membrane characteristics (77). Additionally, a clear separation between the cell outer membrane and DBT was observed in the TEM images suggesting possible exopolysaccharide secretion or a type of chemical interaction (e.g. ionic, hydrophobic); however, additional experiments are required for further conclusions.

PAH hydrophobicity and octane/water coefficient increases with their molecular weight (3, 31). Bioavailability of PAHs of interest is a main limitation for PAH biodegradation in a bioremediation site (31). It has been observed that biostimulation with biosurfactant exogenously added or endogenously produced can enhance bioremediation of hydrophobic chemicals through an increase in bioavailability (41, 43, 80, 121). However, contradicting results have also been reported (24, 41). Our results demonstrated that DBT cometabolism associated with increased PHA production and RL biosynthesis and secretion. Bioavailability of DBT to C3 is a first requirement for its biodegradation. DBT is a hydrophobic compound with a water solubility coefficient of 7.9 μM and an octanol-water partitioning coefficient of 4.44 (12). Foam formation and apparent DBT solubilization were observed after 12 hours of incubation during

cometabolism experiments. Glycerol is a good carbon source for RL production in *Pseudomonas* species (37). The lipid precursor component of the RL molecule is produced in pathways supplied by glycerol (37, 64, 66). Identification of the *rhlABC* genes supported the possibility of RL biosynthesis in C3 (Figure 16, Table 9). In *Burkholderia* species, the *rhlABC* genes reside in the same gene cluster which is responsible for higher biosynthesis of dirhamnolipids over monorhamnolipids (37, 66, 67, 122). The presence of RLs affects DBT biodegradation at early stages of incubation which is supported by the surface tension decrease at day 1 (Figure 18B) and the RL secretion levels quantified with the orcinol assay (Figure 18,A) as well as effects of RL biosynthesis inhibition by HEX and OC on DBT biodegradation (Figure 19). Gutierrez et al. showed that inhibition of RhlA and PhaG enzymes in FAS II pathway by bromoalkanoic acids suppresses production of RLs and PHA in *Pseudomonas* species and this inhibition was dependent on the bromoalkanoic acid used (HEX or OC) (65). This is the first study that utilizes HEX and OC inhibitor in a *Burkholderia* species to investigate their effect of PHA and RL production.

Abdel-Mawgoud et al. demonstrated the direct involvement of β -oxidation via a enoyl-CoA hydratase/isomerase (RhlYZ) (64). FadE (from β -oxidation) and FabF and FabZ (from FAS II) were upregulated with glycerol, indicating that supplementation with glycerol affected both of these pathways. It is uncertain whether one or both lipid pathways (β -oxidation or FAS II) provided the lipid precursors for RL biosynthesis in C3. Both lipid pathways were activated in C3 (**Table 8**). RL biosynthesis was active in all treatments, which was supported by RhlABC enzyme and RL congeners identification. monorhamnolipid Rha-C₁₀-C₁₀ and dirhamnolipids Rha-Rha-C₁₀-C₁₀, Rha-Rha-C₁₀-C₁₂ and Rha-Rha-C₁₂-C₁₂ were identified in 50 mM glycerol and

0.5 mM DBT (Figure 23), whereas, only Rha-C₁₂-C₁₂ monorhamnolipid congener was identified in cultures without glycerol or with HEX or OC inhibitors.

The levels of RLs detected in the extracts of biodegradation cultures associates well with the amount of DBT biodegraded. The cometabolism results show up to an 18-fold increase in DBT biodegradation and a tripling in RL secretion. Inhibition of RL biosynthesis suppresses DBT biodegradation up to 8-fold. Fortification of RLs into cultures without glycerol results in a 1.8-fold increase of DBT biodegradation which further confirm our findings.

The amphipathic properties of RLs suggest multiple functions for RL producers and PAH degraders. Some of these roles are related with hydrophobic chemical solubilization, chemical uptake and biological assimilation (37, 41). RL involvement in cell transport could also increase the biodegradation of hydrophobic chemicals (123). The dual functions of RL production and PAH degradation may confer to the microorganism an evolutionary adaptation to survive in environmental conditions where hydrophobic chemicals are scarce. Bioremediation studies in the site show that microbial abundance is associated with biorespiration (23, 121) and thus chemical biodegradation (24).

Two main mechanisms are proposed for RL interactions with hydrophobic pollutants. One involves chemical solubilization via RL micelle uptake (31), the second, affects cell membrane hydrophobicity for cell attachment and biofilm formation (37, 41). The cometabolism results show up to an 18-fold increase in DBT biodegradation and a tripling in RL secretion. However, the amounts of RLs secreted, especially, in those cultures without glycerol were below the CMC. Above or at the CMC the surface tension of RL is 30 mN/m (37). The proteome

profiling results showed that C3 modified its cell membrane with glycerol supplementation. Based on our results, we proposed that the second mechanism is taking place in C3. Glycerol supported C3 growth and affected RL production and several other metabolic pathways which resulted in enhanced cometabolism of DBT.

10. CHAPTER 6: CONCLUSION AND FUTURE DIRECTIONS

Glycerol induced DBT cometabolism via several mechanisms. The most apparent one was related to an increase in C3 biomass. Extensive literature review, observation of the biodegradation cultures, and analysis and interpretation of preliminary data lead to protein profiling, PHA granule and RL identification and characterization experiments. The results indicated that glycerol induced the expression of proteins related in xenobiotic degradation (phenanthrene, naphthalene and DBT) and changes in lower aromatic metabolic pathways. Broad dioxygenase specificity was also evidenced but this was independent of glycerol supplementation. Metabolomics analysis of DBT metabolites in addition to protein profiling would allow depicting a full DBT catabolic pathway and this will probably varied dependent upon the co-substrates used. DBT as a model chemical showed great potential to further investigate cometabolism of other PAHs. It is important to emphasize that metabolic capability is the first requirement for a successful bioremediation strategy and thus should be considered for the selection of a proper strain or microbial consortium.

Lipid metabolism, PHA production, granule formation and RL biosynthesis and secretion were all metabolic process affected by glycerol and were shown to affect DBT degradation. C3 secreted 3 dirhamnolipid congeners when supplemented with glycerol as opposed to 1 monorhamnolipid with DBT alone or when cells were treated with HEX or OC inhibitor. However, culturing conditions made difficult the purification and characterization process and a tandem mass spectrum of the congeners was not obtained. Characterization and quantification of RLs secreted by C3 from different carbon sources are required to optimize RL production by C3.

The data also suggested changes in membrane fatty acid composition and possible exopolysaccharides secretion. Additional experiments would help evidencing these changes in response to different culturing conditions.

This dissertation utilized glycerol as a co-substrate for DBT cometabolism and RL production. The chemical composition of the crude glycerol fraction from biodiesel production varies greatly. Glycerol in this fraction ranges between 38-96%. Crude glycerol fractions also contain methanol and ash (68). The use of crude glycerol should be investigated for biosurfactant production and DBT degradation. Utilization of a direct supply of crude glycerol from biodiesel production would be attractive to the biodiesel industry to make biodiesel production more cost-effective.

The studies suggested that utilization of glycerol could potentially lead to effectively biodegrade PAHs in contaminated soil. This cometabolism strategy could be applied in combination with bioaugmentation of a suitable microbial consortium (24, 121, 124). Glycerol may trigger a superior response in a bacterial population with a mixture of PAH degraders and RL producers, or both (38–41, 81). An initial analysis of the bacterial population and cellular respiration and PAH biodegradation monitoring over time would be required for a proper assessment of this strategy (23, 24, 121).

Biosurfactants have been used in many different fields (125) and have a promising potential in environmental clean-up of PAHs (31). Patowary *et al.*, (126) suggested that the presence of biosurfactant producers in an optimal bacterial consortium reduced the adaption time of hydrocarbon degrading microorganisms. They reported that decreased in total petroleum

hydrocarbon content correlated with surface tension reduction (126). A RL ratio of 150 mg per Kg of soil was reported for enhanced increase in microbial activity. They also suggested RL introduction to the soil every 30 days (24). It has been reported that the time that soil particles were exposed to diesel influenced the level of adsorption into the soil. This influence was related to the soil organic matter content. As to which a higher biodegradation efficiency was achieved with lower organic matter content (24). However, direct studies on the interaction of soil particles with PAHs and the effects of biosurfactants are scarce and required further investigation.

Glycerol greatly enhanced biodegradation of 0.5 mM DBT by C3. Our studies revealed that complex metabolic networks and cellular mechanisms are induced by glycerol. To our knowledge this is the first report linking these pathways to the biodegradation of DBT. The factors described in this study probably enhance the degradation of heavier PAHs which are more hydrophobic and recalcitrant to degradation.

11. REFERENCES

11.1. WEBSITES CITED

ATSDR website:

1. <https://www.atsdr.cdc.gov/spl/> accessed on July 15, 2016 at 9:44 AM.

Environmental Protection Agency (EPA) website:

2. <https://www.epa.gov/superfund/superfund-national-priorities-list-npl> accessed on October 10, 2016 at 10:11 AM.
3. <https://www.epa.gov/remedytech/remediation-technologies-cleaning-contaminated-sites> accessed on July 21, 2016 at 10:08 AM.

Federal remediation technologies roundtable (FRTR) website:

4. https://frtr.gov/matrix2/top_page.html accessed on July 29, 2016 at 3:42 PM.

Transport website:

5. <http://transportpolicy.net/index.php?title=US: Fuels: Diesel and Gasoline> accessed on 06/16/2015 at 2:49 PM.

Cellular overview of *Pseudomonas aeruginosa* PAO1 (BioCyc database) website:

6. <http://biocyc.org/overviewsWeb/celOv.shtml#> accessed on November 03, 2016 at 12:30 PM.

11.2. PAPERS CITED

1. **Wolfe a, Shimer GH, Meehan T.** 1987. Polycyclic aromatic hydrocarbons physically intercalate into duplex regions of denatured DNA. *Biochemistry* **26**:6392–6396.
2. **Havenga WJ, Rohwer ER.** 1999. Chemical characterization and screening of hydrocarbon pollution in industrial soils by headspace solid-phase microextraction. *J Chromatogr A* **848**:279–295.
3. **Dabestani R, Lvanov IN.** 1999. A Compilation of Physical, Spectroscopic and Photophysical Properties of Polycyclic Aromatic Hydrocarbons. *Photochem Photobiol* **70**:10–34.
4. **Seo J-S, Keum Y-S, Li QX.** 2009. Bacterial degradation of aromatic compounds. *International journal of environmental research and public health*.
5. **Solà M.** 2013. Forty years of Clar's aromatic π -sextet rule. *Front Chem* **1**:4–11.
6. **Portella G, Poater J, Solà M.** 2005. Assessment of Clar's aromatic π -sextet rule by means of PDI, NICS and HOMA indicators of local aromaticity. *J Phys Org Chem* **18**:785–791.
7. **Anthony EJ, Wang J.** 2006. Pilot plant investigations of thermal remediation of tar-contaminated soil and oil-contaminated gravel. *Fuel* **85**:443–450.
8. **Gan S, Lau E V., Ng HK.** 2009. Remediation of soils contaminated with polycyclic aromatic hydrocarbons (PAHs). *J Hazard Mater* **172**:532–549.

9. **Baird WM, Hooven LA, Mahadevan B.** 2005. Carcinogenic polycyclic aromatic hydrocarbon-DNA adducts and mechanism of action. *Environ Mol Mutagen* **45**:106–114.
10. **Soleimani M, Bassi A, Margaritis A.** 2007. Biodesulfurization of refractory organic sulfur compounds in fossil fuels. *Biotechnol Adv* **25**:570–596.
11. **Li M, Wang TG, Simoneit BRT, Shi S, Zhang L, Yang F.** 2012. Qualitative and quantitative analysis of dibenzothiophene, its methylated homologues, and benzonaphthothiophenes in crude oils, coal, and sediment extracts. *J Chromatogr A* **1233**:126–136.
12. **Incardona JP, Collier TK, Scholz NL.** 2004. Defects in cardiac function precede morphological abnormalities in fish embryos exposed to polycyclic aromatic hydrocarbons. *Toxicol Appl Pharmacol* **196**:191–205.
13. **Brinkmann M, Maletz S, Krauss M, Bluhm K, Schiwy S, Kuckelkorn J, Tiehm A, Brack W, Hollert H.** 2014. Heterocyclic aromatic hydrocarbons show estrogenic activity upon metabolization in a recombinant transactivation assay. *Environ Sci Technol* **48**:5892–5901.
14. **Lim MW, Lau E Von, Poh PE.** 2016. A comprehensive guide of remediation technologies for oil contaminated soil — Present works and future directions. *Mar Pollut Bull* **109**:14–45.
15. **Silva A, Delerue-Matos C, Fi??za A.** 2005. Use of solvent extraction to remediate soils contaminated with hydrocarbons. *J Hazard Mater* **124**:224–229.

16. **Yap CL, Gan S, Ng HK.** 2010. Application of vegetable oils in the treatment of polycyclic aromatic hydrocarbons-contaminated soils. *J Hazard Mater* **177**:28–41.
17. **Wang S, Mulligan CN.** 2004. An evaluation of surfactant foam technology in remediation of contaminated soil. *Chemosphere* **57**:1079–1089.
18. **Anitescu G, Tavlariides LL.** 2006. Supercritical extraction of contaminants from soils and sediments. *J Supercrit Fluids* **38**:167–180.
19. **Librando V, Hutzinger O, Tringali G, Aresta M.** 2004. Supercritical fluid extraction of polycyclic aromatic hydrocarbons from marine sediments and soil samples. *Chemosphere* **54**:1189–1197.
20. **Smith MT, Berruti F, Mehrotra AK.** 2001. Thermal Desorption Treatment of Contaminated Soils in a Novel Batch Thermal Reactor. *Ind Eng Chem Res* **40**:5421–5430.
21. **Ferrarese E, Andreottola G, Oprea IA.** 2008. Remediation of PAH-contaminated sediments by chemical oxidation. *J Hazard Mater* **152**:128–139.
22. **Pazos M, Rosales E, Alc??ntara T, G??mez J, Sanrom??n MA.** 2010. Decontamination of soils containing PAHs by electroremediation: A review. *J Hazard Mater* **177**:1–11.
23. **Margesin R, Schinner F.** 2001. Bioremediation (Natural Attenuation and Biostimulation) of Diesel-Oil-Contaminated Soil in an Alpine Glacier Skiing Area. *Appl Environ Microbiol* **67**:3127–3133.

24. **Szulc A, Ambrozewicz D, Sydow M, Ławniczak Ł, Piotrowska-Cyplik A, Marecik R, Chrzanowski Ł.** 2014. The influence of bioaugmentation and biosurfactant addition on bioremediation efficiency of diesel-oil contaminated soil: Feasibility during field studies. *J Environ Manage* **132**:121–128.
25. **Rushton, D.G., A.E. Ghaly KM.** 2007. Assesment of Canadian Regulations and Remediation Methods for Diesel contaminated Soils. *Am J Appl Sci* **7**:465–478.
26. **Pope CJ, Peters WA, Howard JB.** 2000. Thermodynamic driving forces for PAH isomerization and growth during thermal treatment of polluted soils. *J Hazard Mater* **79**:189–208.
27. **Tyagi M, da Fonseca MMR, de Carvalho CCCR.** 2011. Bioaugmentation and biostimulation strategies to improve the effectiveness of bioremediation processes. *Biodegradation* **22**:231–241.
28. **Bodour AA, Drees KP, Maier RM.** 2003. Distribution of biosurfactant-producing bacteria in undisturbed and contaminated arid southwestern soils. *Appl Environ Microbiol* **69**:3280–3287.
29. **Amellal N, Portal J-M, Berthelin J.** 2001. Effect of soil structure on the bioavailability of polycyclic aromatic hydrocarbons within aggregates of a contaminated soil. *Appl Geochemistry* **16**:1611–1619.
30. **Boonchan S, Britz ML, Stanley GA.** 1998. Surfactant-Enhanced Biodegradation of High Molecular Weight Polycyclic Aromatic Hydrocarbons by *Stenotrophomonas maltophilia*. *Biotechnol Bioeng* **59**:482–494.

31. **Makkar RS, Rockne KJ.** 2003. Comparison of synthetic surfactants and biosurfactants in enhancing biodegradation of polycyclic aromatic hydrocarbons. *Environ Toxicol Chem* **22**:2280–2292.
32. **Elliot R, Singhal N, Swift S.** 2010. Surfactants and Bacterial Bioremediation of Polycyclic Aromatic Hydrocarbon Contaminated Soil—Unlocking the Targets. *Crit Rev Environ Sci Technol* **41**:78–124.
33. **Demanèche S, Meyer C, Micoud J, Louwagie M, Willison JC, Jouanneau Y.** 2004. Identification and functional analysis of two aromatic-ring-hydroxylating dioxygenases from a *Sphingomonas* strain that degrades various polycyclic aromatic hydrocarbons. *Appl Environ Microbiol* **70**:6714–6725.
34. **Seo JS, Keum YS, Hu Y, Lee SE, Li QX.** 2007. Degradation of phenanthrene by *Burkholderia* sp. C3: Initial 1,2- and 3,4-dioxygenation and meta- and ortho-cleavage of naphthalene-1,2-diol. *Biodegradation* **18**:123–131.
35. **Tittabutr P, Cho IK, Li QX.** 2011. Phn and Nag-like dioxygenases metabolize polycyclic aromatic hydrocarbons in *Burkholderia* sp. C3. *Biodegradation* **22**:1119–1133.
36. **Singleton DR, Hu J, Aitken MD.** 2012. Heterologous expression of polycyclic aromatic hydrocarbon ring-hydroxylating dioxygenase genes from a novel pyrene-degrading betaproteobacterium. *Appl Environ Microbiol* **78**:3552–3559.
37. **Abdel-Mawgoud AM, Lépine F, Déziel E.** 2010. Rhamnolipids: Diversity of structures, microbial origins and roles. *Appl Microbiol Biotechnol* **86**:1323–1336.

38. **Perfumo A, Banat IM, Canganella F, Marchant R.** 2006. Rhamnolipid production by a novel thermophilic hydrocarbon-degrading *Pseudomonas aeruginosa* AP02-1. *Appl Microbiol Biotechnol* **72**:132–138.
39. **Peng F, Liu Z, Wang L, Shao Z.** 2007. An oil-degrading bacterium: *Rhodococcus erythropolis* strain 3C-9 and its biosurfactants. *J Appl Microbiol* **102**:1603–1611.
40. **Xia W, Du Z, Cui Q, Dong H, Wang F, He P, Tang Y.** 2014. Biosurfactant produced by novel *Pseudomonas* sp. WJ6 with biodegradation of n-alkanes and polycyclic aromatic hydrocarbons. *J Hazard Mater* **276**:489–498.
41. **Noordman WH, Janssen DB.** 2002. Rhamnolipid stimulates uptake of hydrophobic compounds by *Pseudomonas aeruginosa*. *Appl Environ Microbiol* **68**:4502–4508.
42. **Tiehm a.** 1994. Degradation of polycyclic aromatic hydrocarbons in the presence of synthetic surfactants. *Appl Environ Microbiol* **60**:258–263.
43. **Tecon R, Van Der Meer JR.** 2010. Effect of two types of biosurfactants on phenanthrene availability to the bacterial bioreporter *Burkholderia sartisoli* strain RP037. *Appl Microbiol Biotechnol* **85**:1131–1139.
44. **Boldrin B, Tiehm a., Fritzsche C.** 1993. Degradation of phenanthrene, fluorene, fluoranthene, and pyrene by a *Mycobacterium* sp. *Appl Environ Microbiol* **59**:1927–1930.
45. **Kodama K, Umehara K, Shimizu K, Nakatani S, Minoda Y, Yamada K.** 1973. Identification of Microbial Products from Dibenzothiophene and Its Proposed Oxidation Pathway. *Agric Biol Chem* **37**:45–50.

46. **Nojiri H, Habe H, Omori T.** 2001. Bacterial degradation of aromatic compounds via angular dioxygenation. *J Gen Appl Microbiol* **47**:279–305.
47. **Kilbane JJ.** 2006. Microbial biocatalyst developments to upgrade fossil fuels. *Curr Opin Biotechnol* **17**:305–314.
48. **Seo JS, Keum YS, Kyu Cho I, Li QX.** 2006. Degradation of dibenzothiophene and carbazole by *Arthrobacter* sp. P1-1. *Int Biodeterior Biodegrad* **58**:36–43.
49. **Tyagi S, Kramer FR.** 1996. Molecular mechanisms of biocatalytic desulfurization of fossil fuels. *Nat Biotechnol* **14**:303–308.
50. **Monticello DJ.** 2000. Biodesulfurization and the upgrading of petroleum distillates. *Curr Opin Biotechnol* **11**:540–546.
51. **Noda K-I, Watanabe K, Maruhashi K.** 2003. Isolation of the *Pseudomonas aeruginosa* gene affecting uptake of dibenzothiophene in n-tetradecane. *J Biosci Bioeng* **95**:504–511.
52. **Watkins LM, Rodriguez R, Schneider D, Broderick R, Cruz M, Chambers R, Ruckman E, Cody M, Mrachko GT.** 2003. Purification and characterization of the aromatic desulfinate, 2-(2'-hydroxyphenyl)benzenesulfinate desulfinate. *Arch Biochem Biophys* **415**:14–23.
53. **Abin-Fuentes A, Mohamed MES, Wang DIC, Prather KLJ.** 2013. Exploring the mechanism of biocatalyst inhibition in microbial desulfurization. *Appl Environ Microbiol* **79**:7807–7817.

54. **Duarte GF, Rosado AS, Seldin L, De Araujo W, Van Elsas JD.** 2001. Analysis of Bacterial Community Structure in Sulfurous-Oil-Containing Soils and Detection of Species Carrying Dibenzothiophene Desulfurization (dsz) Genes. *Appl Environ Microbiol* **67**:1052–1062.
55. **Kirimura K, Harada K, Iwasawa H, Tanaka T, Iwasaki Y, Furuya T, Ishii Y, Kino K.** 2004. Identification and functional analysis of the genes encoding dibenzothiophene-desulfurizing enzymes from thermophilic bacteria. *Appl Microbiol Biotechnol* **65**:703–713.
56. **Kayser KJ, Cleveland L, Park HS, Kwak JH, Kolhatkar a., Kilbane JJ.** 2002. Isolation and characterization of a moderate thermophile, *Mycobacterium phlei* GTIS10, capable of dibenzothiophene desulfurization. *Appl Microbiol Biotechnol* **59**:737–745.
57. **Maghsoudi S, Kheirloom a., Vossoughi M, Tanaka E, Katoh S.** 2000. Selective desulfurization of dibenzothiophene by newly isolated *Corynebacterium* sp. strain P32C1. *Biochem Eng J* **5**:11–16.
58. **Denome S a., Stanley DC, Olson ES, Young KD.** 1993. Metabolism of dibenzothiophene and naphthalene in *Pseudomonas* strains: Complete DNA sequence of an upper naphthalene catabolic pathway. *J Bacteriol* **175**:6890–6901.
59. **Di Gregorio S, Zocca C, Sidler S, Toffanin A, Lizzari D, Vallini G.** 2004. Identification of two new sets of genes for dibenzothiophene transformation in *Burkholderia* sp. DBT1. *Biodegradation* **15**:111–123.

60. **Gao S, Seo JS, Wang J, Keum YS, Li J, Li QX.** 2013. Multiple degradation pathways of phenanthrene by *Stenotrophomonas maltophilia* C6. *Int Biodeterior Biodegrad* **79**:98–104.
61. **Laurie AD, Lloyd-jones G.** 1999. The *phn* Genes of *Burkholderia* sp . Strain RP007 Constitute a Divergent Gene Cluster for Polycyclic Aromatic Hydrocarbon Catabolism
The *phn* Genes of *Burkholderia* sp . Strain RP007 Constitute a Divergent Gene Cluster for Polycyclic Aromatic Hydrocarbon Cata **181**:531–540.
62. **Evans WC, Evans WC.** 1964. Oxidative Metabolism of Naphthalene by. *Cell* 251–261.
63. **Seo JS, Keum YS, Harada RM, Li QX.** 2007. Isolation and characterization of bacteria capable of degrading Polycyclic Aromatic Hydrocarbons (PAHs) and organophosphorus pesticides from PAH-contaminated soil in Hilo, Hawaii. *J Agric Food Chem* **55**:5383–5389.
64. **Abdel-Mawgoud AM, Lépine F, Déziel E.** 2014. A stereospecific pathway diverts β -oxidation intermediates to the biosynthesis of rhamnolipid biosurfactants. *Chem Biol* **21**:156–164.
65. **Gutierrez M, Choi MH, Tian B, Xu J, Rho JK, Kim MO, Cho YH, Yoon SC.** 2013. Simultaneous Inhibition of Rhamnolipid and Polyhydroxyalkanoic Acid Synthesis and Biofilm Formation in *Pseudomonas aeruginosa* by 2-Bromoalkanoic Acids: Effect of Inhibitor Alkyl-Chain-Length. *PLoS One* **8**.
66. **Costa SGV a O, Déziel E, Lépine F.** 2011. Characterization of rhamnolipid production by *Burkholderia glumae*. *Lett Appl Microbiol* **53**:620–627.

67. **Toribio J, Escalante AE, Soberón-Chávez G.** 2010. Rhamnolipids: Production in bacteria other than *Pseudomonas aeruginosa*. *Eur J Lipid Sci Technol* **112**:1082–1087.
68. **Yang F, Hanna M a, Sun R.** 2012. Value-added uses for crude glycerol--a byproduct of biodiesel production. *Biotechnol Biofuels* **5**:13.
69. **da Silva GP, Mack M, Contiero J.** 2009. Glycerol: A promising and abundant carbon source for industrial microbiology. *Biotechnol Adv* **27**:30–39.
70. **Lin EC.** 1976. Glycerol dissimilation and its regulation in bacteria. *Annu Rev Microbiol* **30**:535–578.
71. **Voegele RT, Sweet GD, Boos W.** 1993. Glycerol kinase of *Escherichia coli* is activated by interaction with the glycerol facilitator. *J Bacteriol* **175**:1087–1094.
72. **Tepper BS.** 1964. Modification of cellular constituents during growth of mycobacterium phlei. *Am Rev Respir Dis* 75–82.
73. **Rehm BH a, Mitsky T a., Steinbüchel A.** 2001. Role of Fatty Acid de novo Biosynthesis in Polyhydroxyalkanoic Acid (PHA) and Rhamnolipid Synthesis by Pseudomonads: Establishment of the Transacylase (PhaG)-Mediated Pathway for PHA Biosynthesis in *Escherichia coli*. *Appl Environ Microbiol* **67**:3102–3109.
74. **Choi MH, Xu J, Gutierrez M, Yoo T, Cho YH, Yoon SC.** 2011. Metabolic relationship between polyhydroxyalkanoic acid and rhamnolipid synthesis in *Pseudomonas aeruginosa*: Comparative ¹³C NMR analysis of the products in wild-type and mutants. *J Biotechnol* **151**:30–42.

75. **De Eugenio LI, Galán B, Escapa IF, Maestro B, Sanz JM, García JL, Prieto MA.** 2010. The PhaD regulator controls the simultaneous expression of the pha genes involved in polyhydroxyalkanoate metabolism and turnover in *Pseudomonas putida* KT2442. *Environ Microbiol* **12**:1591–1603.
76. **Jurasek L, Marchessault RH.** 2002. The role of phasins in the morphogenesis of poly(3-hydroxybutyrate) granules. *Biomacromolecules* **3**:256–261.
77. **Di Martino C, Catone M V., López NI, Raiger Iustman LJ.** 2014. Polyhydroxyalkanoate Synthesis Affects Biosurfactant Production and Cell Attachment to Hydrocarbons in *Pseudomonas* sp. KA-08. *Curr Microbiol* **68**:735–742.
78. **Pham TH, Webb JS, Rehm BH a.** 2004. The role of polyhydroxyalkanoate biosynthesis by *Pseudomonas aeruginosa* in rhamnolipid and alginate production as well as stress tolerance and biofilm formation. *Microbiology* **150**:3405–3413.
79. **Lee HOJ, Choi MH, Kim TUN, Yoon SC.** 2001. Accumulation of Polyhydroxyalkanoic Acid Containing Large Amounts of Unsaturated Monomers in *Pseudomonas fluorescens* BM07 Utilizing Saccharides and Its Inhibition by 2-Bromooctanoic Acid. *Appl Environ Microbiol* **67**:4963–4974.
80. **Whang LM, Liu PWG, Ma CC, Cheng SS.** 2008. Application of biosurfactants, rhamnolipid, and surfactin, for enhanced biodegradation of diesel-contaminated water and soil. *J Hazard Mater* **151**:155–163.

81. **Nie M, Yin X, Ren C, Wang Y, Xu F, Shen Q.** 2010. Novel rhamnolipid biosurfactants produced by a polycyclic aromatic hydrocarbon-degrading bacterium *Pseudomonas aeruginosa* strain NY3. *Biotechnol Adv* **28**:635–643.
82. **Dobler L, Vilela LF, Almeida R V., Neves BC.** 2016. Rhamnolipids in perspective: Gene regulatory pathways, metabolic engineering, production and technological forecasting. *N Biotechnol* **33**:123–135.
83. **Zhu K, Rock CO.** 2008. RhlA converts ??-hydroxyacyl-acyl carrier protein intermediates in fatty acid synthesis to the ??-hydroxydecanoyl-??-hydroxydecanoate component of rhamnolipids in *Pseudomonas aeruginosa*. *J Bacteriol* **190**:3147–3154.
84. **Miller DJ, Zhang YM, Rock CO, White SW.** 2006. Structure of RhlG, an essential β -ketoacyl reductase in the rhamnolipid biosynthetic pathway of *Pseudomonas aeruginosa*. *J Biol Chem* **281**:18025–18032.
85. **Tavares LFD, Silva PM, Junqueira M, Mariano DCO, Nogueira FCS, Domont GB, Freire DMG, Neves BC.** 2013. Characterization of rhamnolipids produced by wild-type and engineered *Burkholderia kururiensis*. *Appl Microbiol Biotechnol* **97**:1909–1921.
86. **Ochsner URS a, Reiser J, Fiechter A.** 1995. Production of *Pseudomonas aeruginosa* Rhamnolipid Biosurfactants in Heterologous Hosts . These include : Production of *Pseudomonas aeruginosa* Rhamnolipid Biosurfactants in Heterologous Hosts **61**:3503–3506.

87. **Rahim R, Ochsner UA, Olvera C, Graninger M, Messner P, Lam JS, Soberón-Chávez G.** 2001. Cloning and functional characterization of the *Pseudomonas aeruginosa* rhIC gene that encodes rhamnosyltransferase 2, an enzyme responsible for di-rhamnolipid biosynthesis. *Mol Microbiol* **40**:708–718.
88. **Zhu K, Rock CO.** 2008. RhIA converts β -hydroxyacyl-acyl carrier protein intermediates in fatty acid synthesis to the β -hydroxydecanoyl- β -hydroxydecanoate component of rhamnolipids in *Pseudomonas aeruginosa*. *J Bacteriol* **190**:3147–3154.
89. **Bastiaens L, Springael D, Wattiau P, Verachtert H, Harms H, DeWachter R, Diels L.** 2000. Isolation of adherent polycyclic aromatic hydrocarbon (PAH) -degrading bacteria using PAH-sorbing carriers. *Appl Environ Microbiol* **66**:1834–1843.
90. **Akhtar N, Ghauri M a., Anwar M a., Akhtar K.** 2009. Analysis of the dibenzothiophene metabolic pathway in a newly isolated *Rhodococcus* spp. *FEMS Microbiol Lett* **301**:95–102.
91. **Dephoure N, Gygi SP.** 2011. A solid phase extraction-based platform for rapid phosphoproteomic analysis. *Methods* **54**:379–386.
92. **Kessner D, Chambers M, Burke R, Agus D, Mallick P.** 2008. ProteoWizard: Open source software for rapid proteomics tools development. *Bioinformatics* **24**:2534–2536.

93. **Chambers MC, Maclean B, Burke R, Amodei D, Ruderman DL, Neumann S, Gatto L, Fischer B, Pratt B, Egertson J, Hoff K, Kessner D, Tasman N, Shulman N, Frewen B, Baker T a, Brusniak M-Y, Paulse C, Creasy D, Flashner L, Kani K, Moulding C, Seymour SL, Nuwaysir LM, Lefebvre B, Kuhlmann F, Roark J, Rainer P, Detlev S, Hemenway T, Huhmer A, Langridge J, Connolly B, Chadick T, Holly K, Eckels J, Deutsch EW, Moritz RL, Katz JE, Agus DB, MacCoss M, Tabb DL, Mallick P.** 2012. A cross-platform toolkit for mass spectrometry and proteomics. *Nat Biotechnol* **30**:918–920.
94. **Tabb DL, Fernando CG, Chambers MC.** 2008. MyriMatch: highly accurate tandem mass spectral peptide identification by multivariate hypergeometric analysis. *J Proteome Res* **6**:654–661.
95. **Ma ZQ, Dasari S, Chambers MC, Litton MD, Sobecki SM, Zimmerman LJ, Halvey PJ, Schilling B, Drake PM, Gibson BW, Tabb DL.** 2009. IDPicker 2.0: Improved protein assembly with high discrimination peptide identification filtering. *J Proteome Res* **8**:3872–3881.
96. **Tabb DL.** 2007. IDPicker Overview.
97. **Griffin NM, Yu J, Long F, Oh P, Shore S, Li Y, Koziol JA, Schnitzer JE.** 2010. Label-free, normalized quantification of complex mass spectrometry data for proteomic analysis. *Nat Biotechnol* **28**:83–89.

98. **Polpitiya AD, Qian WJ, Jaitly N, Petyuk VA, Adkins JN, Camp DG, Anderson GA, Smith RD.** 2008. DAnTE: A statistical tool for quantitative analysis of -omics data. *Bioinformatics* **24**:1556–1558.
99. **Irie Y, Parsek MR.** 2014. *Pseudomonas Methods and Protocols*. *Pseudomonas Methods Protoc* **1149**:271–279.
100. **Laabei M, Jamieson WD, Lewis SE, Diggle SP, Jenkins ATA.** 2014. A new assay for rhamnolipid detection—important virulence factors of *Pseudomonas aeruginosa*. *Appl Microbiol Biotechnol* **98**:7199–7209.
101. **Price NPJ, Ray KJ, Vermillion K, Kuo TM.** 2009. MALDI-TOF mass spectrometry of naturally occurring mixtures of monorhamnolipids and dirhamnolipids. *Carbohydr Res* **344**:204–209.
102. **Price NPJ.** 2006. Oligosaccharide structures studied by hydrogen-deuterium exchange and MALDI-TOF mass spectrometry. *Anal Chem* **78**:5302–5308.
103. **Valle RP, Huang CL, Loo JSC, Zuo YY.** 2014. Increasing hydrophobicity of nanoparticles intensifies lung surfactant film inhibition and particle retention. *ACS Sustain Chem Eng* **2**:1574–1580.
104. **Seo JS, Keum YS, Li QX.** 2013. Metabolomic and proteomic insights into carbaryl catabolism by *Burkholderia* sp. C3 and degradation of ten N-methylcarbamates. *Biodegradation* **24**:795–811.
105. **Jendrossek D.** 2009. Polyhydroxyalkanoate granules are complex subcellular organelles (carbonosomes). *J Bacteriol* **191**:3195–3202.

106. **Richardson DJ.** 2000. Bacterial respiration: A flexible process for a changing environment. *Microbiology* **146**:551–571.
107. **Balachandran C, Duraipandiyar V, Balakrishna K, Ignacimuthu S.** 2012. Petroleum and polycyclic aromatic hydrocarbons (PAHs) degradation and naphthalene metabolism in *Streptomyces* sp. (ERI-CPDA-1) isolated from oil contaminated soil. *Bioresour Technol* **112**:83–90.
108. **Meena LS, Chopra P, Vishwakarma RA, Singh Y.** 2013. Biochemical characterization of an S-adenosyl-methionine-dependent methyltransferase (Rv0469) of *Mycobacterium tuberculosis*. *Biol Chem* **394**:871–877.
109. **Chiang PK, Gordon RK, Tal J, Zeng GC, Doctor BP, Gordon K.** 1996. S-Adenosylmethionine and methylation **10**:471–480.
110. **Déziel E, Lépine F, Milot S, Villemur R.** 2000. Mass spectrometry monitoring of rhamnolipids from a growing culture of *Pseudomonas aeruginosa* strain 57RP. *Biochim Biophys Acta - Mol Cell Biol Lipids* **1485**:145–152.
111. **Hennessee CT, Li QX.** 2016. Effects of PAH Mixtures on Degradation, Gene Expression, and Metabolite Production in Four *Mycobacterium* species. *Appl Environ Microbiol* **2011**:AEM.00100-16.
112. **Deutscher J.** 2008. The mechanisms of carbon catabolite repression in bacteria. *Curr Opin Microbiol* **11**:87–93.
113. **Wackett LP.** 1996. Co-metabolism: Is the emperor wearing any clothes? *Curr Opin Biotechnol* **7**:321–325.

114. **Kimura N, Nishi A, Goto M, Furukawa K.** 1997. Functional analyses of a variety of chimeric dioxygenases constructed from two biphenyl dioxygenases that are similar structurally but different functionally. *J Bacteriol* **179**:3936–3943.
115. **Suen W, Haigler BE, Eq-ol a L, Air T, Base F.** 1996. DNT : Similarity to Naphthalene Dioxygenase. *Microbiology* **178**:4926–4934.
116. **T MJ, Seo J, Keum Y, Li QX.** 2011. Comparative Protein and Metabolite Profiling Revealed a Metabolic Network in Response to Multiple Environmental Contaminants in. *J Agric Food Chem* 2876–2882.
117. **Piccoli S, Andreolli M, Giorgetti A, Zordan F, Lampis S, Vallini G.** 2014. Identification of aldolase and ferredoxin reductase within the dbt operon of *Burkholderia fungorum* DBT1. *J Basic Microbiol* **54**:464–469.
118. **Pini CV, Bernal P, Godoy P, Ramos JL, Segura A.** 2009. Cyclopropane fatty acids are involved in organic solvent tolerance but not in acid stress resistance in *Pseudomonas putida* DOT-T1E. *Microb Biotechnol* **2**:253–261.
119. **York GM, Junker BH, Stubbe J, Sinskey a. J.** 2001. Accumulation of the PhaP phasin of *Ralstonia eutropha* is dependent on production of polyhydroxybutyrate in cells. *J Bacteriol* **183**:4217–4226.
120. **Venkateswar Reddy M, Mawatari Y, Yajima Y, Seki C, Hoshino T, Chang YC.** 2015. Poly-3-hydroxybutyrate (PHB) production from alkylphenols, mono and poly-aromatic hydrocarbons using *Bacillus* sp. CYR1: A new strategy for wealth from waste. *Bioresour Technol* **192**:711–717.

121. **Lin TC, Pan PT, Young CC, Chang JS, Chang TC, Cheng SS.** 2011. Evaluation of the optimal strategy for ex situ bioremediation of diesel oil-contaminated soil. *Environ Sci Pollut Res* **18**:1487–1496.
122. **Hörmann B, Müller MM, Syldatk C, Hausmann R.** 2010. Rhamnolipid production by *Burkholderia plantarii* DSM 9509T. *Eur J Lipid Sci Technol* **112**:674–680.
123. **Bai G, Brusseau ML, Miller RM.** 1997. Influence of a rhamnolipid biosurfactant on the transport of bacteria through a sandy soil. *Appl Environ Microbiol* **63**:1866–1873.
124. **Horvath RS.** 1972. Microbial co-metabolism and the degradation of organic compounds in nature. *Bacteriol Rev* **36**:146–155.
125. **Reis R, Pacheco G, Pereira a, Freire D.** 2013. *Biosurfactants: Production and Applications*. New York InTech.
126. **Patowary K, Patowary R, Kalita MC, Deka S.** 2016. Development of an efficient bacterial consortium for the potential remediation of hydrocarbons from contaminated sites. *Front Microbiol* **7**:1–14.

12. ANNEXED

Table 13. Full description of significantly abundant proteins (p-value < 0.05). Proteins are shown in alphabetic order. Treatments were: A, 0.5 mM DBT; B, 50 mM glycerol; C, 50 mM glycerol and 0.5 mM DBT; D, 50 mM glycerol, 0.5 mM DBT and 2 mM OC. Proteins were extracted at day 2. Three biological replicates were analyzed in each treatment. Mean normalized value is shown in each treatment. The LogFC represents the glycerol*DBT interaction term.

UniProt ID	Protein description	Relative abundance by treatment				LogFC	P-value
		A	B	C	D		
Q93NA6	2,3-dihydroxy-2,3-dihydrophenylpropionate dehydrogenase	1.08	0.36	1.59	1.52	1.70	0.007
A0A0M4PT16	2-dehydropantoate 2-reductase	0.00	0.00	1.07	0.00	3.36	0.005
B1JU41	50S ribosomal protein L15	0.99	0.89	1.05	1.24	1.20	0.044
B5WTF5	50S ribosomal protein L15	0.99	0.89	1.05	1.24	1.20	0.044
A0A0D5V6G6	50S ribosomal protein L7/L12	1.22	0.75	0.96	1.42	1.24	0.019
A0A0D5VNH8	6-phosphogluconate dehydrogenase, decarboxylating	0.00	0.94	0.44	0.00	-2.03	0.005
A0A0D5V8G0	ABC transporter family protein	1.39	0.18	0.57	0.27	-1.85	0.024
A0A0D5VCE5	ABC transporter family protein	1.13	0.98	0.44	0.27	-2.04	0.006
A0A088TW83	ABC transporter, solute-binding protein	0.00	0.94	0.49	0.00	-2.11	0.041
A0A0D5VDU6	Acetaldehyde dehydrogenase 2	0.00	0.60	1.53	0.00	2.85	0.000
A0A0D5V7J1	Acetyl-coenzyme A synthetase	0.00	0.91	0.00	0.00	-3.66	0.002
A0A0M3TWC5	Acetyl-coenzyme A synthetase	0.00	0.91	0.00	0.00	-3.66	0.002
A0A0D5VDE2	Acetylornithine aminotransferase	1.68	1.57	0.96	1.52	-1.55	0.010
A0A0D5VBP8	Acetyltransferase component of pyruvate dehydrogenase complex	1.49	1.22	0.63	0.84	-2.19	0.003
C4AQ27	Acyl-CoA synthase	0.99	0.18	0.20	0.00	-3.33	0.014
A0A0D5VM16	Aldo/keto reductase family protein	0.00	1.20	0.20	0.00	-2.41	0.017
A0A0D5VJE9	Alpha amylase, catalytic domain protein	0.00	1.38	0.69	0.00	-4.61	0.000
A0A0D5VMD4	Amino acid adenylation domain protein	0.00	2.57	0.00	0.00	-6.41	0.000
A0A0D5V9V2	Aminomethyltransferase folate-binding domain protein	0.00	1.07	0.00	0.00	-3.69	0.002

Table 13 (continued). Full description of significantly abundant proteins (p-value < 0.05). Proteins are shown in alphabetic order. Treatments were: A, 0.5 mM DBT; B, 50 mM glycerol; C, 50 mM glycerol and 0.5 mM DBT; D, 50 mM glycerol, 0.5 mM DBT and 2 mM OC. Proteins were extracted at day 2. Three biological replicates were analyzed in each treatment. Mean normalized value is shown in each treatment. The LogFC represents the glycerol*DBT interaction term.

UniProt ID	Description	Relative abundance by treatment				LogFC	P-value
		A	B	C	D		
A0A0D5VEW3	Aminomethyltransferase	0.64	1.20	0.57	0.53	-1.72	0.021
A0A0D5VF93	Aminopeptidase N	0.00	1.37	0.46	0.00	-1.86	0.036
A0A0D5V5Y2	Aminotransferase class I and II family protein	1.32	1.23	0.83	1.10	-1.70	0.005
A0A0D5VLM9	Aminotransferase class-III family protein	0.72	1.34	0.00	0.00	-4.75	0.000
A0A0D5VB61	Arginine-tRNA ligase	0.62	1.48	0.20	0.54	-2.30	0.011
R9W162	Aromatic-ring-hydroxylating dioxygenase	1.73	0.42	1.58	2.17	1.39	0.033
B2T171	Aspartate 1-decarboxylase	0.58	0.00	0.00	1.34	2.38	0.027
A0A0D5VFE6	Aspartate-tRNA ligase	0.00	1.07	0.00	0.00	-2.65	0.011
A0A0M4NYD7	ATP:cob(I)alamin adenosyltransferase	1.22	0.23	1.60	1.55	1.99	0.001
A0A0D5VJR3	Bacterial extracellular solute-binding family protein	0.00	0.13	0.91	1.20	1.92	0.045
A0A0D5VFF5	Bacterial extracellular solute-binding family protein	1.39	1.64	1.36	1.13	-1.00	0.047
A0A0N0IDK4	Beta-eliminating lyase family protein	0.00	1.02	0.00	0.00	-3.41	0.006
A0A0D5VBD8	Carbohydrate-binding family V/XII	0.00	1.00	0.62	0.00	-2.41	0.017
A0A0D5VFX6	Chaperone protein DnaK	1.40	0.98	0.24	1.45	-1.20	0.022
A0A0D5V7V8	Chaperone protein HtpG	1.80	0.88	0.00	1.34	-2.21	0.002
A0A0D5VDT3	Chaperone SurA	2.01	1.68	2.33	2.21	1.18	0.016
Q13SY2	Chemotaxis response regulator protein-glutamate methyltransferase	0.00	0.93	0.20	0.00	-2.11	0.040
A0A0D5VBP4	Chromosome partition protein Smc	0.85	1.16	0.42	0.00	-2.36	0.001
A0A0D5V8E3	CTP synthase	0.00	1.03	0.20	0.27	-3.29	0.000
O86041	Cupin	1.23	1.52	1.28	0.27	-1.55	0.008
A0A0D5VI43	Cyclic peptide transporter family protein	0.00	1.19	0.69	0.00	-1.80	0.021
A0A0D5VJG9	D-alanine-poly(Phosphoribitol) ligase, subunit 1	0.00	2.92	0.00	0.00	-6.71	0.000
G5L3J5	Dihydrodipicolinate synthase/N-acetylneuraminase lyase	2.42	0.46	2.42	2.34	2.45	0.000

Table 13 (continued). Full description of significantly abundant proteins (p-value < 0.05). Proteins are shown in alphabetic order. Treatments were: A, 0.5 mM DBT; B, 50 mM glycerol; C, 50 mM glycerol and 0.5 mM DBT; D, 50 mM glycerol, 0.5 mM DBT and 2 mM OC. Proteins were extracted at day 2. Three biological replicates were analyzed in each treatment. Mean normalized value is shown in each treatment. The LogFC represents the glycerol*DBT interaction term.

UniProt ID	Description	Relative treatment by abundance				LogFC	P-value
		A	B	C	D		
A0A0D5VK03	Dihydroxy-acid dehydratase	0.23	1.16	0.63	0.27	-1.80	0.027
A0A0D5VH17	DNA polymerase I	0.00	0.94	0.20	0.00	-3.56	0.003
A0A0D5VD44	DNA-directed RNA polymerase subunit beta	0.45	1.16	0.25	0.80	-2.15	0.004
A0A0D5VAX2	DNA-directed RNA polymerase subunit beta'	0.85	1.26	0.97	0.68	-4.00	0.000
A0A0M5LFU7	DSBA oxidoreductase	1.82	0.00	0.00	0.41	-3.31	0.001
A0A0D5VBB3	Efflux pump membrane family protein	0.00	0.00	1.54	0.27	4.26	0.000
A0A0D5VCE6	Elongation factor G	0.49	1.16	0.00	0.00	-5.01	0.000
A0A0D5VEA5	Endoribonuclease L-PSP family protein	0.26	0.23	0.20	1.10	2.65	0.039
B2T4A8	Enoyl-[ACP] reductase [NADH]	0.00	1.07	0.00	0.00	-4.07	0.000
A0A0D5V781	Enoyl-CoA hydratase/isomerase family protein	0.00	1.11	0.44	0.00	-2.11	0.013
A0A0M4P2D0	Extracellular solute-binding protein family 5	0.00	0.30	0.96	0.00	1.86	0.044
A0A0D5VBT1	Flagellar motor switch protein FliG	0.94	0.00	0.00	0.00	-3.23	0.006
Q93CN7	Putative monooxygenase alpha subunit	2.02	1.62	2.02	1.87	1.89	0.007
A0A0D5VB09	Flavoheмоprotein	1.64	0.00	0.00	1.34	-1.89	0.042
A0A0D5V7V5	FMN-dependent NADH-azoreductase	0.45	0.18	1.35	1.77	5.75	0.000
A0A0D5VLU1	Glucose-6-phosphate 1-dehydrogenase	0.23	1.01	0.33	0.00	-2.72	0.004
A0A0D5VBW3	Glutamate synthase (Ferredoxin)	0.00	1.02	0.00	0.27	-4.26	0.000
Q13V40	Glutamate-1-semialdehyde 2,1-aminomutase	0.00	0.93	0.00	0.00	-2.70	0.037
A0A0D5V9H7	Glutamine-fructose-6-phosphate aminotransferase [isomerizing]	0.00	1.20	0.00	0.00	-3.36	0.007
A0A0D5V FY1	Glycerol-3-phosphate dehydrogenase	0.00	1.07	1.94	0.53	1.76	0.003
A0A0D5VMH1	Glycine betaine/L-proline transport ATP binding subunit	1.57	0.31	0.00	0.00	-5.23	0.000
Q13SR6	Glycine dehydrogenase (decarboxylating)	1.02	1.22	0.33	1.10	-1.34	0.029

Table 13 (continued). Full description of significantly abundant proteins (p-value < 0.05). Proteins are shown in alphabetic order. Treatments were: A, 0.5 mM DBT; B, 50 mM glycerol; C, 50 mM glycerol and 0.5 mM DBT; D, 50 mM glycerol, 0.5 mM DBT and 2 mM OC. Proteins were extracted at day 2. Three biological replicates were analyzed in each treatment. Mean normalized value is shown in each treatment. The LogFC represents the glycerol*DBT interaction term.

UniProt ID	Description	Relative abundance by treatment				LogFC	P-value
		A	B	C	D		
A0A0D5VAC2	Glycine-tRNA ligase beta subunit	1.30	1.79	0.73	0.27	-2.09	0.001
A0A0D5VCV1	Glycolate oxidase, subunit GlcD	0.00	1.23	0.20	0.00	-2.52	0.011
A0A0D5V8X4	Heme ABC exporter, ATP-binding protein CcmA	1.40	0.60	0.00	0.00	-4.99	0.000
A0A0D5V647	Heme ABC exporter, ATP-binding protein CcmA	0.26	1.16	0.00	0.00	-4.01	0.001
A0A0D5VD28	Hsp70 family protein	1.36	0.66	0.00	0.27	-3.67	0.001
G5L3J5	Hydratase-aldolase	1.98	1.27	2.33	2.40	1.97	0.000
A0A0D5VIM7	Intracellular multiplication and macrophage-killing family protein	0.36	1.12	0.20	0.00	-3.18	0.000
A0A0D5VJ60	Isocitrate dehydrogenase, NADP-dependent	0.49	1.89	0.25	0.00	-3.64	0.000
A0A0D5VAW4	Isocitrate lyase	0.26	1.35	0.69	0.00	-2.14	0.002
A0A0D5VEQ0	Isoleucine-tRNA ligase	0.00	1.23	0.33	0.00	-1.95	0.026
A0A0N0ZGK7	Lactoylglutathione lyase	0.58	0.48	0.42	1.24	1.52	0.046
A0A0D5VBP9	LPS export ABC transporter ATP binding protein	1.40	0.62	0.33	0.27	-1.90	0.019
A0A0D5VBW4	LTXXQ motif family protein	0.72	0.99	1.43	1.20	1.50	0.023
A0A0D5V5U8	Malic enzyme, NAD binding domain protein	0.23	1.39	1.10	0.00	-1.11	0.036
A0A0D5V6I0	Malic enzyme, NAD binding domain protein	1.36	1.50	0.86	1.30	-1.92	0.001
A0A0D5V9M1	NAD dependent epimerase/dehydratase family protein	0.45	1.07	0.20	0.53	-4.44	0.000
A0A0D5V8Z7	NADH-quinone oxidoreductase	1.02	1.29	0.00	0.00	-4.96	0.000
A0A0M4NP56	Naphthalene 1,2-dioxygenase	1.68	0.23	1.66	1.76	1.26	0.044
A0A0D5VK45	Nitrate reductase, alpha subunit	2.55	0.42	0.25	2.01	-2.34	0.001
A0A0D5VM92	Nitrate reductase, beta subunit	2.05	0.13	0.00	1.34	-3.43	0.000
A0A0D5VE52	NlpB/DapX lipofamily protein	0.58	1.10	0.49	0.00	-2.68	0.007
A0A0D5VDA6	OsmC-like family protein	0.00	0.13	0.83	1.10	2.62	0.016
A0A0D5VD61	Outer membrane/peptidoglycan-associated (Lipo)protein	2.06	1.62	1.46	2.02	-1.45	0.005

Table 13 (continued). Full description of significantly abundant proteins (p-value < 0.05). Proteins are shown in alphabetic order. Treatments were: A, 0.5 mM DBT; B, 50 mM glycerol; C, 50 mM glycerol and 0.5 mM DBT; D, 50 mM glycerol, 0.5 mM DBT and 2 mM OC. Proteins were extracted at day 2. Three biological replicates were analyzed in each treatment. Mean normalized value is shown in each treatment. The LogFC represents the glycerol*DBT interaction term.

UniProt ID	Description	Relative abundance by treatment				LogFC	P-value
		A	B	C	D		
Q143E5	Outer-membrane lipoprotein carrier protein	0.64	1.06	0.96	0.26	-1.86	0.040
A0A0D5VG00	Oxoglutarate dehydrogenase (Succinyl-transferring), E1 component	1.49	1.15	0.42	1.20	-2.29	0.000
C7DQY6	PAH dioxygenase small subunit	1.45	1.40	1.12	0.92	-1.28	0.036
A0A0D5VLZ1	Peptidase M1 family protein	0.00	1.38	0.25	0.00	-2.50	0.012
A0A0D5VEM2	Peptidase M3 family protein	0.64	1.13	0.00	0.69	-2.69	0.003
A0A0D5VMS9	Peptidyl-prolyl cis-trans isomerase	0.49	0.85	1.05	1.10	2.41	0.003
Q13X57	Peptidyl-prolyl cis-trans isomerase	1.02	1.15	1.60	1.63	1.09	0.037
A0A0D5VH07	Peroxiredoxin, Ohr subfamily protein	0.23	0.50	0.96	1.10	2.44	0.008
A0A0N1KL01	Phasin family domain protein	2.03	2.13	2.26	1.96	-1.34	0.005
A0A0D5VCV0	Phosphatidylethanolamine-binding family protein	0.23	0.66	0.96	1.24	2.01	0.030
A0A0D5V9F1	Phosphoenolpyruvate carboxylase	0.00	1.81	1.17	0.00	-1.27	0.042
A0A0D5VDY9	Phosphoenolpyruvate synthase	0.59	1.16	0.00	0.53	-3.14	0.000
A0A0D5VER0	Phosphoenolpyruvate-proteinphosphotransferase	0.45	0.71	0.00	0.00	-3.32	0.009
B2SXE3	Phosphoenolpyruvate-protein phosphotransferase	0.36	0.93	0.00	0.00	-3.90	0.001
A0A0D5V8K8	Phosphoglycerate kinase	0.00	1.25	0.82	0.27	-1.64	0.019
A0A0N0IEG4	Phosphomethylpyrimidine synthase	0.49	0.93	0.00	0.00	-4.36	0.000
A0A0D5VDM4	Phosphoribosyl transferase domain protein	0.72	0.41	1.19	1.42	1.92	0.012
A0A0D5V925	Phosphoribosylformylglycinamide synthase	0.23	1.80	0.00	0.00	-5.42	0.000
A0A0Q5H1G7	Poly(R)-hydroxyalkanoic acid synthase	0.23	0.00	0.83	0.80	2.77	0.011
W6X074	Poly(R)-hydroxyalkanoic acid synthase, class I	0.41	0.00	0.54	0.95	2.09	0.043
A9BZX2	Poly(R)-hydroxyalkanoic acid synthase, class I	0.00	0.13	0.83	0.80	2.51	0.017
A0A0N7JU12	Polyhydroxyalkanoic acid synthase	1.19	0.00	0.00	0.00	-3.75	0.007

Table 13 (continued). Full description of significantly abundant proteins (p-value < 0.05). Proteins are shown in alphabetic order. Treatments were: A, 0.5 mM DBT; B, 50 mM glycerol; C, 50 mM glycerol and 0.5 mM DBT; D, 50 mM glycerol, 0.5 mM DBT and 2 mM OC. Proteins were extracted at day 2. Three biological replicates were analyzed in each treatment. Mean normalized value is shown in each treatment. The LogFC represents the glycerol*DBT interaction term.

UniProt ID	Description	Relative abundance by treatment				LogFC	P-value
		A	B	C	D		
A0A0D5VFS8	Protein-export protein SecB	0.99	0.60	0.33	1.30	1.96	0.012
Q93CP1	Putative isomerase	1.93	0.00	0.00	0.41	-3.50	0.000
Q93CP1	Putative isomerase	1.09	0.90	0.25	0.27	-2.50	0.006
A0A0D5VIB5	Putative NADH dehydrogenase/NAD(P)H nitroreductase	0.59	1.37	1.98	2.02	1.29	0.017
A0A0M4P147	Putative serine protein kinase, PrkA	0.00	1.44	0.25	0.00	-3.27	0.000
A0A0N0IFY8	Putative translation initiation inhibitor, yjgF family	1.42	0.60	0.63	0.95	-1.96	0.021
A0A0D5VE80	Pyruvate dehydrogenase E1 component	1.82	1.42	1.05	0.80	-1.56	0.003
A0A0D5V9F4	Pyruvate kinase	0.23	1.32	0.96	0.27	-1.78	0.011
Q3JLM3	Rhamnosyltransferase 2	1.00	0.43	0.00	0.00	-4.34	0.001
A2RWE5	Rhamnosyltransferase II	0.94	0.43	0.00	0.00	-4.34	0.001
A0A0D5V939	Ribonuclease E	0.00	1.12	0.25	0.00	-2.45	0.002
A0A0D5VDW9	Ribose-phosphate pyrophosphokinase	1.36	0.62	0.46	0.53	-2.24	0.040
A0A0D5VLP3	RNA polymerase sigma factor RpoD	0.00	1.01	0.33	0.00	-2.56	0.002
A0A0D5VEZ5	RNA polymerase-binding transcription factor DksA	0.72	0.62	1.10	0.95	1.11	0.048
A0A0D5VFS0	RND transporter, hydrophobe/amphiphile efflux-1 family protein	1.17	0.61	0.00	0.69	-3.95	0.000
A0A0D5VCJ1	S1 RNA binding domain protein	0.49	1.00	0.00	0.69	-3.38	0.001
A0A0D5VDD8	Serine hydroxymethyltransferase	0.00	0.93	1.10	0.00	-1.70	0.002
A0A0D5V9T1	Short chain dehydrogenase family protein	0.00	1.13	0.20	0.00	-2.29	0.024
A0A0D5VPP2	Short chain dehydrogenase family protein	0.00	0.00	1.75	0.26	4.66	0.000
A0A0D5VG50	Signal transducing histidine kinase, homodimeric domain protein	1.32	0.88	0.79	0.54	-1.16	0.038
A0A0D5VFC1	Soluble lytic murein transglycosylase L domain protein	0.45	1.23	0.63	0.00	-2.56	0.011

Table 13 (continued). Full description of significantly abundant proteins (p-value < 0.05). Proteins are shown in alphabetic order. Treatments were: A, 0.5 mM DBT; B, 50 mM glycerol; C, 50 mM glycerol and 0.5 mM DBT; D, 50 mM glycerol, 0.5 mM DBT and 2 mM OC. Proteins were extracted at day 2. Three biological replicates were analyzed in each treatment. Mean normalized value is shown in each treatment. The LogFC represents the glycerol*DBT interaction term.

UniProt ID	Description	Relative abundance by treatment				LogFC	P-value
		A	B	C	D		
A0A0D5V720	Succinyl-CoA ligase [ADP-forming] subunit beta	1.63	1.22	1.05	1.24	-1.08	0.039
A0A0D5V735	Sulfate ABC transporter, sulfate-binding family protein	0.23	0.84	1.67	1.00	1.31	0.016
A0A0D5VNY2	Sulfurtransferase	0.00	0.93	0.00	0.00	-3.21	0.011
A0A0M3TVK8	Tautomerase	0.00	0.00	0.44	0.95	3.74	0.004
A0A0M3TVE7	Threonine synthase	0.00	0.92	0.00	0.00	-3.83	0.001
A0A0D5V9J4	Threonine--tRNA ligase	0.62	1.55	0.49	0.26	-2.70	0.010
A0A0D5V7D0	Thymidylate kinase	0.99	0.89	0.33	0.27	-1.74	0.036
A0A0D5VMA4	TonB dependent receptor family protein	2.36	0.00	0.00	0.54	-4.91	0.000
A0A0D5VNE5	TonB-dependent siderophore receptor family protein	0.00	1.09	0.37	0.00	-3.57	0.003
A0A0D5VMB8	TonB-dependent siderophore receptor family protein	1.38	2.24	1.18	0.52	-2.69	0.000
A0A0D5VGP4	TonB-dependent siderophore receptor family protein	0.00	2.02	1.43	0.27	-1.23	0.039
A0A0N0ZGN2	Transketolase	1.71	1.44	0.73	1.28	-1.93	0.001
A0A0D5VJ16	Type VI secretion ATPase, ClpV1 family	0.00	1.93	0.73	0.00	-2.07	0.002
A0A0D5VDN9	Uncharacterized protein	0.00	0.99	0.44	0.00	-2.01	0.005
A0A0N0IFW9	Uncharacterized protein	1.32	0.13	0.46	0.27	-4.72	0.000
A0A0M4P0G0	Uncharacterized protein	0.81	1.02	1.06	1.10	-2.15	0.009
A0A0D5VEE7	Uncharacterized protein	0.00	0.96	0.20	0.00	-3.96	0.001
A0A0D5VGK4	Uncharacterized protein	0.23	1.07	0.69	0.00	-2.00	0.010
A0A0D5VPU9	Uncharacterized protein	0.45	1.86	2.05	0.41	1.61	0.006
A0A0D5VNT3	Uncharacterized protein	0.23	0.23	0.20	1.30	2.46	0.014
A0A0D5VIL6	Uncharacterized protein	0.00	1.01	0.00	0.00	-3.41	0.006
A0A0M3TVK2	Uncharacterized protein	0.23	0.36	1.51	1.00	2.12	0.001
A0A0D5VCB1	YceI-like domain protein	0.96	1.39	0.91	0.80	-1.75	0.024